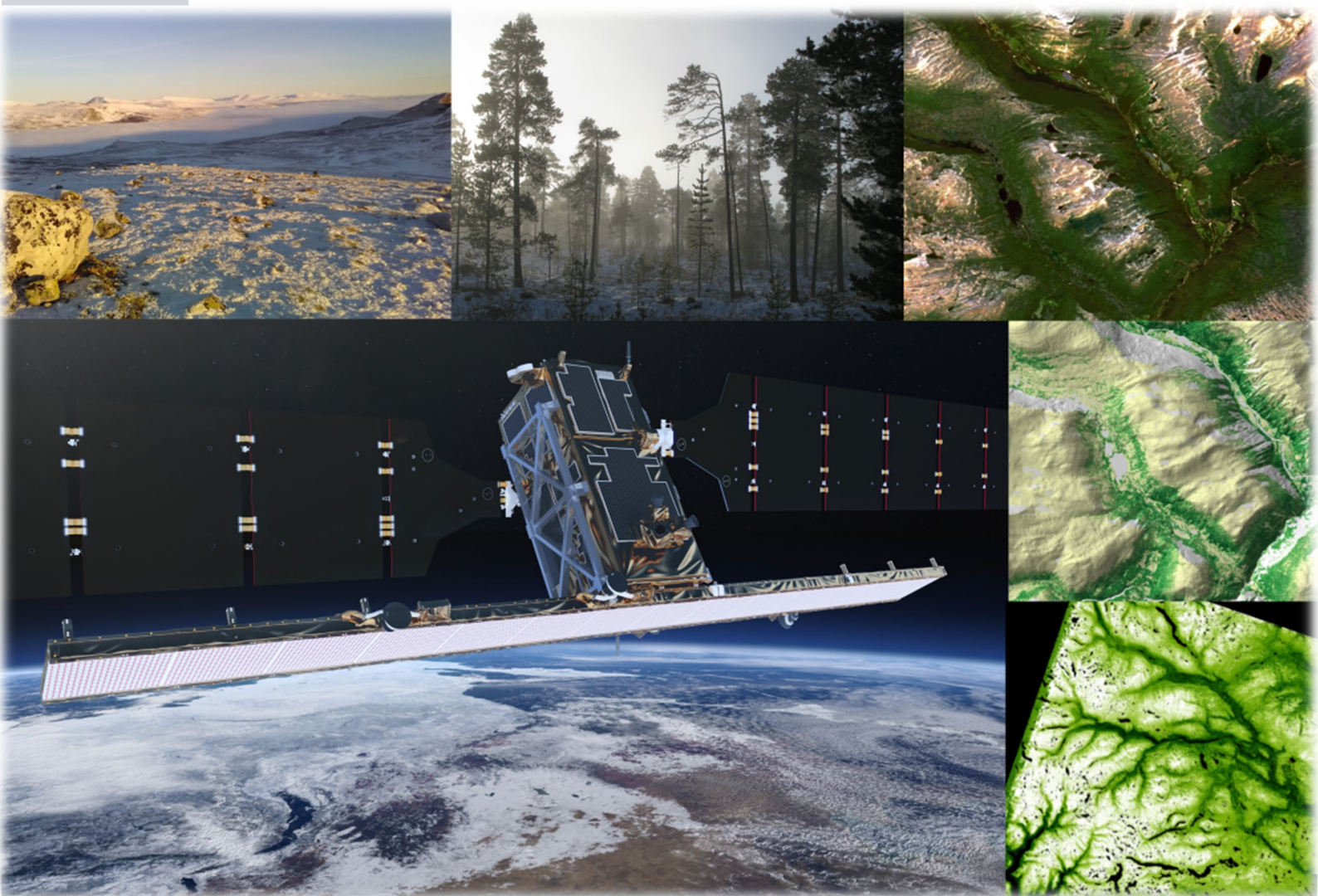**1545**

NINA Report

# Sentinel4Nature: Estimating environmental gradients and properties using remote sensing

Stefan Blumentrath, Arnt-Børre Salberg, Zofie Cimburova, Vegar Bakkestuen, Lars Erikstad, Megan Nowell, Martin Kermit



NINA

Norwegian Institute for Nature Research

# NINA Publications

**NINA Report (NINA Rapport)**
This is NINA's ordinary form of reporting completed research, monitoring or review work to clients. In addition, the series will include much of the institute's other reporting, for example from seminars and conferences, results of internal research and review work and literature studies, etc. NINA Report may also be issued in a second language where appropriate.

**NINA Special Report (NINA Temahefte)**
As the name suggests, special reports deal with special subjects. Special reports are produced as required and the series ranges widely: from systematic identification keys to information on important problem areas in society. NINA special reports are usually given a popular scientific form with more weight on illustrations than a NINA Report.

**NINA Factsheet (NINA Fakta)**
Factsheets have as their goal to make NINA's research results quickly and easily accessible to the general public. Fact sheets give a short presentation of some of our most important research themes.

**Other publishing**
In addition to reporting in NINA's own series, the institute's employees publish a large proportion of their scientific results in international journals, popular science books and magazines.

# Sentinel4Nature: Estimating environmental gradients and properties using remote sensing

Blumentrath, Stefan
Salberg, Arnt-Børre
Cimburova, Zofie
Bakkestuen, Vegar
Erikstad, Lars
Nowell, Megan
Kermit, Martin

**Norwegian Institute for Nature Research**

AVAILABILITY
Open

PUBLICATION TYPE
Digital document (pdf)

QUALITY CONTROLLED BY
Siri Lie Olsen

SIGNATURE OF RESPONSIBLE PERSON
Kristin Thorsrud Teien (sign.)

CLIENT(S)/SUBSCRIBER(S)
European Space Agency

CLIENT(S) REFERENCE(S)
C4000111621 Sentinel4Nature

CLIENTS/SUBSCRIBER CONTACT PERSON(S)
Veronique Dowson

COVER PICTURE
Top left: Thin and sparse snow cover at Hjerkinn © S. Blumentrath,
Top middle: Snow covered forest © O.T. Sandlund,
Top right: Sentinel-2 RGB image from Sunndalen © Z. Cimburova,
Down left: Sentinel-1 in orbit © ESA/ATG medialab,
Middle left: Modelled tree canopy cover © Z. Cimburova,
Down left: Modelled day of snow melt © A-B Salberg.

KEY WORDS
Norway, Oslofjord, Lurøykalven, Hjerkinn, Sunndalen, environmental gradients, snow cover, tree canopy cover, remote sensing, Sentinel imagery, data fusion, modelling, NiN, PRODEX, ESA, NRS

NØKKELORD
Norge, Oslofjorden, Lurøykalven, Hjerkinn, Sunndalen, lokale komplekse miljøvariabler (LKM), snødekkebetinget vekstsesongreduksjon, tresjiktstetthet , fjernmåling, Sentinel, data fusion, modellering, NiN, PRODEX, ESA, NRS

# Abstract

In 2014, the European Space Agency (ESA) launched the first Sentinel satellite as one of a series of complementary sensors that together form the Sentinel mission family. It is part of to-day's most ambitious Earth Observation Program: Copernicus. At the same time, a new system for describing, mapping and analysing nature in Norway (NiN) has been developed (Halvorsen et al. 2015). One of the leading principles in NiN is to account for gradual transitions in nature and thus to focus on the underlying environmental gradients and properties (e.g. related to climate, soil, etc.) that govern the occurrence of species and associated nature types.

The aim of the Sentinel4Nature project (financed by ESAs PRODEX funds) has been to develop and advance an approach to remote sensing that focuses on monitoring basic environmental gradients and properties and utilizes fusion of different data sources (different sensors as well as auxiliary data). In this context, the suitability of remote sensing to identify environmental gradients in the NiN classification system has been assessed.

Based on expert judgement and a literature review, it was estimated that satellite remote sensing can be a useful source of information for more than 50 % of the 61 environmental gradients in NiN. The majority of the most suitable gradients is related to land cover as well as presence of water or snow in the landscape.

From the most suitable gradients, 1) reduced growing season due to prolonged snow-lie and 2) tree canopy cover, were selected for case studies that were conducted in one to four study sites across Southern- and Central-Norway. For 1), the date of snow melt was estimated from a time series of Landsat8 and Sentinel-1 observations and for 2), the percentage of canopy cover per pixel was modelled using Sentinel-1 and Sentinel-2 data. In both cases fairly accurate models could be developed that improve the current possibilities to map or model vegetation structures or species occurrences. Fusion of imagery from different sensors (in particular radar and optical) significantly improved the model performance. Auxiliary data was less important than expected. However, data on terrain has been important during image enhancement and correction.

Although the presented methods already perform quite well, future adjustments and improvements in the processing chains and also parameter tuning have to be expected when used at larger extents and especially towards arctic environments of the Scandinavian peninsula.

Stefan Blumentrath, NINA, Gaustadalléen 21, NO-0349 Oslo. stefan.blumentrath@nina.no
Arnt-Børre Salberg, NR, Gaustadalléen 23a, NO-0373 Oslo. arnt-borre.salberg@nr.no
Zofie Cimburova, NINA, Gaustadalléen 21, NO-0349 Oslo. zofie.cimburova@nina.no
Megan Nowell,  NINA, Gaustadalléen 21, NO-0349 Oslo. megan.nowell@nina.no
Vegar Bakkestuen,  NINA, Gaustadalléen 21, NO-0349 Oslo. vegar.bakkestuen@nina.no
Lars Erikstad,  NINA, Gaustadalléen 21, NO-0349 Oslo. lars.erikstad@nina.no
Martin Kermit, NR, Gaustadalléen 23a, NO-0373 Oslo. martin.kermit@nr.no

# Sammendrag

Blumentrath, S., Salberg, A.-B., Cimburova, Z., Bakkestuen, V., Erikstad, L., Nowell, M., Kermit, M. 2018. Sentinel4Nature: Beregning av miljøgradienter og egenskaper ved hjelp av fjernmåling. NINA Rapport 1545. Norsk institutt for naturforskning.


I 2014 ble den første Sentinel-satellitten skutt opp av Den europeiske romfartsorganisasjon (ESA) som en del av en serie komplementere sensorer som til sammen danner Sentinel-familien. Disse inngår i dagens mest avanserte jordobservasjonsprogram: Copernicus. På samme tid ble det nye systemet for beskrivelse, kartlegging og analyse av natur i Norge (NiN) utviklet (Halvorsen et al. 2015). Et av grunnprinsippene i NiN er å redegjøre for gradvise over-ganger i naturen og å fokusere på underliggende miljøvariabler (f.eks. lokale komplekse miljø-variabler (LKM) knyttet til bla. klima, jordforhold, osv.) som påvirker forekomsten av arter og naturtyper.

Formålet med Sentinel4Nature-prosjektet (som ble finansiert as ESAs PRODEX-program) har vært å utvikle og forbedre en tilnærming til fjernmåling som fokuserer på overvåking av under-liggende miljøvariabler og egenskaper, og som benytter seg av data fra ulike kilder (både ulike sensorer og supplerende data på f.eks. terreng). I denne sammenhengen ble det også vurdert om satellitt-fjernmåling kan bidrar til kartlegging av de ulike miljøvariablene i NiN.

Basert på en ekspertvurdering og litteratur-studie ble det estimert at satellitt-basert fjernmåling kan være en nyttig informasjonskilde for mer enn 50 % av de 61 lokale komplekse miljøvariab-lene in NiN. Flesteparten av miljøvariablene der fjernmåling kan bidra positivt er knyttet til areal-dekke eller forekomsten av vann eller snø i landskapet.

Blant de mest egnete miljøvariablene ble 1) snødekkebetinget vekstsesongreduksjon og 2) tre-sjiktstetthet valgt ut som case-studier som ble gjennomført i en til fire studieområder i Sør- and Midt-Norge. For 1) ble snøsmeltingsdato estimert fra en tidsserie av Landsat8- og Sentinel-1-observasjoner og for 2) ble prosentandel trekronedekning per piksel modellert basert på Senti-nel-1-og Sentinel-2-data. I begge casene oppnådde de utviklede modellene rimelig høy presisjon og kunne forbedre dagens muligheter til å forklare eller modellere vegetasjonsstrukturer og arts-forekomster. Fletting av bildedata fra ulike sensorer (særlig kombinert bruk av radar- og optiske data) forbedret modellene vesentlig. Supplerende romlige variabler, f.eks. terrengindekser, var mindre viktig enn forventet. Terrengdata har imidlertid spilt en viktig rolle i bildeforbedring og -korreksjon.

Selv om de utviklede metodene allerede fungerer rimelig bra, kan det forventes at framtidige tilpasninger og forbedringer i prosesseringskjedene og parameterne blir nødvendig dersom mo-dellene skal brukes landsdekkende og spesielt i nordlige og arktiske strøk på den Skandinaviske halvøy.

Stefan Blumentrath, NINA, Gaustadalléen 21, NO-0349 Oslo. stefan.blumentrath@nina.no
Arnt-Børre Salberg, NR, Gaustadalléen 23a, NO-0373 Oslo. arnt-borre.salberg@nr.no
Zofie Cimburova, NINA, Gaustadalléen 21, NO-0349 Oslo. zofie.cimburova@nina.no
Megan Nowell, NINA, Gaustadalléen 21, NO-0349 Oslo. megan.nowell@nina.no
Vegar Bakkestuen, NINA, Gaustadalléen 21, NO-0349 Oslo. vegar.bakkestuen@nina.no
Lars Erikstad, NINA, Gaustadalléen 21, NO-0349 Oslo. lars.erikstad@nina.no
Martin Kermit, NR, Gaustadalléen 23a, NO-0373 Oslo. martin.kermit@nr.no

# Contents

# Foreword

Shortly after the first Sentinel satellites were launched in 2014, the Norwegian Institute for Nature Research (NINA) and the Norwegian Computing Center (NR) received funding from ESAs PRODEX program to explore the potential of the satellite remote sensing for the new mapping system «Nature in Norway» (NiN) that had been established roughly at the same time. This report presents the final results of the project and updates and extends the earlier status report:

Blumentrath, S, Nowell, M. S., Salberg, A.-B., Kermit, M. A., Bakkestuen, V., Erikstad, L., Bernhardt, J. 2016. Sentinel4Nature: Estimating environmental gradients and properties using remote sensing. NINA Kortrapport 6. Norsk institutt for naturforskning.

We are especially grateful to the members of our advisory board:
- Arild Lindgaard from the Norwegian Biodiversity Information Centre
- Ellen Arneberg from the Norwegian Environment Agency
- Johan Danielsen from the Norwegian Environment Agency

for their valuable comments and suggestions during progress meetings.

We also want to thank Guro Dahle Strøm, Vigdis Lonar Barth and Anja Strømme from the Norwegian Space Center as well as Veronique Dowson from the European Space Agency (ESA) for their support during the project and of course ESA for financing it.

Finally, our thanks go to our colleagues from NINA Annika Hofgaard, Dagmar Hagen, Nina Eide, Marianne Evju, Siri Lie Olsen, Jørn Olav Løkken and Lars Rød Eriksen for providing data and biological expertise to the project.

November 2018

Stefan Blumentrath

Principal investigator

# 1 Introduction

The European Space Agency (ESA) Sentinels constitute the first series of operational satellites responding to the Earth Observation needs of the European Union (EU). In spring 2014, Sentinel-1 satellite, the first in the Sentinel mission family, was launched by the ESA as part of today's most ambitious Earth Observation Program: Copernicus (European Space Agency 2010). The family of missions from Sentinel-1 to Sentinel-6 (not launched), will carry a wide range of technologies, such as radar and multi-spectral imaging instruments for land, ocean and atmospheric monitoring. For example, Sentinel-1 is imaging global landmasses, coastal zones, sea-ice, polar areas, and shipping routes at high resolution, and covering the global ocean. This method ensures a reliability of service required by operational services and a consistent long-term data archive built for applications based on long time series. Sentinel-2 with an innovative wide swath high-resolution multispectral imager with 13 spectral bands can be used to determine various plant indices such as leaf area chlorophyll and water content indexes. These Sentinel missions aim to provide the public with free Earth Observation data with unchallenged spectral, temporal and spatial resolution for a wide range of purposes. They will undoubtedly offer new and unique possibilities for environmental assessments, monitoring and management.

At the same time, a new system for describing, mapping and analysing Nature in Norway (NiN) has been developed (Halvorsen et al. 2015). One of the leading principles in NiN is to account for gradual transitions in nature and thus to focus on the underlying environmental gradients and properties (e.g. related to climate, soil, etc.) that govern the occurrence of species and associated nature types. The specific recognition of gradual transitions in nature and a systematic use of spatial and temporal scales in NiN can be seen as a contrast to most of the other classification systems applied in European countries (see Ichter et al. 2014). Although NiN is a specific system for Norway and does not cover the whole range of environmental conditions in Europe, it can be seen as a comprehensive list of important environmental gradients and properties with a pan-European relevance, especially in hard-rock-coast and alpine environments that cover large extents of Norway.

The Sentinel4Nature project financed by ESA's PRODEX program, therefore, seeks to investigate the methodological potential of detecting and modelling the NiN environmental gradients using Sentinel imagery. Further, developing new approaches in nature monitoring will provide stakeholders, managers and researchers working with environment management with more valuable information.

# 2 Aim and expected benefits of the project

The main objective of the Sentinel4Nature project is to develop and advance a novel approach to remote sensing, which focuses on monitoring basic environmental gradients and properties (covering physical, chemical and biological components as well as their interactions). It is based on the hypothesis that the recently launched Sentinel satellites, with their increased temporal, spatial and spectral resolution, as well as increased spatial coverage (compared to e.g. Landsat), will provide valuable information that may be used to map and monitor basic environmental gradients. Here the aim is to, a) identify the potential of Sentinel imagery for modelling and identifying environmental gradients, b) explore how satellite imagery can be applied in order to support various sectors in their need for area information. This includes integration with other relevant datasets such as e.g. Digital Elevation Models (DEM) using data fusion techniques to optimize the results (Salberg et al. 2013, Ichter et al. 2014).

The Sentinel4Nature project explores the usefulness of remote sensing techniques for identifying environmental gradients in the NiN classification system. The work is based on the hypothesis that monitoring of environmental gradients and their changes can provide environmental researchers, managers and policy makers with valuable information because:

- Monitoring environmental gradients can serve as an early warning system for changes in ecosystem processes and functioning and thereby improve targeted responses, because one can expect that characteristics of the underlying environmental gradients change before organisms react to it and e.g. vegetation changes.

- Environmental gradients can also be indicators of the quality of different nature types, as they allow more fine scaled mapping at continuous scales. Therefore, modelling and identifying them will provide additional information about e.g. ecological conditions within mapped nature types of special interest.

- Information on environmental gradients can allow for a broader scope of possible applications, compared to more traditional vegetation mapping. For example, the pattern of snow cover in Arctic or alpine areas is not only important for vegetation structure, but also for the Arctic or alpine fauna.

- Another hypothesis is that gradients can be monitored with a higher robustness compared to e.g. complex vegetation or land cover type mapping, because the focus is on single environmental characteristics and not on multiple vegetation classes/types, and continuous data are generated instead of discrete classes. Also, training data for gradients can often be measured or mapped in a more objective and quantitative way, while delineation and classification of habitat types in the field can lead to substantial differences among different observers (Eriksen et al. 2018).

For the reasons above, it can be expected that a gradient-based approach will be useful for indicator systems developed across European (in Norway for example the Nature Index - NI), which are meant as tools for guiding environmental policies. The gradient-based approach can fit nicely into the Driving Force, Pressure, State, Impact, and Response concept (DPSIR assessment framework – European Environment Agency), which is an extended version of the OECD's countries (Organisation for Economic Co-operation and Development) pressure-state-response model implanted in the 1980s. In this causal framework interactions between humans and the environment are assessed in terms of the DPSIR components (see also Pirrone et al. 2005, Stanners et al. 2007). The proposed gradient-based approach to remote sensing and monitoring aims at identifying underlying characteristics or trends in nature (pressures and impacts). It may therefore help policy and decision makers but also scientists to identify links between pressures and impacts and the current state of the environment and thus to identify reasons or drivers of change.

Furthermore, the gradients listed in the NiN system overlap with the concept Essential Climate Variables (ECV, Bojinski et al. 2014) and Essential Biodiversity Variables (EBV). The latter have been identified by the Group on Earth Observations Biodiversity Observation Network (GEO BON) to "become the window into the biodiversity observation systems upon which researchers, managers and decisions makers at different levels can better interact while they do their jobs" (Group on Earth Observations Biodiversity Observation Network 2016). Thus, the project has the potential to provide linkages to the global activities of GEO BON. In Norway, comparable activities where mapping ecological gradients is of relevance are the ecological base map initiative (Norwegian Ministry of Climate and Environment 2016) as well as the work related to the development of a comprehensive technical system for the determination of good ecological condition (Nybø & Evju 2017).

Finally, the project will give environmental management institutions an assessment of the potential that the Sentinel satellites will provide within remote sensing-based nature management, both in terms of mapping and modelling, but also for detecting changes caused by e.g. climate or intervention. The project will also contribute to the use of satellite-based and cost-effective methods for collecting environmental information and support the analysis of nature types, and thereby contribute to the implementation of NiN in Norwegian management institutions. For nature management institutions, like the Norwegian Environment Agency, improved analysis of mountain areas will be vital for the management and surveillance of national parks which are found to large extent in these areas.

The work will be carried out through case studies on selected environmental gradients and properties with relevance for alpine and coastal ecosystems. Alpine and coastal ecosystems are ecosystems of special interest in many European countries, as coastal zones and mountains are habitats for species of European interest and are particularly vulnerable to environmental changes (direct or indirect human pressures such as climate or land use changes) (Pachauri et al. 2014, Vermaat et al. 2017).

# 3 The suitability of remote sensing (Sentinel) for estimating environmental gradients and properties in NiN

A first step in the Sentinel4Nature project was to explore the suitability of satellite-based sensing (in particular Sentinel satellites) for identifying and modelling environmental gradients and properties in NiN.

Local complex environmental variables (hereafter referred to as environmental gradients and properties) are the smallest building blocks of the NiN system to describe and map Nature in Norway across scales (Halvorsen et al. 2015). Environmental gradients represent gradual changes in environmental conditions, while environmental properties represent rather distinct features of the environment. The important characteristic of both of these elements in NiN is that they affect the abundance of species and species composition with a relatively long-lasting effect. The NiN nature types are defined based on changes in species compositions along the different environmental gradients and properties of the system. Thus, environmental gradients and properties represent the main structuring element of the NiN system. **Figure 1** shows an idealized exchange of indicator species abundances along a hypothetical environmental gradient.
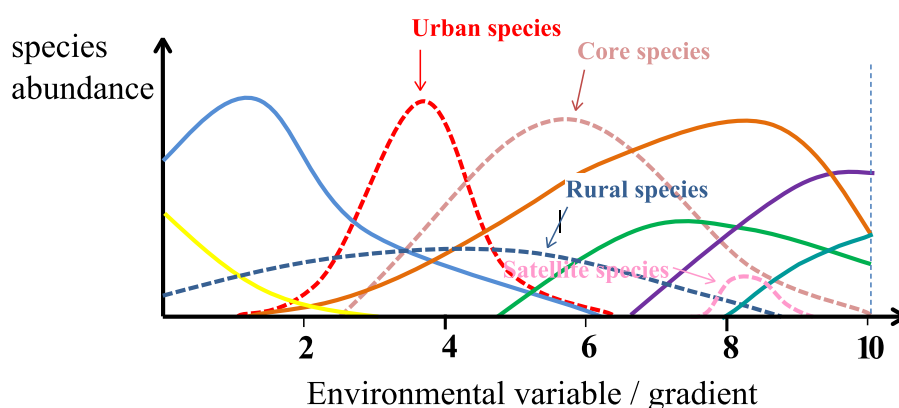


*Figure 1* Idealized changes in species abundances along a hypothetical environmental gradient (modified from Halvorsen et al. 2016), that are used as a guiding principle in NiN.

In this chapter, an assessment of the suitability of remote sensing for estimating environmental gradients and properties in NiN is presented (chapters 3.1 and 3.2). This assessment was the basis for the selection of suitable gradients for case studies in the Sentinel4Nature project (chapter 3.3).

## 3.1 Assessing the suitability of remote sensing for estimating environmental gradients and properties in NiN

In the system Nature in Norway (NiN) version 2.0, there are 61 local complex environmental variables (hereafter referred to as environmental gradients) listed, which are known to influence species occurrence in nature (Halvorsen et al. 2015, see also **Table 1** and the electronic appendix for an overview). For these environmental gradients the potential of satellite remote sensing

has been assessed for estimating and modelling them in space and time. The assessment was conducted as an expert judgement, supported by a literature review.

Criteria used during this assessment are:
- the observable properties of the imagery (spectral response, image structures)
- suitable and available sensors
- the required spatial resolution
- the need for time series
- additional required data sources
- existing and related examples

These criteria also stress the main challenges, which may occur when utilizing remote sensing for estimating environmental gradients and properties. Spatial and spectral resolution is one of the main challenges across all gradients. Spatial resolution, i.e. pixel size, implies the minimum size of an observed feature. Products of current satellite missions are usually not in sub-meter resolution. In the case that higher precision is required, other methods, e.g. UAV-based remote sensing are needed. Spectral resolution refers to the number and range of spectral bands. In general, much more information can be derived from hyperspectral imagery than from multispectral imagery (e.g. Sentinel-2 mission). Finally, a large challenge concerns the availability of time-series necessary for the remote sensing of many environmental gradients. Even if the frequency of satellite imaging is high, the weather conditions (e.g. cloud cover) might make a scene unusable. However, even if technological obstacles prevent the direct usage of remote sensing, it can in many cases be utilized as a pre-product or background data for further analysis.

## 3.2 Suitability of remote sensing for environmental gradients and properties in NiN

Each environmental gradient was evaluated in terms of its potential for remote sensing. Five grades of suitability were assigned:
- **achievable** if necessary technologies are currently available,
- **feasible** if remote sensing is theoretically possible, but some uncertainties regarding either spatial or temporal resolution or topics of interest exist,
- **challenging** if remote sensing is theoretically possible, but significant uncertainties regarding either spatial or temporal resolution or topics of interest exist,
- **currently not feasible** if remote sensing is not possible with current technology,
- **not relevant** if the environmental gradient is not relevant to remote sensing technology.

**Table 1** contains the overall results of this evaluation. The detailed assessment and applied criteria are provided in a spreadsheet, that follows this document as an underlineelectronic appendix.

*Table 1: Potential for remote sensing for environmental gradients in NiN*

| Potential | NiN gradients |
|---|---|
| Achievable | Avalanche exposure, Drought period, Flood regime, Landslide exposure, Reduced growing-season due to prolonged snow-lie, Sand stabilization (shore and dune development), Semi-natural agricultural management intensity type, Soil scarification, Tree canopy cover, Water Saturation |
| Feasible | Freshwater humus content, Geothermal influence, Marine salinity, Mire surface character, Permafrost, Sedimentation-induced disturbance, Slope dependent disturbance intensity, Soil flow |
| Challenging | Agricultural management intensity, Coastal influence, Content of organic material, Depth-related light attenuation , Erosion exposure, Ground influenced by frost heaving, Ground/sea- and riverbed strongly influenced by human disturbance, Hay- |

| | making influence, Historical environmental stress, Ice disturbance along shorelines and rivers, Seminatural ground/sea- and riverbed influenced by limited human disturbance, Severity of drought, Size classes (waterbodies), Slow Primary Succession, Slow primary Succession on coral sea beds, Turbidity, Water supply, Wind deflation |
|---|---|
| Currently not feasible | Anoxia, Arid terrestrial salinity, Bedrock with special chemical content, Lime richness, Natural manuring, Peat formation, Salt-enriched coastal ground, Strength of rheogenous water supply, Strongly human influenced waterbodies, Water movement energy, Water spraying intensity, Water sprinkling, Water-induced disturbance |
| Not relevant | Connectivity, Depth-zonation in deep fjords, Dominating Particle size-class, Drought exposure, Erosion Resistance (in graded sediments), Fine-material content (in graded sediments), Freshwater with special chemical content, Light zonation in cave openings, Ocean depth zonation, Particle size, Special sorted sediments, Type of rheogenous water supply |

Altogether, identifying and modelling through remote sensing was found achievable for 10 out of 61 environmental gradients. The common observable property of these gradients is land cover, detected using Sentinel-2 visible and near-infrared spectral bands. Vegetation indices such as the Normalized Difference Vegetation Index (NDVI) or water indices such as the Normalized Difference Water Index (NDWI) may be utilized as pre-products. Landslide exposure is for example related to an absence of vegetation cover, indicated by low NDVI values, in addition to sufficient steep terrain slopes. In addition, products of Sentinel-1 and Sentinel-3 missions may be utilized to observe properties such as texture (tree canopy cover) or surface temperature (reduced growing-season due to prolonged snow-lie). The suitability of remote sensing for these environmental gradients is also supported by previous studies (Mulder et al. 2011, Gao 1996, McFeeters 1996). Here, developing solutions that utilize the new Sentinel sensors and possibly new methodological approaches, can help to improve the information quality of remote sensing products for these gradients.

Satellite remote sensing was evaluated as theoretically possible (feasible or challenging) for 26 more environmental gradients. The main uncertainties about the suitability of remote sensing for these gradients concern the spatial, spectral (coastal influence) or temporal (soil flow) resolution. In some cases, the suitability of remote sensing depends on the scale of measurement – e.g. salinity is well measurable in coarser scale but challenging at a local scale.

Finally, 12 environmental gradients were assessed as not relevant. In these gradients, physical barriers, such as rocks or water may prevent from identifying and modelling through remote sensing (e.g. light zonation in cave openings). These gradients also describe small-scale local conditions, rare cases, or concern fine categorization (e.g. Fine-material content (in graded sediments)). However, even in these cases, remote sensing can facilitate the identification and modelling of these environmental gradients by providing pre-products or background data (e.g. in order to model Drought exposure, NDVI can be utilized as a pre-product).

The general conclusion is that despite many technological obstacles (e.g. spatial, spectral and temporal resolution), remote sensing can be utilized as a pre-product across many gradients.

## 3.3 Gradients from NiN selected for case studies

From the NiN gradients where it is expected that remote sensing is suitable to map them in space and time, the gradients "Reduced growing-season due to prolonged snow-lie" and "Tree canopy cover" were selected for further case studies. Both are relevant for mountain and/or coastal ecosystems. At the same time, the methodology to address them is relatively different due to

different observable properties, different temporal dynamics and both are expected to benefit from combining different data sources, including data from different Sentinels (1 and 2).

### 3.3.1 Reduced growing-season due to prolonged snow-lie (SV, NiN 2.0)

In Arctic and alpine areas, an important factor for the occurrence of plant species is the duration of snow cover (**Figure 2**). The length of the snow cover season determines the length of the growing season and thereby the time the species have to complete their life cycle. Here, snow-beds represent the most extreme cases, which are only snow-free for a few weeks during the summer months. In snow-beds, very few species are found. The environmental gradient "reduced growing season due to snow-lie" (SV) is one of the most important factors for variation in species composition in mountain and tundra ecosystems and strongly impacts the alpine plant communities.

However, at some locations in the mountain areas, it is the stability of the snow cover and not the length of the snow cover season that determines the species composition. Areas without a stable snow cover are highly exposed to strong wind and frost during the winter. In order to survive in such places, the species need to be able to cope with tough conditions without any protective snow cover. The snow cover stability is directly related to the thickness of the snow cover, which again is based on the amount of precipitation and the strength of the wind.
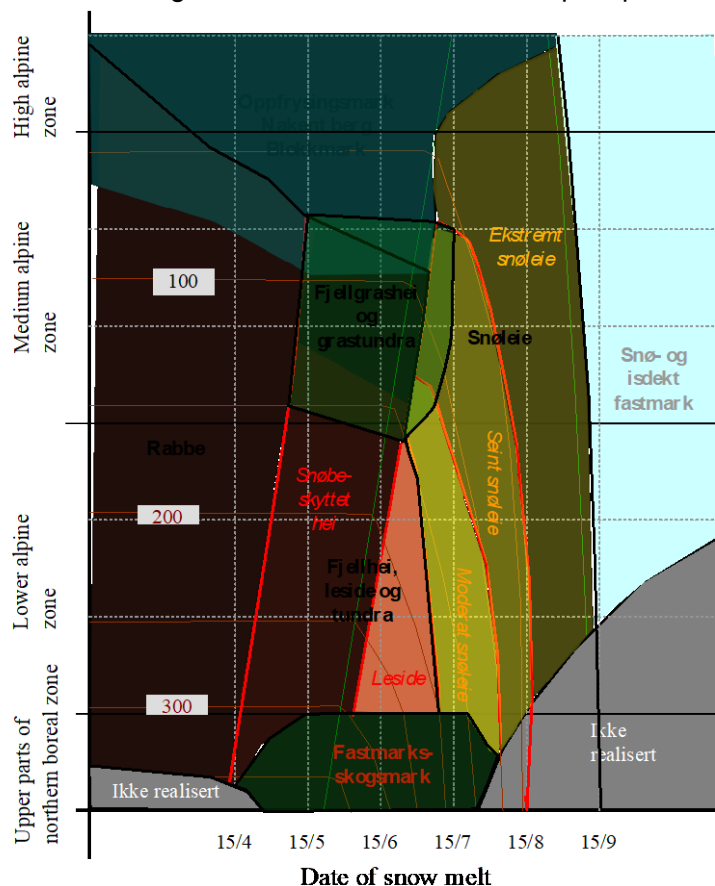


*Figure 2* Occurrence of nature types in Norwegian mountains depending on altitudinal belt and date of snow melt (modified from Halvorsen et al. 2016). Green lines indicate the beginning and end of the growing season. Rabbe: Ridge, Snøleie: Snow-bed, Snø og isdekt fastmark, Snow and ice-covered land, Fjellgrashei og grastundra : Mountain grassland and tundra, Fjellhei, leside og tundra: Mountain, leeward and tundra, Ikke realisert: unrealized, Oppfrysingsmark: frost turbation, Nakent berg: bare rock, Blokkmark: boulders

The reduced growing season due to snow-lie (SV) as well as the snow cover stability are two very important environmental gradients in the upland and tundra regions. Since both are strongly related to the snow cover, satellite-based sensors may be used to monitor them. Satellite sensors have been widely used to map the snow-covered areas and cryosphere (see e.g. Scherer et al. 2005, Maher et al. 2012, Crawford e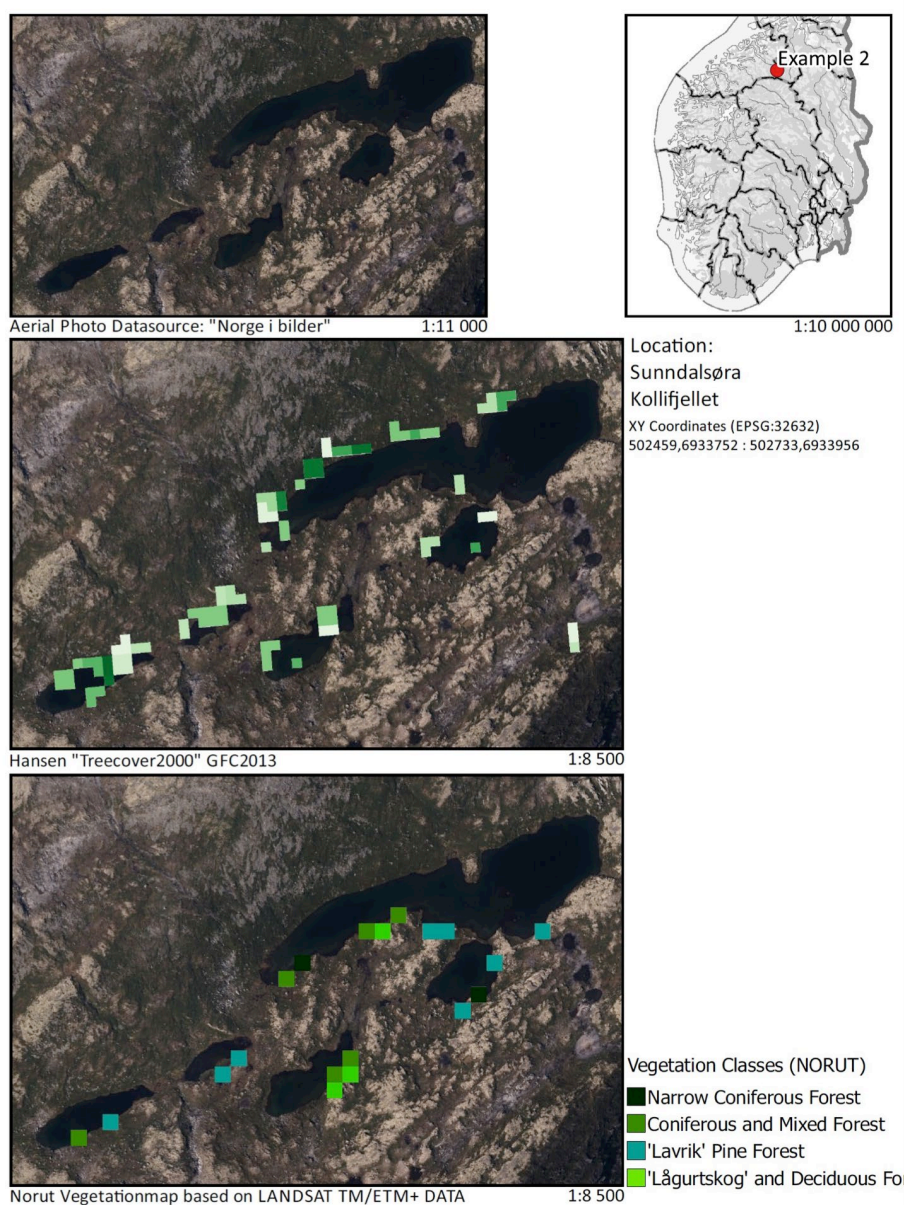t al. 2013, Metsamaki et al. 2014). Mapping snow cover duration over time can provide information about possible effects of climate change in this regard, and in consequence on vegetation patterns in mountain and tundra regions.

### 3.3.2 Tree canopy cover (TT, NiN 1.0)

The density of tree canopy cover is one of the most important environmental factors for both forest species which can be found underneath the tree crowns and for species that do not tolerate growing in shady environment (e.g. alpine plants). Thus, tree canopy cover is an important structuring factor for vegetation. It affects the occurrence of species and species compositions in several ways. First, canopy cover reduces the availability of light and precipitation that reaches the species under the trees. Second, with an increased canopy cover, the input of dead organic matter (litter) increases. Tree canopy cover is furthermore related to several other gradients in NiN like Drought exposure (UE), Severity of drought (UF), or Wind deflation (VI) from NiN 2.0, as well as Deforestation (BA), Forest regrowth (GG), and Reduction of tree cover density (TR).

Beyond its relevance as a habitat for certain species, tree canopy cover is of vital interest for management in many other regards, including economic activities (forestry), $CO_2$-accounting, natural hazards, as well as landscape and nature conservation (e.g. in terms of maintaining open cultural landscapes). Furthermore, tree canopy cover is an important variable for characterizing the forest-tundra-ecotone and, as such, is of special interest for research on effects of climate change. Forest encroachment has the potential to significantly change ecosystem structure and functions in Norwegian mountain areas, but the speed and pattern of forest encroachment are disputed (see e.g. Bryn et al. 2018).

For this reasons, tree canopy cover has been of high interest for previous remote sensing projects. However, both classical classification approaches (like NORUT's vegetation map, Johansen 2009) and more gradient-like approaches (like in Hansen et al. 2013) struggle especially with "mixed signal" - pixels at the land-water interface. **Figure 3** shows lakes in an alpine area in Norway where pixels along the shorelines were falsely associated with tree canopy cover. The combination of radar and optical sensors with Sentinel-1 and Sentinel-2 can help addressing these issues, together with pre-processing techniques like e.g. spectral unmixing.

Aerial Photo Datasource: "Norge i bilder"  1:11 000

1:10 000 000

Location:
Sunndalsøra
Kollifjellet

XY Coordinates (EPSG:32632)
502459,6933752 : 502733,6933956

Hansen "Treecover2000" GFC2013  1:8 500

Vegetation Classes (NORUT)
Narrow Coniferous Forest
Coniferous and Mixed Forest
'Lavrik' Pine Forest
'Lågurtskog' and Deciduous Fo

Norut Vegetationmap based on LANDSAT TM/ETM+ DATA  1:8 500

**Figure 3** Errors in forest detection in existing remote sensing products along the land / water interface.

# 4 Case study sites

Case study sites for the Sentinel4Nature project have been chosen depending on the selected case study gradients, which are "Reduced growing-season due to prolonged snow-lie" (SV, NiN 2.0) and "Tree canopy cover (TT, NiN 1.0)". In order to study the detectability of the environmental gradients named above, the following case study sites in Norway were chosen (see **Figure 4**):

- Oslofjord
- Lurøykalven
- Hjerkinn
- Sunndalen

Together they cover a wide range of environmental conditions both with regards to climate and topography. In addition, these sites have been and are part of earlier or on-going research activities.
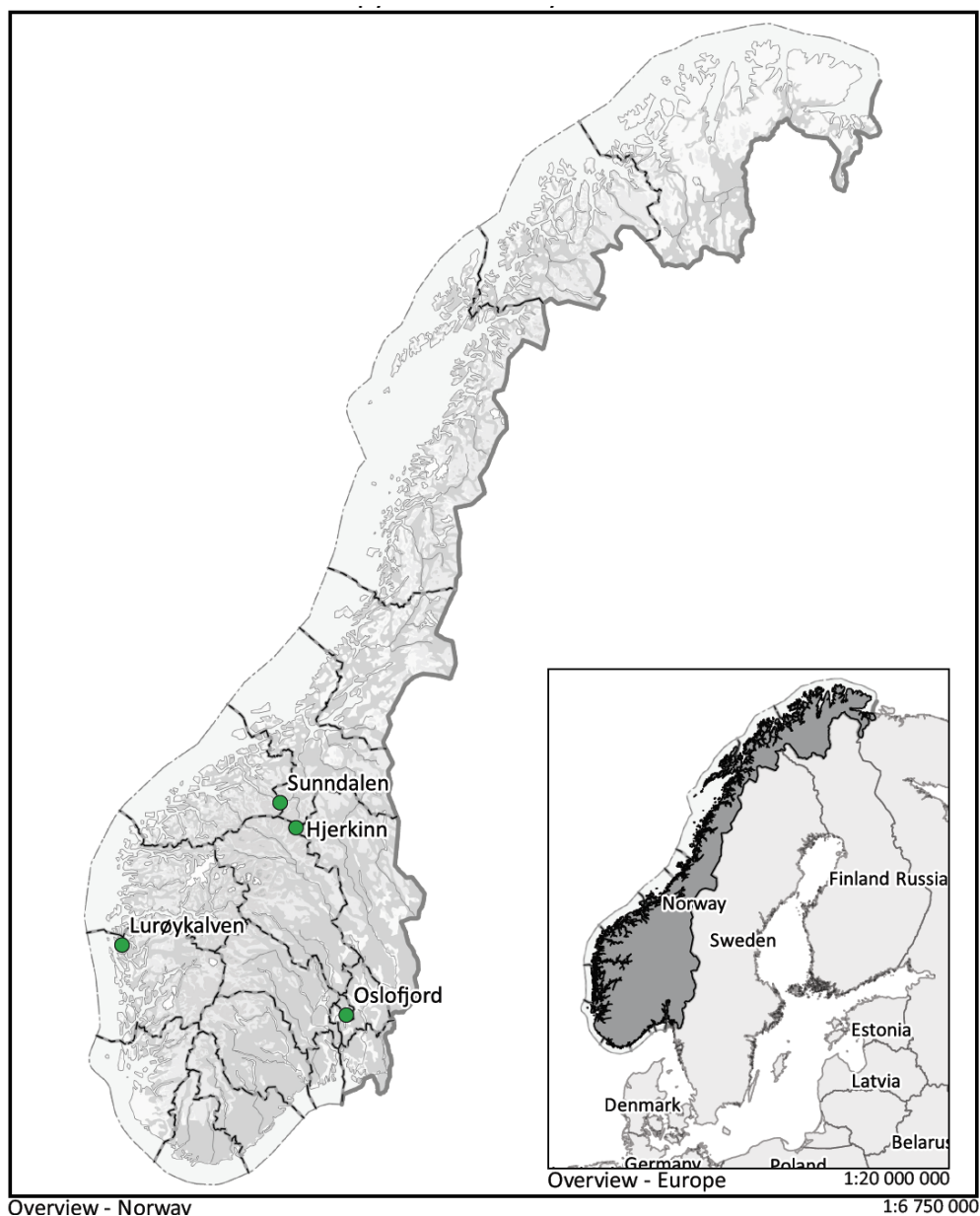


**Figure 4** *Location map of the four case study sites in the Sentinel4Nature project.*

# 4.1 Oslofjord

The Oslofjord study area is located in south-east Norway (59° 53'N 10° 42'E). This lowland area is characterized by a hilly terrain and located at the transition between oceanic and continental climate. The landscape consists of a mixed habitat mosaic with the fjord, islands, forests and human infrastructure (see **Figure 5**). The average annual temperature is reasonably stable and ranges from -0.6 to 3.4°C. Precipitation is fairly constant throughout the year. The city of Oslo surrounds the four islands included in the case study. The islands of Gressholmen and Rambergøya are moderately inhabited, while Ormøya and Malmøya have more human infrastructure (**Figure 6**).

Topics to be studied in the Oslofjord case study site are the gradient "Tree canopy cover" and the usefulness of data fusion and scale effects in the small-scale vegetation se-



**Figure 5** Landscape at the Oslofjord (Photo: Anne Sverdrup-Thygeson)

quences in this area (see **Figure 7**). The tree canopy cover gradient is of particular relevance for the inner Oslofjord region because forest expansion is a threat to open cultural landscapes here, especially the prioritized and endangered habitats of calcareous grassland.
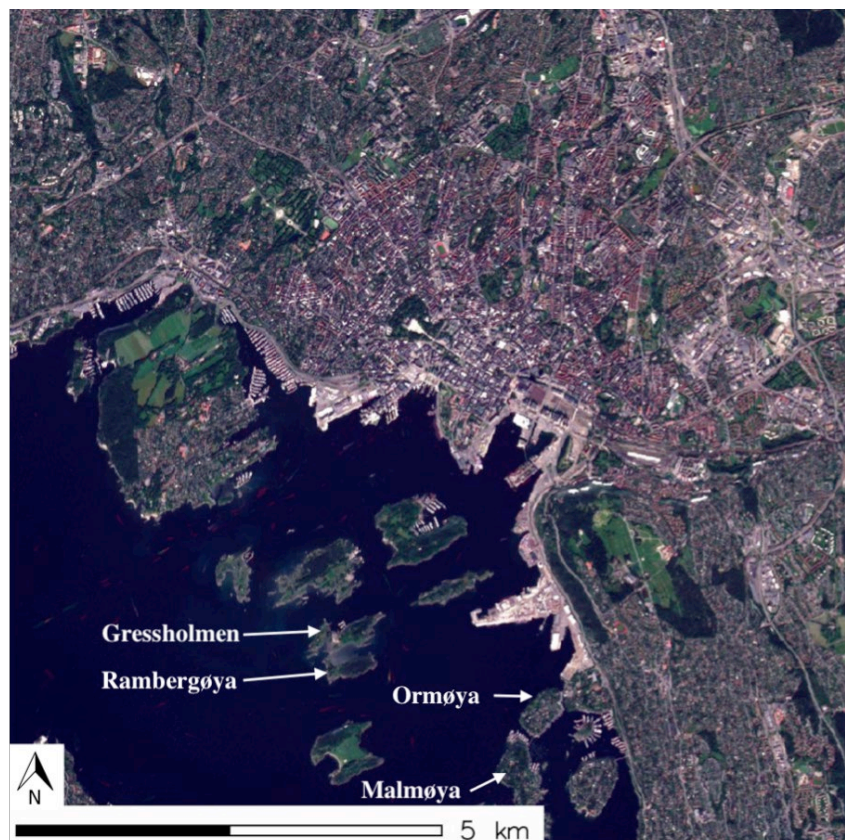


**Figure 6** Sentinel-2 RGB image from Oslofjord case study site with the islands Gressholmen, Rambergøya, Ormøya and Malmøya.
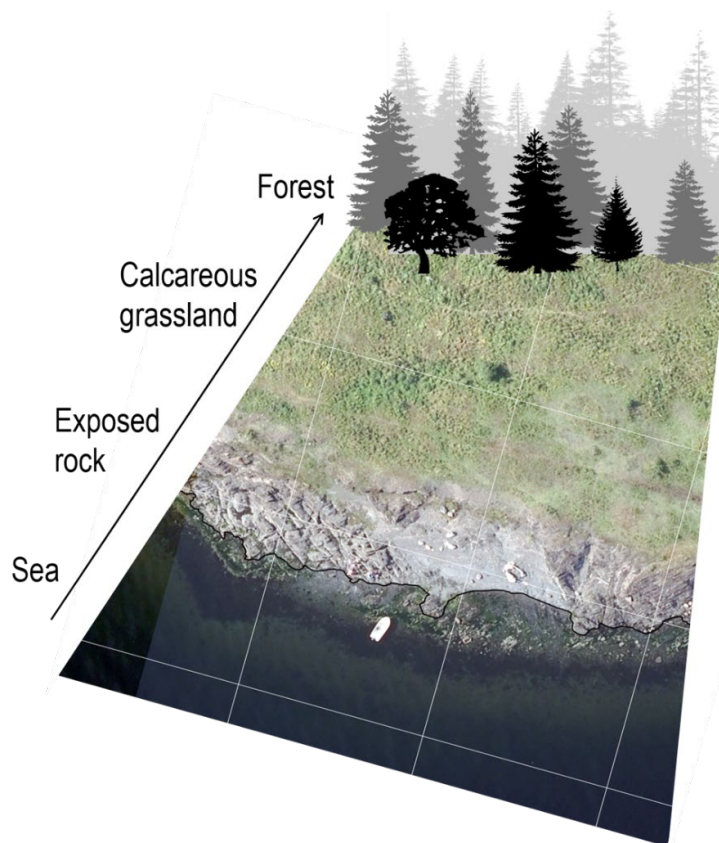
**Figure 7** *Example of a vegetation sequence in the Oslofjord case study, representing succession from unvegetated gravel, through sparsely vegetated calcareous grassland and further stages of succession to forest.*

## 4.2 Lurøykalven

Located in western Norway, Lurøykalven is an island about 50 km north-west of Bergen (60° 42'N 5° 4'E) (see **Figure 8** and **Figure 9**). The study site consists of coastal lowlands with a hilly terrain. The island has an oceanic climate and contains the prioritized nature type coastal heathland, that is threatened by forest re-growth/expansion. Conservation measures are applied to maintain these open cultural landscapes. The average annual temperature ranges from 1.3 to 5.3°C with rainfall falling predominantly in autumn. Lurøykalven has very little human infrastructure. Main topic to be studied in Lurøykalven is the gradient "Tree canopy cover". In this context the usefulness of data fusion and scale effects are important aspects in the small-scale vegetation mosaic in Lurøykalven.



**Figure 8** *Landscape at Lurøykalven (Photo: Vegar Bakkestuen)*
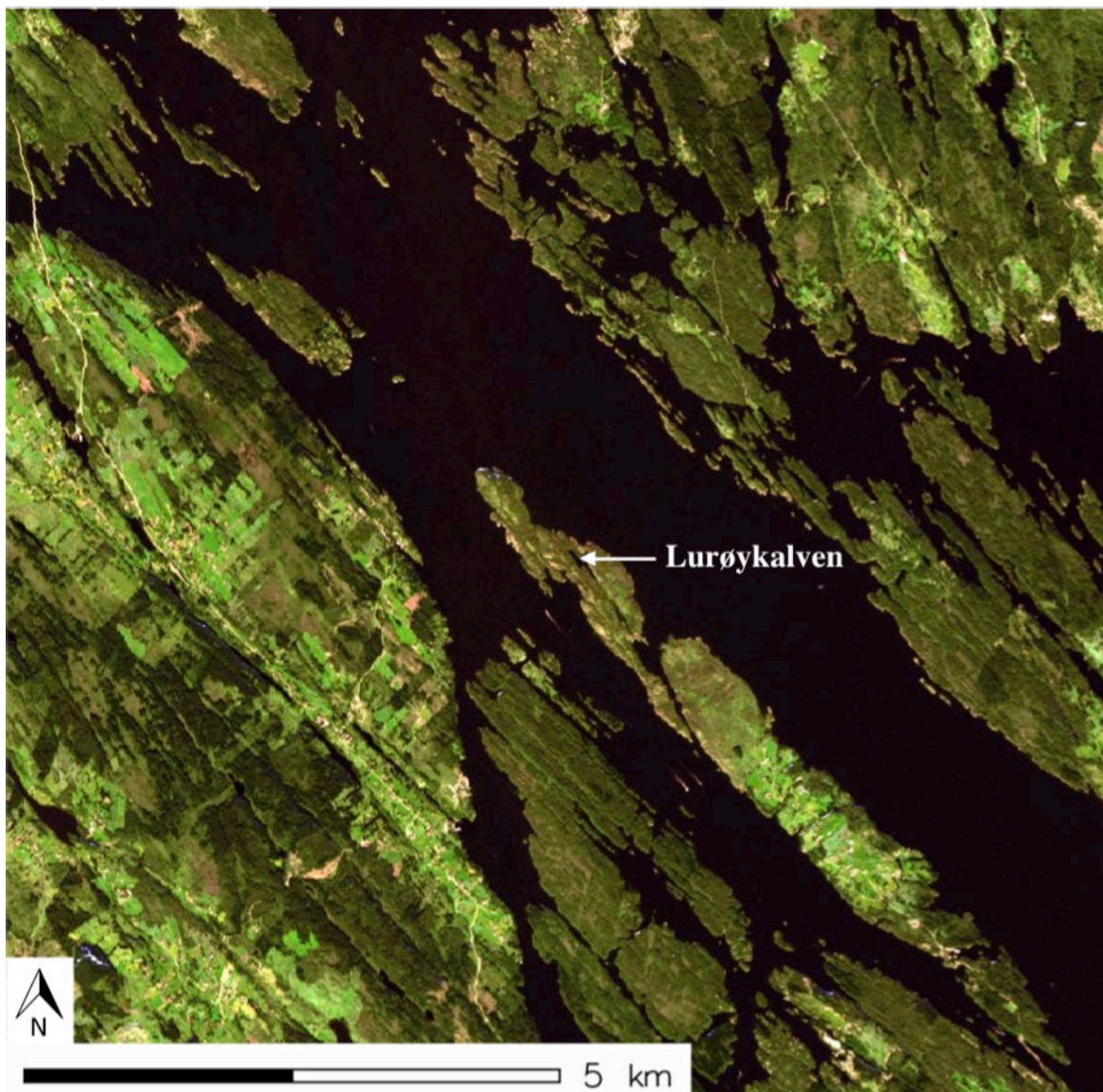
*Figure 9 Sentinel-2 RGB image from Lurøykalven case study site*

## 4.3 Hjerkinn

The study area Hjerkinn is located in the Norwegian mountain region Dovrefjell (62° 13'N, 9° 27'E), between 1000 and 1500 m above sea level (**Figure 10**). It represents a mountain area in the central to eastern parts of Norway, with relatively continental climate. The study site includes boreal to mainly low alpine vegetation zones. The landscape has mountainous terrain, characterized by small-scale patterns with shrub, lichen, mire or tree dominated habitats as well as gravel, bare rock and human infrastructure. NINA has many on-going research activities in the area - including long-term monitoring and restoration projects – making it a natural candidate as a case study site for developing and evaluating remote sensing methodologies.
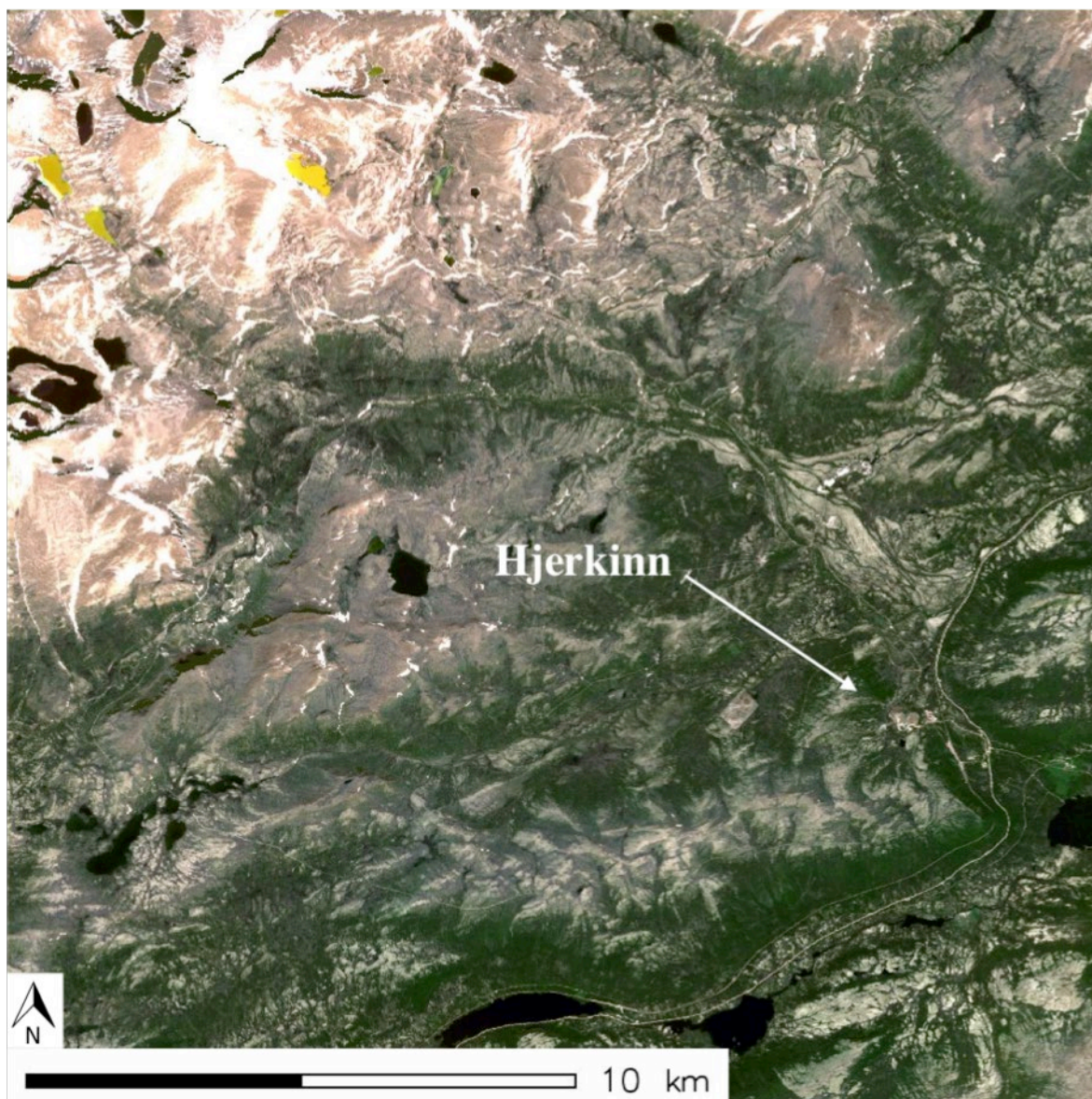
*Figure 10* Sentinel-2 RGB image from Hjerkinn case study site

Most of Hjerkinn's area is located above and around the forest line. **Figure 11** shows the typical landscape at the study site during melting season. The image was acquired on May 19 2013, and shows that the ridge vegetation was becoming visible, but there were still large areas covered with snow. Topics to be studied at Hjerkinn are both the "Tree canopy cover" gradient and the gradient "Reduced growing-season due to prolonged snow-lie".
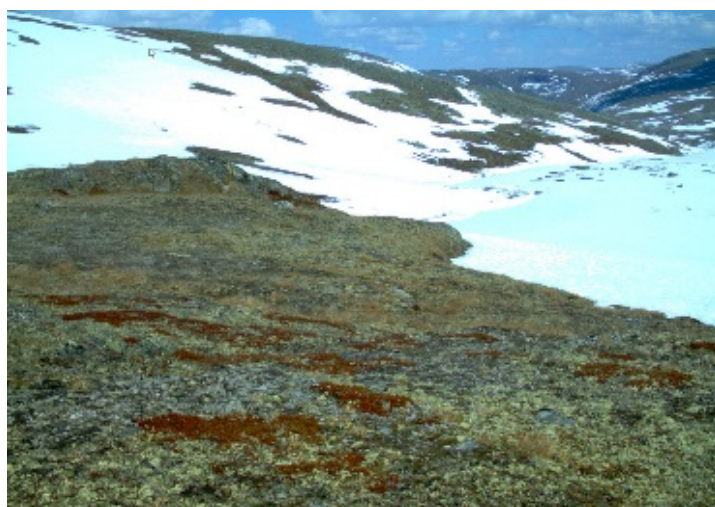


*Figure 11* Landscape at Hjerkinn (Photo: Lars Erikstad)

## 4.4 Sunndalen

The study area Sunndalen is, like Hjerkinn, a mountain area in the Dovrefjell region (62° 34'N 9° 2'E) (see **Figure 12**). It covers boreal to alpine climate zones, but the terrain is steeper compared to Hjerkinn, with deep valleys. Being in central Norway, the climate is relatively continental. A reason for choosing Sunndalen as a case study was to establish a link to the project ECOFUNC, funded by the Norwegian research council (RCN grant MILJØ2015, project number: 244557), where the products from the Sentinel4Nature project will be evaluated with respect to their benefits for understanding mountain ecosystems and their changes.

The topic to be studied in Sunndalen is the "Tree canopy cover" gradient, with a special focus on the forest-tundra ecotone dynamics.
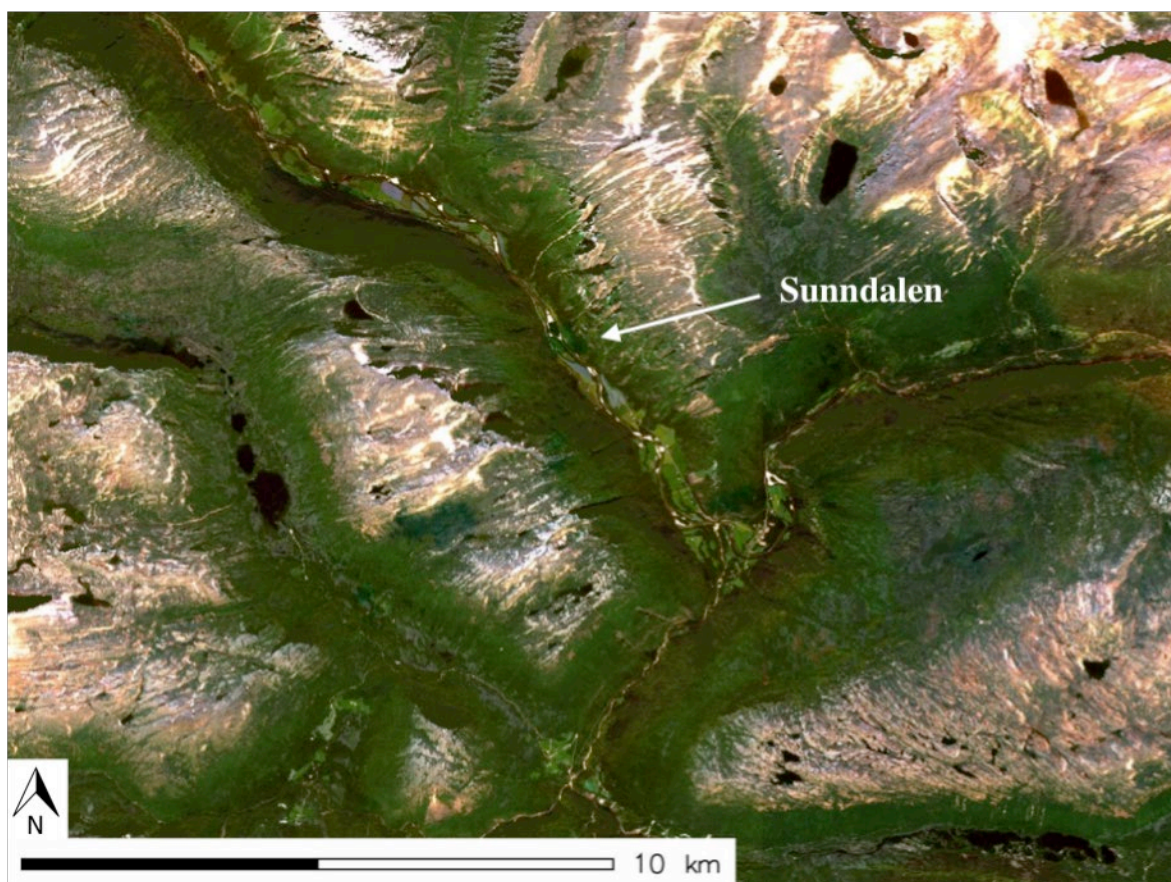


**Figure 12** *Sentinel-2 RGB image from Sunndalen case study site*

# 5 Data fusion for improved estimation of environmental gradients from remote sensing data

A key component of the Sentinel4Nature project is to connect Sentinel data with other geospatial datasets such as aerial images, terrain models and indices derived from them as well as thematic maps by means of data fusion (Salberg et al. 2013, Ichter et al. 2014). This requires adjusting differently gridded data against each other.

Although it "can significantly improve our ability to assess the distribution as well as the horizontal and vertical structure of ecosystems", image fusion has until recently been applied only to a very limited degree in ecological applications (Schulte to Bühne & Pettorelli 2018). Therefore, the Sentinel4Nature project set out to evaluate four different approaches to data fusion:

1. Aggregation: combining high-resolution data (such as orthophotos or terrain models derived from LiDAR) with coarser satellite data.
2. Sharpening: combining lower resolution with higher resolution data by means of resampling to reduced pixel size
3. Merging: a combination of the two approaches above which meets at an intermediate resolution
4. Object-oriented data fusion: Another approach to data fusion is to merge characteristics of data with different resolution in image objects which were derived by segmentation of high-resolution raster data.

A special focus is put on the object-oriented data fusion technique. The hypothesis is that the use of spatial structures ("image objects") acquired from a segmentation of relevant (higher resolution) data layers will lead to a more realistic geographical representation of environmental patterns. The use of such segments, as well as grids with different resolution, allows for several aggregation techniques, e.g. based on variance or average or similar statistics, which may be utilized for improved analysis (Blaschke 2010).

In order to identify suitable data fusion strategies, technical and methodological aspects are relevant, such as the trade-off between spatial and spectral resolutions (He et al. 2011), the amount of data to process and the availability and more or less unbiased coverage (regarding space, time and content) of especially the high resolution data. In addition, characteristics of the spatial pattern to be observed (e.g. size and shape of terrain structures which govern the small-scale snow pattern) are important in these regards.

Unfortunately, Schulte to Bühne & Pettorelli (2018) find that
- the lack of reported reasons for decisions regarding data fusion in existing studies together with
- difficulties to report all data analysis steps to a reproducible level of detail make it hard to learn from existing experience.

What ancillary data (e.g. terrain indices) is suitable to fuse with different satellite data depends very much on the individual objective, here the environmental gradient in question. The same applies to decisions on what sensors - with possibly different resolution - that are relevant to combine in order to improve modelling results, The tree canopy cover gradient (chapter 6.2), for example, is much less affected by terrain structure compared to the gradient on reduced growing-season due to prolonged snow-lie (chapter 6.1).

Therefore, data fusion strategies are discussed in respective chapters for modelling the two selected case study gradients.

# 6 Modelling environmental gradients and properties in space and time in a data fusion setting

For the two environmental gradients selected as cases from the total of 61 environmental gradients in NiN, remote sensing and spatial data was pre-processed, models were developed, validated and refined. This data processing, model development and refinement was carried out in an iterative process, whose results are documented in this chapter. Data produced in this project can be accessed here: http://geodata.nina.no/search/?title__icontains=Sentinel4Nature

## 6.1 Develop, evaluate and refine a model for Reduced growing-season due to prolonged snow-lie (SV, NiN 2.0)

Contrary to the Landsat based schemes proposed by Crawford et al. (2013) and Maher et al. (2012), the aim in the Sentinel4Nature project is to derive satellite-based maps that describe the spatial distribution of the date of snow melt, with corresponding uncertainties. The date of snow melt defines usually the start of the growing season in Norwegian mountains and thus corresponds to named environmental gradient.

### 6.1.1 Data preparation and data fusion
Snow-covered areas are often easy to identify in optical satellite images. However, there are many factors that may influence the performance of an automatic system for monitoring the spatial snow cover distribution. These include:
- *Spatial resolution*: For low and medium resolution images, it is often a snow cover fraction that is estimated, since the area of the pixel unit is not completely snow covered (Metsamaki et al. 2014).
- *Band configuration*: Some sensors have thermal bands or bands that are sensitive to cirrus clouds (e.g. Landsat-8 and Sentinel-2). Use of data from these bands will often improve the performance with respect to distinguishing snow from clouds (Zhu & Woodcock 2012).
- *Temporal resolution*: In order to estimate date of snow melt, satellite data with high temporal resolution is needed. The estimation of snow cover stability may be particularly challenging since this requires monitoring of the snow cover during the full winter season when there is limited daylight. For areas in the far north, this is almost impossible using optical satellite data.
- *Land cover*: Some vegetation types can mislead the recognition of snow-covered areas. For example, lichen rich ridge vegetation have a very high albedo and may therefore be confused with snow.

Some ancillary information may be used to improve the performance:
- *Other sensors*: Synthetic-aperture radar (SAR) is suitable for identifying wet snow (Nagler & Rott 2000), and Sentinel-1 may therefore be used in the melting season to locate snow patches. A major benefit with SAR is that it penetrates clouds. However, a major drawback is that dry snow cannot be detected with C-band SAR since the radar signals penetrates dry snow. Hence, we cannot reliably distinguish dry snow from bare ground.
- *Precise elevation model*: Altitude indices like topographic position index (TPI), insolation, slope, or aspect may be used to improve the identification of snow-beds.
- *History*: If previous snow cover distribution maps are available, these may be used as prior information on where snow-beds and areas with less snow cover stability are located.

However, in this project the model for the date of snow melt has been developed without the two latter auxiliary data types and is only based on a time series of satellite imagery. The resulting pure remote sensing product is then evaluated with regards to possible contributions of terrain

information (chapter 6.1.5). The method proposed makes use of Landsat-8 images as the primary source of data for estimating the probability for snow cover in each pixel at a given day of the year. The reason for selecting Landsat-8 over Sentinel-2 was mainly related to the availability of data at the start of the project, and that Landsat-8 has thermal channels that provide valuable information for separating clouds from snow. However, provided that a good cloud-masking algorithm is available, Sentinel-2 should also be used.

Even when all available imagery since the Landsat-8 satellite that was put into service in 2013 is being used; the number of cloud-free observations is still limited. To gain more observations, data from the Sentinel-1 satellites is added to the available optical images from Landsat-8. Sentinel-1 provides data from a synthetic aperture radar (SAR) sensor. As SAR is not affected by cloud cover, gaps in the Landsat-8 time series may be filled. SAR sensors are not sensitive to snow in general, as electromagnetic waves penetrate the surface when the snow is dry. On the other hand, SARs operating at C-band frequencies are sensitive to wet snow due to the presence of liquid water (Rott & Matzler, 1987) and have been used to estimate snow cover in mountain areas, such as the Himalayas (Thakur et al. 2013).

The data from the Sentinel-1 satellite can therefore only provide positive observations of the presence of wet snow, whereas the non-presence of wet snow cannot always be treated as a snow free observation. However, detections of wet snow are of particular importance in this study as they provide valuable observations at a point in time close to the snow melting day.

The data fusion consists of projecting all satellite data to the same spatial grid, detecting if a given pixel is snow covered, and adding snow maps from each time-instant (and sensor) to the time series. Hence, the processing chain may easily be extended with new sensor data, as long as they provide estimate of the snow extent. Details about the algorithm is described in the next chapter.

## 6.1.2 Model development

Landsat satellites have a revisiting frequency of 16 days, which leads to a limited temporal resolution when estimating the date of snow melt for a given year. Taking cloud conditions into account, there may potentially be prolonged periods where no clear observations are available during the critical snow melting season. For this reason, data from multiple years must be aggregated. The challenge is then to combine the temporal profile of several melting seasons, as the annual variation in snow conditions may vary greatly. At a particular year, there might be less precipitation and the snow melt starts early, whereas for another year, conditions may be colder and more snow rich, thus the melting begins very late. To address the variation over different melting seasons, we propose to model the snow cover at a given location, or pixel in the satellite image, using a binomial distribution. The binomial distribution reflects the two conditions where snow is present or not. The probability of snow at a given time is estimated by means of a generalized linear model (GLM).

The proposed methodology consists of the following steps:

1. **Preprocessing of Landsat-8 images**: The available Landsat images were converted to Top of the Atmosphere (TOA) reflectance images using the corresponding metadata. From the metadata, also the annual day number (Julian day) was extracted and an image stack sorted after the relative day number rather than acquisition date, was created. Clouds were detected by classifying each Landsat pixel into the following classes: Clouds, snow, green vegetation, brown land cover, and water (Salberg 2011). Masks were created to filter out water and clouds from the image stack. Cloud shadows and terrain shadows often cause problems when analysing optical data. By using information about the sun elevation angle and terrain topography, cloud shadows and terrain shadows could be estimated (Salberg 2011). However, in this analysis, removal of cloud shadows was not considered necessary.

2. ***Preprocessing of Sentinel-1 SAR images***: To correct the SAR imagery for terrain variation and systematic influences on the radiometry, the flattening gamma terrain correction method (Small 2011) was applied.

3. ***Snow detection***: For the Landsat-8 images, the normalized difference snow index (NDSI) was used to identify snow cover. The NDSI takes advantage of the information in the green and SWIR wavelength bands and was calculated for each image pixel not identified as cloud or open water by

$$NDSI = \frac{B_2 - B_5}{B_2 + B_5}$$

Here $B_k$ denotes Landsat band k of the TOA reflectance image. Pixels satisfying $NDSI > 0.6$ were identified as snow covered, thus indicating only high confidence detections (Zhu & Woodcock 2012).

Changes in the backscatter coefficient were used to detect wet snow in the SAR images. The SAR difference images created during the pre-processing steps were compared against a fixed threshold set at 4dB. Dark areas (lower than the threshold) were identified as covered with wet snow.

4. ***Estimation of the snow cover probability***: Both Landsat-8 and SAR images from Sentinel-1 were merged into a common image stack ordered according to the Julian day, after subsetting the images to only include the overlapping area covered by both image types.

For each pixel at a given location, a set of snow cover observations $y_1, y_2, ..., y_N$ were available. The value of $y_k$ was set to 1 if the respective pixel in the corresponding image was snow covered, thus indicating positive snow detections. For the Landsat-8 images, pixels without snow cover were set to $y_k=0$, as these pixels indicate a positive detection of an area without snow. This is not true for the SAR images, and pixels that did not indicate wet snow were filtered out, due to the fact that non-presence of wet snow cannot be interpreted as an observation of an area without snow.

Alongside the image stack, a set of corresponding time instants $t_1, t_2, ..., t_N$ were available, ordered according to the day in the year they were acquired, ensuring that $t_{k+1} \geq t_k$. Please note that since the images may have been acquired from different years such that $y_{k+1}$ may be equal 1 even if $y_k$ is equal to 0. Assuming that the day of snow melt happens later in the year than January 1st, all pixels were defined as snow covered on this day, thus ensuring stability in the estimate. In normal years, this is a reasonable assumption for mountain regions in Northern Europe.

For every pixel in the image stack, the probability for snow was estimated using a GLM with binomial distribution and logit link function. The probability for snow for time instant k can be written as

$$p_k = \text{logit}^{-1}(\eta_k) = \frac{\exp(\eta_k)}{1 + \exp(\eta_k)},$$

where $\eta_k = a_0 + a_1 t_k$. The parameters $a_0$ and $a_1$ were estimated from the snow cover observations $y_1, y_2, ..., y_N$ and corresponding time instants $t_1, t_2, ..., t_N$ using an iterative re-weighted linear regression algorithm (McCullagh & Nelder, 1989).

Note that the binomial distribution also applies if there are multiple observations on the same Julian day (from different years) in the stack. In this case, we simply change the

number of trials $n_i$ to the number of observations and $y_i$ to the sum of snow covered observations on that day.

To handle the data separation problem we have used a Bayesian GLM approach, where the parameters $a_0$ and $a_1$ are modelled as Cauchy distributed variables with mean values equal to 0 and -5.0, respectively, and scale parameters equal to 10.0 and 4.0 (Gelman et al. 2008).

5. **_Estimation of the date for snow melt_**: The date for snow melt cover is estimated as the time instant where the probability of snow is less than a given threshold. Here, this threshold was set to $p_{th} = 25\%$. The date for snow melt may then be estimated as

$$t_{melt} = \frac{\left(\log\left(\frac{p_{th}}{1-p_{th}}\right) - \widehat{a}_0\right)}{\widehat{a}_1}.$$

6. **_Estimation of uncertainty_**: Since the GLM is based on an iterative re-weighted linear regression, one may estimate the uncertainty to $\widehat{a}_0$ and $\widehat{a}_1$. A 90% confidence interval to $t_{melt}$ may then be written as

$$t^u_{melt} = \frac{\left(\log\left(\frac{p_{th}}{1-p_{th}}\right) - \widehat{a}_0 + 1.645\sigma\right)}{\widehat{a}_1}$$

$$t^l_{melt} = \frac{\left(\log\left(\frac{p_{th}}{1-p_{th}}\right) - \widehat{a}_0 - 1.645\sigma\right)}{\widehat{a}_1},$$

where

$$\sigma^2 = \text{var}(\widehat{a}_0) + \text{var}(\widehat{a}_1)t^2_{melt} + \text{cov}(\widehat{a}_0, \widehat{a}_1)t_{melt}.$$

The uncertainty of the date for snow melt is then defined to be: $(t^u_{melt} - t^l_{melt})/2$.

## 6.1.3 Validation data

In contrast to the tree canopy cover gradient (see chapter 6.2.2), in-situ data is not a hard requirement for training/developing the model on reduced growing-season due to prolonged snow-lie because of the clear, and known reflectance pattern of snow in satellite imagery. However, the high spatio-temporal resolution and variation that this model is based on, is particularly challenging regarding the collection of appropriate validation data because the latter has to be able to capture this spatio-temporal variation. For evaluation the following data sources were selected:

- Surface temperature data from temperature loggers
- Species occurrence data from the Global Biodiversity Information Facility (GBIF)
- Vegetation plot data collected with regards to snow cover duration (Evju et al. 2012)

In the Sentinel4Nature project the possibility to use orthorectified images from time-lapsed wildlife camera traps for validation was also explored and tested. Due to technical and administrative challenges, this approach could not be developed into a production-ready protocol within the project time frame. This development is therefore covered in a separate report (Blumentrath et al. 2018).

### 6.1.3.1  Surface temperature data from temperature loggers

It is possible to detect snow cover periods in data series from temperature and moisture loggers that are placed on the ground. When a temperature logger is covered by snow, the temperature and moisture measures stabilize, and their variation over a 24-hour period drops compared to the situation where there is no snow. Therefore, snow-covered periods can be identified in the temperature logger data by the low variation in temperature per day at or below 0 degrees Celsius under snow cover (see **Figure 13**).

From other projects conducted in NINA (Eide 2017), temperature logger data were obtained for the Hjerkinn case study site. The loggers were placed along altitudinal gradients (amongst others) directly on the ground and cover the years 2010 - 2016. They were programmed to monitor the temperature at a two hours interval. This makes them particularly suitable for the detection of date of snow melt.
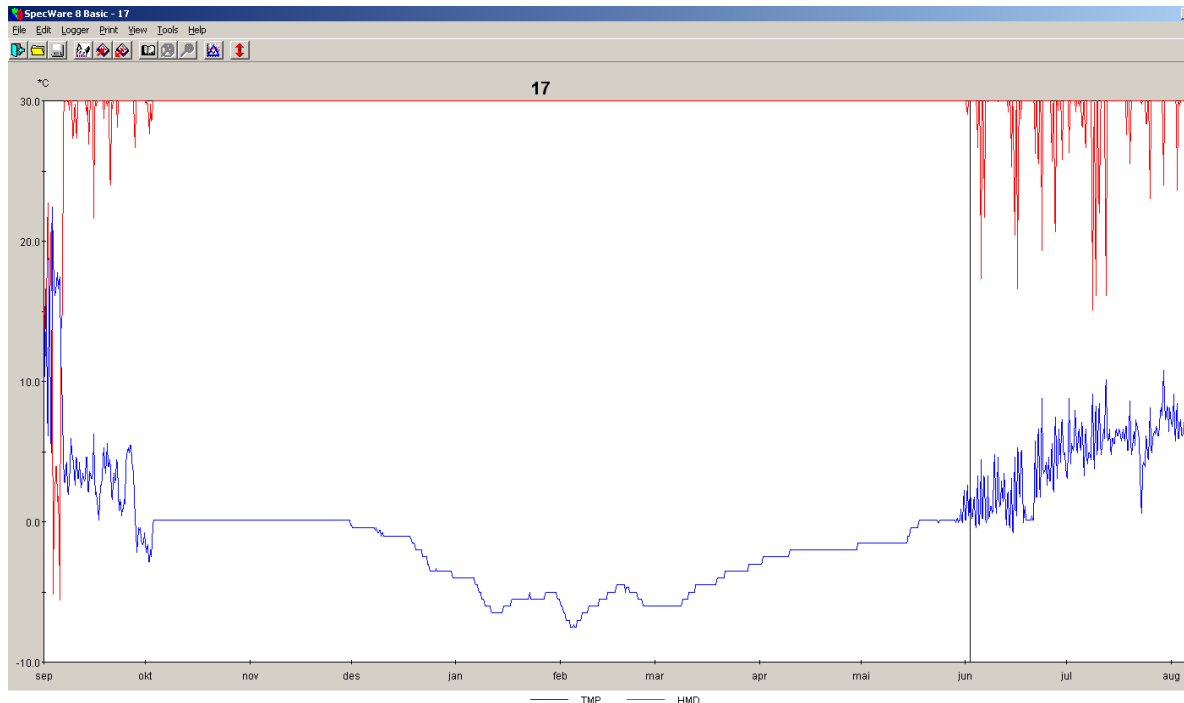


*Figure 13* *Plot of temperature logger data (Eide 2017) from September (left) to August (right). The temperature logger data can be used to measure snow melt. The red line represents moisture, while the blue line is the temperature. The period with low variation of temperature and moisture in the centre of the plot (October to June) indicates that the logger is covered by snow.*

Temperature and moisture logger data represent a means to evaluate the accuracy of the model regarding the physical snow cover condition. They also provide indications of a variability of the snow cover between years. Given that the model is based on aggregated data across years, model accuracy is to be judged within this natural variation.

For verification purposes of the estimated day of snow melt, available temperature loggers from Eide (2017) were used to confirm the presence or non-presence of snow. From the raw logger measurements, the number of temperature registrations and the average temperature per day were computed. In addition, the minimum and maximum temperature, as well as the standard deviation and variance of the temperature during each 24-hour period were calculated.

Days with snow cover were identified by setting a threshold to the daily variation and the maximum logged temperature. Here, a day showing a maximum temperature less than 1℃, and a temperature variance less than 1℃ was classified as snow covered. All other days were identified as no-snow measurements.

### 6.1.3.2   Species occurrence data from the Global Biodiversity Information Facility (GBIF)
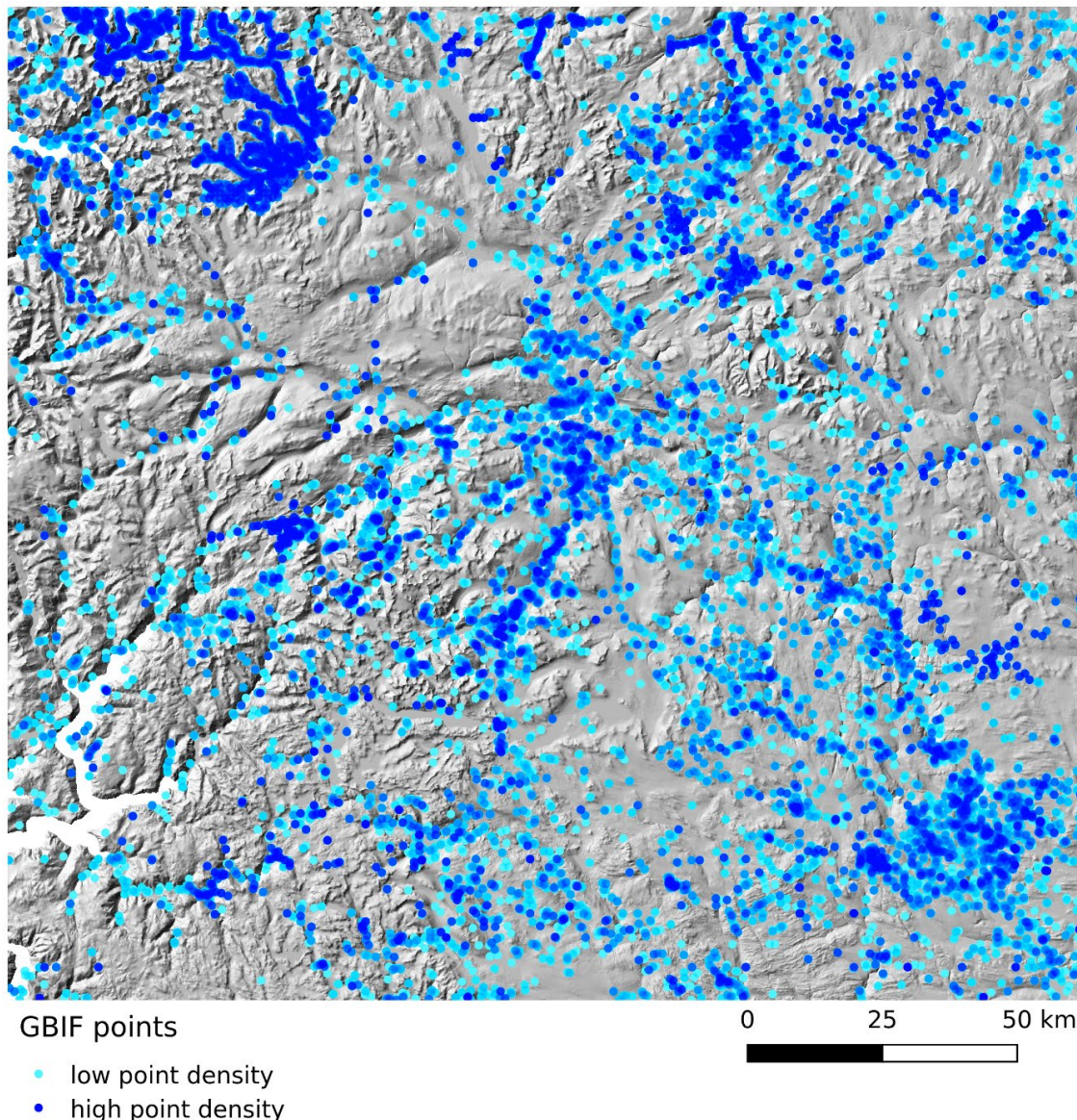Another means of evaluating the model on reduced growing-season due to prolonged snow-lie is using a bio-indicator approach. From studies by Odland & Munkejord (2008) the sensitivity to

snow cover conditions is known for a list of ca. 100 vascular plant species. For those species, ca. 160,000 geo-located occurrence records were fetched from the Global Biodiversity Information Facility (GBIF) for the Hjerkinn case study site (**Figure 14**) using the *v.in.pygbif* module in GRASS GIS (Blumentrath & Kudrnovsky 2016). These records were then assigned with the snow indicator value developed by Odland & Munkejord (2008) at a scale from 0 to 9, where 0 represents chionophobic plants, meaning plants with little tolerance to snow cover, and 9 represents chionophilic plants which are able to tolerate longer duration of snow cover and thus have a competitive advantage at places with long-lasting snow cover. Odland & Munkejord's (2008) Snow Index was also a major source for the definition of the respective gradient in the Nature in Norway (NiN) system[1].

The linkages between the physical snow cover (as expressed by the model) and the distribution of vegetation patterns represent the core of the NiN system with regards to this gradient. In the model evaluation, these linkages are explored both visually by plotting the data and an ordinal regression analysis. The ordinal regression is also used to compare model versions developed in the project and to track model improvements. Finally, ordinal regression using the species occurrence data is used to assess how much the satellite remote sensing-based model improves our ability to represent the snow cover gradient compared to an alternative model using only terrain data.

---

[1] https://artsdatabanken.no/Pages/179767 (in Norwegian)

GBIF points

- low point density
- high point density

*Figure 14 Occurrences of species with known sensitivity to snow cover at the Hjerkinn case study site (colours indicate number of occurrences at a location – light blue: low number of occurrences to dark blue: high number of occurrences)*

### 6.1.3.3 Vegetation plot data collected with regards to snow cover duration

Within the area of the case study site at Hjerkinn, Evju et al. (2012) collected data on frequency of plant species within vegetation plots along the snow cover gradient from unstable snow cover (ridge, "rabbe") through sheltered areas with relatively constant snow cover ("leeside") to areas with prolonged snow cover (snow bed, "snøleie") (see **Figure 15**). These data were assigned with the estimated day of snowmelt from the model on reduced growing-season due to prolonged snow-lie.

The species found in the plots were classified with regards to their sensitivity to snow cover both using Odland & Munkejord (2008) (similar to GBIF data in chapter 6.1.3.2) and expert judgement (Olsen 2017). The relatively low number of observations in this dataset limits the possibilities to analyse it statistically. Relations between modelled day of snow melt and vegetation pattern, are only plotted and interpreted visually.
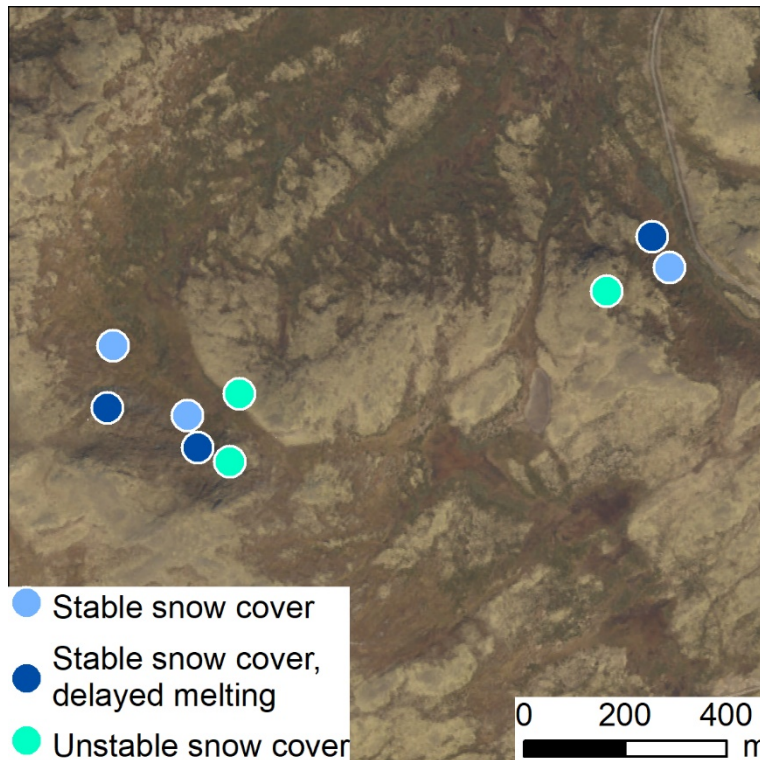
*Figure 15* Vegetation plot data collected with regards to snow cover duration (Evju et al.2012)

### 6.1.4 Results

The dates for snow melt and corresponding uncertainty were estimated from Landsat 8 images at path/row 199/017. All available images of this area since the launch of the satellite in 2013 until 2017 were considered for this study. Images taken later in the year than day 238 (corresponding to August 26th) were not used, as this day is close to when the melting season ends and new snow fall may be expected. The total image count over the four years of satellite data was 42 images to be used in the study.

Sentinel-1 data from the 2015 season were applied, and 31 scenes overlapping with the chosen study area in the melting period between the days 60 and 206 (corresponding to March 1st and July 25th) were cropped to fit the Landsat 8 images and included in the study. **Figure 16** shows the selected study area as well as detailed close up examples of Sentinel-1 and Landsat 8 images.
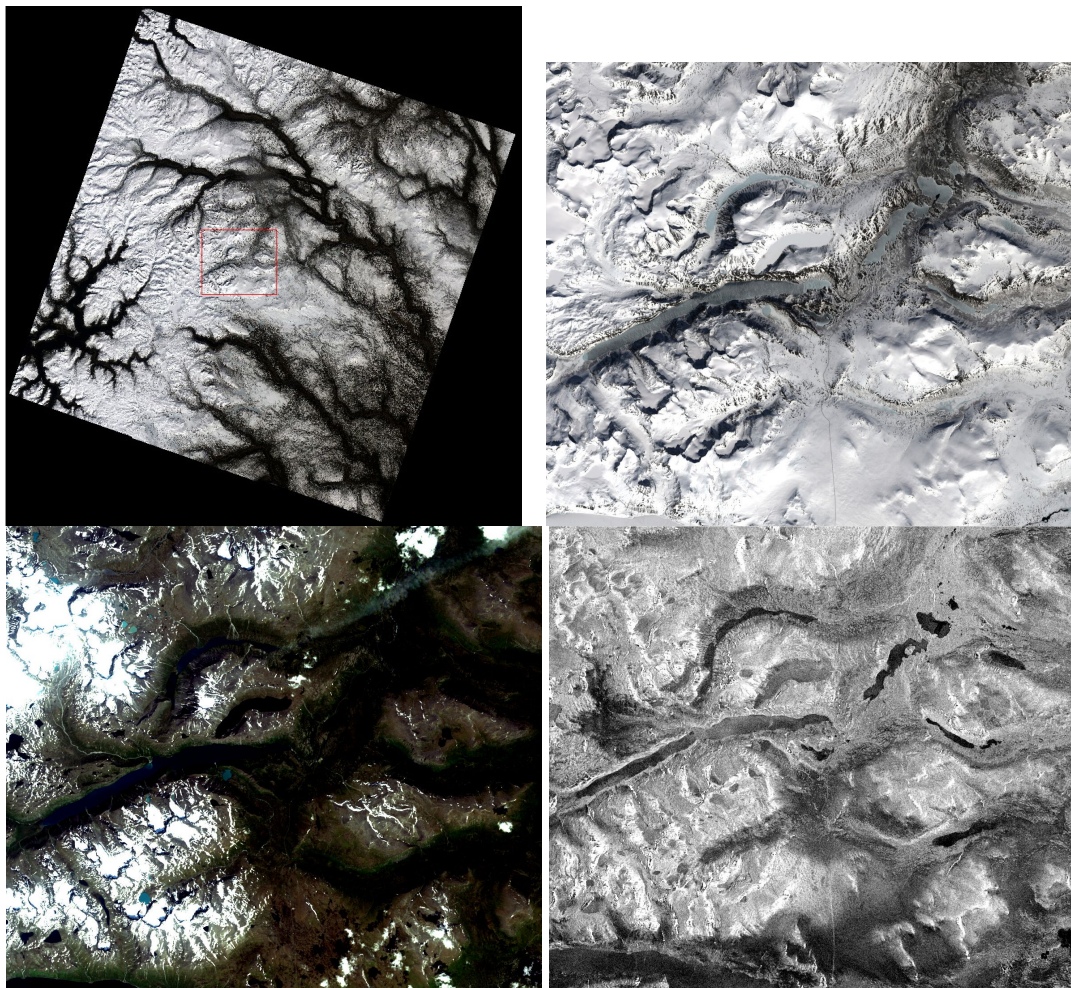
**Figure 16** *The study scene from Dovrefjell and examples of images from Landsat-8 and Sentinel-1. Top left: The study scene with example area marked with a red square. Top right: Landsat-8 RGB image of example area from Day 110 (April 20th 2015). Bottom left: Landsat-8 RGB image of example area from Day 200 (July 19thth 2013). Bottom right: Sentinel-1 SAR synthetic image from Day 132 (May 12th 2015)*

Using the proposed GLM based methodology, we generated a continuous map with Landsat resolution (30 m) of the estimated dates for snow melt. The spatial variation of the estimated dates for snow melt was huge for the study area, with a mean value equal to 125.3 and standard deviation equal to 59.3 (**Figure 17**). The GLM methodology allows to produce a corresponding uncertainty map. The estimated uncertainties were for some areas large and varied substantially across the area (**Figure 17**).

A similar spatial pattern for the dates of snow melt was observed when using both Landsat-8 and Sentinel-1 (**Figure 18**). However, compared to using only Landsat-8 data, the average mean value has increased to day 152.2, with a standard deviation of 45.3.
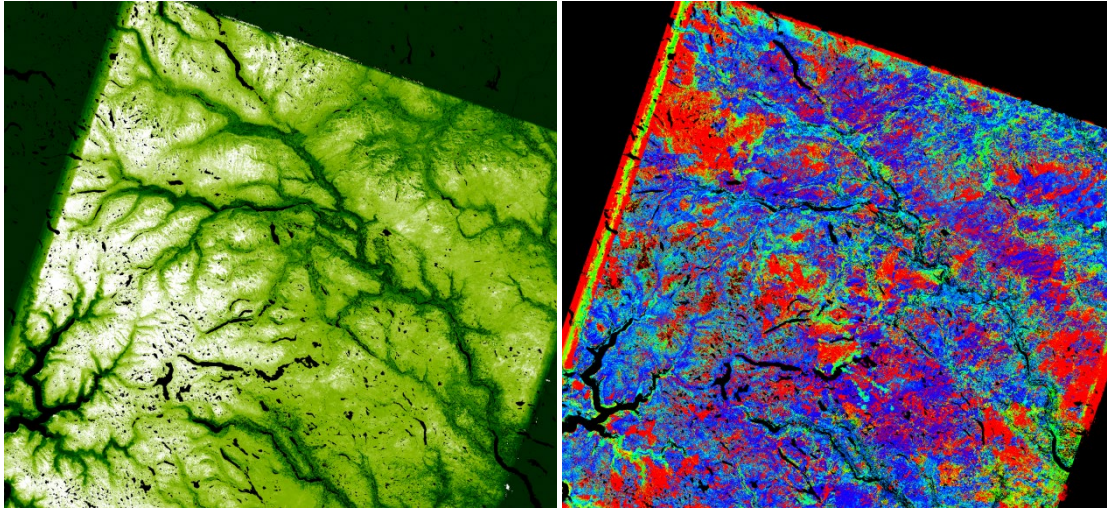
**Figure 17** *The estimated dates for snow melt (left image) and corresponding uncertainties esti-mates (right image) for the study area based on Landsat-8. Left image: For the dates of snow melt image the colour scale corresponds to day number, from day 1 (dark green) to day 220 (white). Right image: The black areas in the image corresponds to no data e.g. masked water bodies. For the estimated uncertainties image the rainbow colour scale corresponds to the de-gree of uncertainty (90% confidence interval, from 0 (yellow) via green and blue to 100 days (red)).*
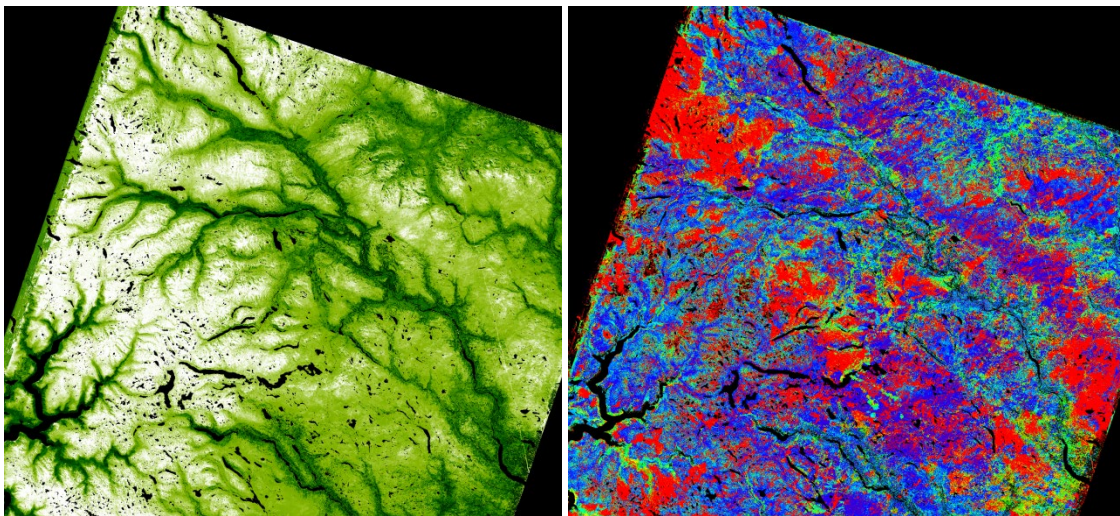


**Figure 18** *The estimated dates of snow melt cover (left image) and corresponding uncertain-ties estimates (right image) for the study area based on Landsat-8 and Sentinel-1. Left image: The dates of snow melt image the colour scale corresponds to day number, from day 1 (dark green) to day 238 (white). Right image: The black areas in the image corresponds to no data e.g. masked water bodies. For the estimated uncertainties image the rainbow colour scale cor-responds to the degree of uncertainty (90% confidence interval, from 0 (black) via green and blue to 100 days (red)).*

## 6.1.5 Evaluation

### 6.1.5.1   Surface temperature data from temperature loggers

For evaluation of the final developed model based on Landsat8 and Sentinel-1 data. results were compared to temperature logger measurements (see chapter 6.1.3.1). For the pixels at the log-ger locations, the model, the underlying satellite data and the temperature measurements were

combined in a plot over a time axisis (**Figure 19**). For all the panels in **Figure 19**, except one, the overall uncertainty was about ±25 days over the period from 2013 to 2017. For the location with higher uncertainty (snow cover probability for row 890, col 4016) the uncertainty was about ±50 days. The higher uncertainty was, most likely, caused by a false SAR snow detection in the summer period. For this location we also observe that the temperature loggers indicate an unstable snow cover, with many snow free days during the winter.
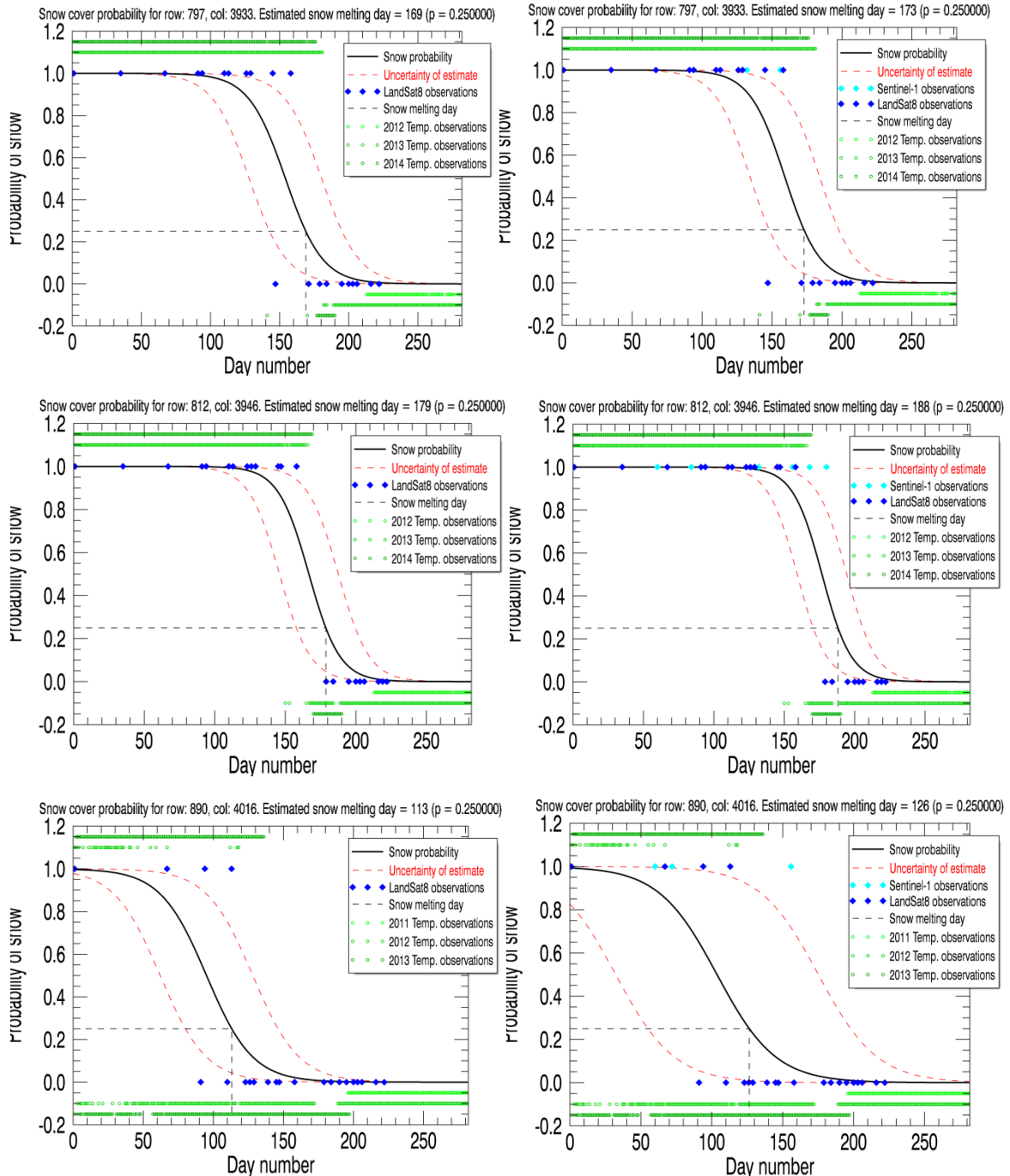


*Figure 19* *Probability for snow as a function of day-number (black curve), with corresponding confidence interval (red curves). The left curves correspond to Landsat-8 observation only, whereas the right curves correspond to Landsat-8 and Sentinel-1 observations. The snow observations (blue circles) and estimated probability (using the GLM based methodology) for snow (black line), with corresponding 90% uncertainty confidence interval (red lines) for four different locations (pixels). The black dashed lines show the estimated date of snow melt (using a 25% probability threshold).*

The probability curves shown in **Figure 19**, and a number of curves corresponding to other locations (not shown here), show that the date for snow melt is later when it is estimated using both Landsat-8 and Sentinel-1, compared to when only Landsat8 data is used.

### 6.1.5.2 Species occurrence data from the Global Biodiversity Information Facility (GBIF)

The following plots (**Figure 20** and **Figure 21**) visualise the frequency at which plants of the different snow tolerance classes were found at locations with different estimated days of snow melt in the model. In general, the plots show that the developed model corresponds with the occurrence of snow sensitive species as plant species with a higher snow index are more abundant in locations with a later estimated day of snow melt. In the plots only the most recent records from GBIF (recorded 2010 and later) were used, because these provide the closest temporal match to the satellite imagery used. Inclusion of older records has been tested and their inclusion results in a significant decrease in correlation between snow index classes and the modelled day of snow melt. This can be either due to changes in environmental conditions (e.g. earlier snow melt) or due to less geometric precision in older plant species records from GBIF.

In addition, altitude turned out to have a significant influence on the relation between modelled day of snow melt and occurrence of species with different snow indices. Excluding occurrences records below 1000m altitude (which roughly marks the forest line at Hjerkinn) (**Figure 20**) led to a more stable and continuous increase of relative occurrence of the species with higher snow indices at later estimated days of snow melt, compared to using no filter on altitude (**Figure 21**).
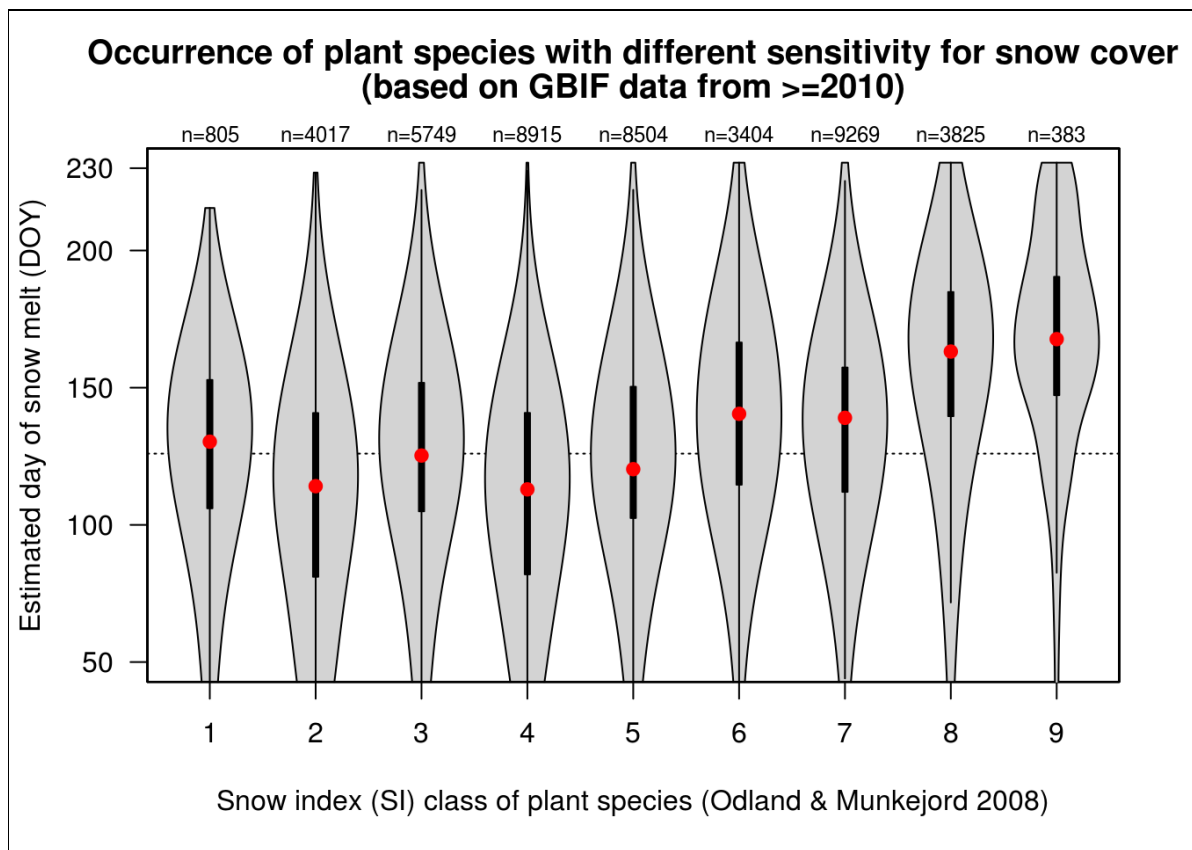


*Figure 20 Violin plot representing the recordings of species with Odland & Munkejord's (2008) Snow Index in GBIF and the modelled day of snowmelt; GBIF data limited to records from after 2010. The thick black bar in the centre represents the interquartile range, the thin black line extended from it represents the 95% confidence intervals, and the red dot is the median.*

A possible explanation for this observation can be that plant species with intermediate snow indices (in contrast to those at the two ends of the snow index scale) often can be found in lowlands and forests. There, the snow generally melts earlier than in the mountains. Furthermore, forest canopy is an obstacle to detecting snow melt on the ground from satellite imagery and limits the models ability to correctly detect the actual day of snow melt on the ground and not the snow melt at the canopy of higher vegetation. This indicates that the model is more robust in the mountain areas, where the snow cover gradient at the same time is of most relevance.
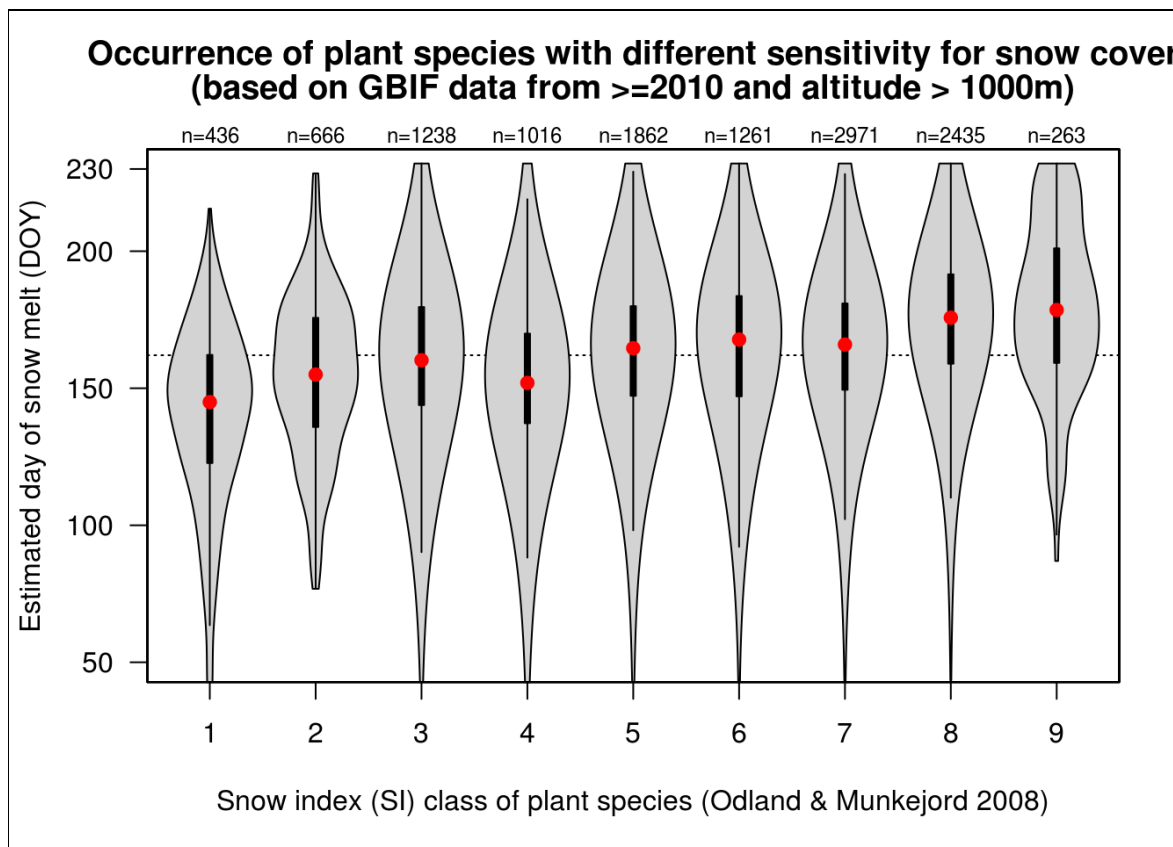


***Figure 21*** *Violin plot representing the recordings of species with Odland & Munkejord's (2008) Snow Index in GBIF and the modelled day of snowmelt; GBIF data limited to records from after 2010 and above 1000m altitude. The thick black bar in the centre represents the interquartile range, the thin black line extended from it represents the 95% confidence intervals, and the red dot is the median.*

The relationship between the snow tolerance of the plants and the estimated day of snow melt has been further analysed using an ordinal regression (CLM). The regression analysis of the data from GBIF shows a highly significant correlation between modelled day of snowmelt and occurrence of snow sensitive species (**Table 1**). Furthermore, the relationship identified by the ordinal regression between the snow index of the occurring plant species and the modelled day of snowmelt at the species location varies significantly across the different snow index classes (per class estimates of the CLM not shown here). Also here the relationship is much more robust and shows much less variation within higher snow index classes, especially compared to intermediate snow index classes. This supports findings from the visual inspection (**Figure 20** and **Figure 21**) that the model performs best in the areas where snow cover is truly prolonged, meaning where snow-bed habitats and plant communities related to them are located. These areas represent the particularly relevant end of the scale for this NiN gradient.

*Table 2 Performance of ordinal regression models explaining snow index of the species occurrences in GBIF filtered by age (records newer than 2010) and altitude in addition (only records above 1000 m), using four versions of the developed remote sensing product (v2016_landsat: version from 2016 with only Landsat8 input, v2016_landsat_s1: version from 2016 with both Landsat8 and Sentinel-1 input, v2018_landsat: version from 2018 with only Landsat8 input, v2018_landsat_s1: version from 2018 with both Landsat8 and Sentinel-1 input)*

| Ordinal regression (clm) | | | |
|---|---|---|---|
| Model | Estimate Std. | Error z value | Pr(>\|z\|) |
| Snow Index ~ snow_model_v2018_landsat_s1 | 0.0125561 | 0.0003073 | <2e-16 *** |
| Snow Index [> 1000m alt.] ~ snow_model_v2018_landsat_s1 | 0.0166524 | 0.0007723 | <2e-16 *** |

**Table 2** shows a comparison of the performance of ordinal regression models that are supposed to explain the relation between the occurrences of plant species that represent different snow index classes and

- the estimated day of snow melt from different versions of the developed remote sensing products
- just auxiliary data, like the digital elevation model and relevant environmental variables derived from those, as well as a
- combination of the two above

Model results show that adding auxiliary terrain data only marginally improves the performance of the latest, pure remote sensing product (v2018_landsat_s1). Gains in explanatory power are mostly provided by land surface temperature during summer (EuroLST_BIO10, Metz, Rocchini & Neteler 2014) and altitude, which also can be seen as a proxy for temperature in this area. Furthermore, the remote sensing products outperform even very complex models without satellite data.

The official, country-wide available terrain model with 10m resolution the tested terrain parameters are based on, is unfortunately usually of relatively limited quality in the Norwegian mountains. Here, standard deviation in altitude is ~ between 4 to 6 meter (Kartverket 2013). This terrain model thus does not very well capture more small-scale terrain structures that can have a significant influence on where snow accumulates or is blown off.

In any case, the model performance comparison suggests that the developed remote sensing product significantly improves our current ability to model spatial patterns of the occurrence of snow-dependent plant species in the Norwegian mountain and that in provides information that is not available in the other tested auxiliary data.

*Table 3 Performance of ordinal regression models explaining snow index of the species occur-rences in GBIF filtered by age (records newer than 2010) and altitude (only records above 1000 m), using four versions of the developed remote sensing product (v2016_landsat: version from 2016 with only Landsat8 input, v2016_landsat_s1: version from 2016 with both Landsat8 and Sentinel-1 input, v2018_landsat: version from 2018 with only Landsat8 input, v2018_land-sat_s1: version from 2018 with both Landsat8 and Sentinel-1 input) as well as altitude from the 10 m Digital Elevation Model (DEM) (Kartverket 2013) and topographic indices derived from it (wind exposure, topographic convergence, global solar radiation) as well as Land Surface Tem-perature during summer (EuroLST_BIO10).*

| GBIF data from | >=2000 | | >=2000 and altitude > 1000m | |
|---|---|---|---|---|
| Ordinal regression (clm) | AIC | rank | AIC | rank |
| Snow Index ~ v2016_landsat | 161787 | 13 of 16 | 58252 | 11 of 16 |
| Snow Index ~ v2016_landsat_s1 | 160822 | 9 of 16 | 58157 | 9 of 16 |
| Snow Index ~ v2018_landsat | 160742 | 8 of 16 | 58106 | 7 of 16 |
| Snow Index ~ v2018_landsat_s1 | 160497 | 6 of 16 | 58038 | 6 of 16 |
| Snow Index ~ v2018_landsat_s1 * altitude | 159722 | 1 of 16 | 57870 | 1 of 16 |
| Snow Index ~ v2018_landsat_s1 * wind_exposure | 160400 | 4 of 16 | 58032 | 3 of 16 |
| Snow Index ~ v2018_landsat_s1 * topo_convergence | 160371 | 3 of 16 | 58032 | 4 of 16 |
| Snow Index ~ v2018_landsat_s1 * GlobalRadiation | 160490 | 5 of 16 | 58035 | 5 of 16 |
| Snow Index ~ v2018_landsat_s1 * EuroLST_BIO10 | 159798 | 2 of 16 | 57894 | 2 of 16 |
| Snow Index ~ altitude | 161080 | 12 of 16 | 58488 | 13 of 16 |
| Snow Index ~ wind_exposure | 164053 | 14 of 16 | 58838 | 16 of 16 |
| Snow Index ~ topographic_convergence | 164094 | 15 of 16 | 58800 | 14 of 16 |
| Snow Index ~ GlobalRadiation_doy_100_235 | 164157 | 16 of 16 | 58819 | 15 of 16 |
| Snow Index ~ EuroLST_BIO10 | 161076 | 11 of 16 | 58430 | 12 of 16 |
| Snow Index ~ altitude * topo_convergence + … | 160715 | 7 of 16 | 58151 | 8 of 16 |
| Snow Index ~ EuroLST_BIO10 * topo_convergence + … | 160857 | 10 of 16 | 58201 | 10 of 16 |

### 6.1.5.3 Vegetation plot data collected with regards to snow cover duration

Plotting the vegetation data from Evju et al. (2012) against the modelled day of snow melt shows that the vegetation data does not include extreme snow-lie sites with significantly prolonged snow cover (see **Figure 22**). The maximum day of the year for modelled snow melt at the loca-tions of the vegetation data is day 200, which corresponds to 19 July (in non-leap-years). This represents the lower bound for the occurrence of vegetation types related to delayed snow melt, while extreme snow-lie vegetation can be found in Norwegian mountains in areas where the snow does not melt before September (see **Figure 2**).
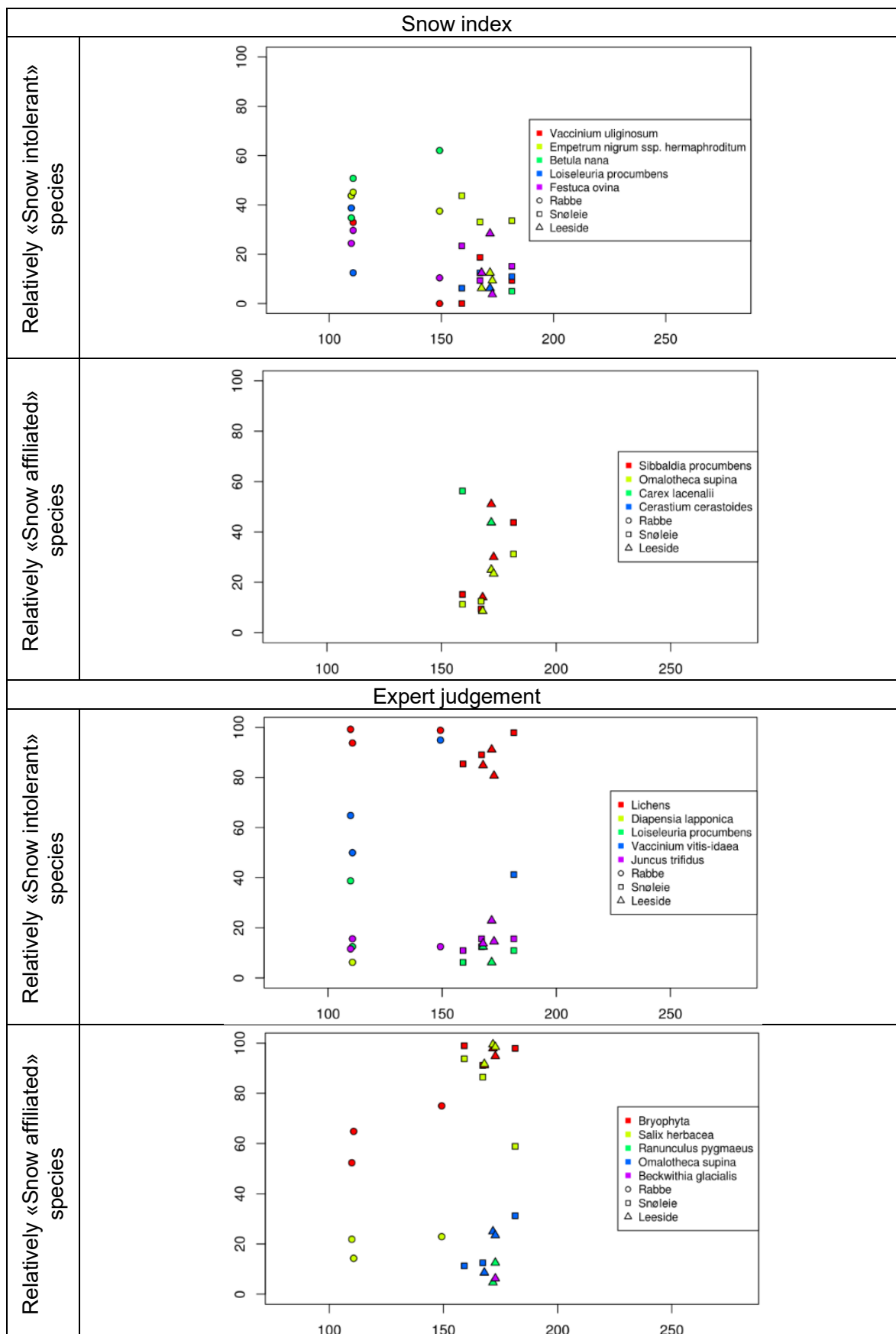
**Figure 22** *Snow sensitive species from vegetation plot data over modeled day for snowmelt (x-axis: relative frequency per site, y-axis: average estimated day of snow melt)*

However, the plots above clearly show for both the expert judgements and the Snow Index by Odland & Munkejord (2008), that:

- snow affiliated species are almost exclusively found at locations with the latest dates of modelled snowmelt,
- the frequency of snow intolerant species decreases with later modelled day of snow melt
- the order of the in-situ data locations when looking at the modelled day of snow melt matches the classification of the locations by the data collectors regarding the duration of snow cover. Locations with prolonged snow-lie ("Snøleie") are found at later estimated dates of snow melt, locations with intermediate duration of snow cover in the middle and locations with short and unstable snow cover at earlier dates.
- locations that represent areas with unstable snow cover contain the highest variation regarding the day of snowmelt (they span most number of days).

All in all, the vegetation plot data shows a clear relationship between modelled day of snow melt and occurrence of snow sensitive species. This indicates that the model is able to represent effect of snow cover duration on the vegetation in the mapped sites.

## 6.1.6 Discussion and conclusions
Given enough data, we are able to estimate the dates for snow melt for mountain areas with fairly high accuracy (**Figure 18**). The use of Sentinel-1 data provided us with more observations. However, a major drawback with SAR for snow cover monitoring is that it can only detect wet snow and cannot distinguish dry snow from bare ground. Thus, we are only able to use positive snow cover detections from Sentinel-1 to estimate the date for melted snow cover. This introduces a bias into our estimates by shifting the dates for snow melt towards a later day. This is observed with a later average date for melted snow cover when using Sentinel-1 data (day 152.2), compared to Landsat-8 only (day 125.3). This was also confirmed by the probability curves (**Figure 19**).

The model evaluation (chapter 6.1.5) showed clear and significant correlation between modelled estimates for the gradient "Reduced growing-season due to prolonged snow-lie" and occurrence of relevant indicator species. This confirms that model estimates are not only reasonably technically accurate, but also ecologically meaningful and provide ecological information that would not have been available at that extent and spatio-temporal resolution otherwise. The developed remote sensing product improves our abilities to explain species occurrence in space and time. However, evaluation of modelling results also gave indication for the following possible future improvements:
- The accuracy of the estimates is sensitive to the snow cover stability and the quality of the observations. For cases when the snow cover varies during the winter season or from one winter to the next, the uncertainty will be higher than for cases when the snow cover is stable during the winter. This has been confirmed by the evaluation using species occurrence data. Thus, it can be meaningful to accompany the model with an estimate on snow cover stability. The latter was described as an environmental gradient in NiN Version 1.0 (https://www.artsdatabanken.no/Pages/137938). For such a model much of the described pre-processing chain (chapter 6.1.1) could be repurposed.
- Especially in the lower end of the gradient the model rather represents instable snow cover (locations where snow is blown off) than early snow "melt". Thus, labelling it the estimate "modelled day of snow melt" can be misleading and should probably rather be referred to as a "snow cover duration index".
- Due to the nature of satellite imagery it can be expected that the algorithm would not work for areas with dense forest cover. In forest the observation of snow is often hindered by the canopy of especially coniferous trees, leading to an underestimating of the snow cover extent. In order to apply the algorithm in lowlands and especially areas with higher

and woody vegetation, it would be required to reduce the effect the forest canopy cover. This may be achieved by including e.g. the two-way forest canopy transmissivity into the snow cover extent estimation (Metsämäki et al. 2015). However, as the NiN gradient "Reduced growing-season due to prolonged snow-lie" is most relevant in mountain areas, scope of and results from the model could simply be limited to those areas and a mask could be applied for lowlands.

In addition, it can be recommended to improve several other aspects before the method can be considered operational for usage. These include: (1) The use of Sentinel-2 images in order to obtain more samples in the time series, and thereby reduce the uncertainty. However, one challenge with Sentinel-2 is the lack of thermal bands that are useful to discriminate snow from clouds. (2) The use of improved cloud and cloud shadow detection in order to reduce the number of misclassified pixels. We experimented by using the cloud detection method proposed by Zhu and Woodcock (2012), but this tended to classify small snow patches as clouds and was therefore not applicable for our purpose. (3) The use of improved pre-processing of the optical data, including topographic normalization and further image registration (Crawford et al. 2013) in order to reduce effects of terrain shadow.

The proposed method may also be used to predict changes of the climatic snow cover duration. This can be achieved by comparing the dates of snow-melt from two consecutive time-series. The quality of the change detection will depend strongly on the number of observations and time duration they are acquired over. A time series duration of at least 5-10 years are expected to be necessary, and 50 observations per time series should be collected.

## 6.2 Develop, evaluate and refine a model for Tree canopy cover (TT, NiN 1.0)

The second gradient selected for a case study was Tree canopy cover. Also here, data was specifically collected, pre-processed and analysed, and developed models were evaluated. Processing is documented at https://github.com/NINAnor/sentinel4nature.

### 6.2.1 Data preparation and data fusion
Multitemporal data from both pairs of Sentinel-1 (A and B) and Sentinel-2 (A and B) were chosen as the main data source for the Tree canopy cover model. Both sensors have a known potential for vegetation, and especially forest monitoring. Sentinel-1 is particularly interesting for monitoring of boreal forests, where it can be hard to get images from optical satellites with little or no cloud cover. Forested areas (appearing green on the RGB composite) have relatively high backscatter intensities in both polarizations (especially in VH) and relatively low difference between the two polarizations when compared to the agricultural cropland (Dostálová et al. 2016).

Satellite images for all years where data was available - 2015-2017 for Sentinel-1 and 2016-2017 for Sentinel-2 – were downloaded and pre-processed (see **Figure 23**).
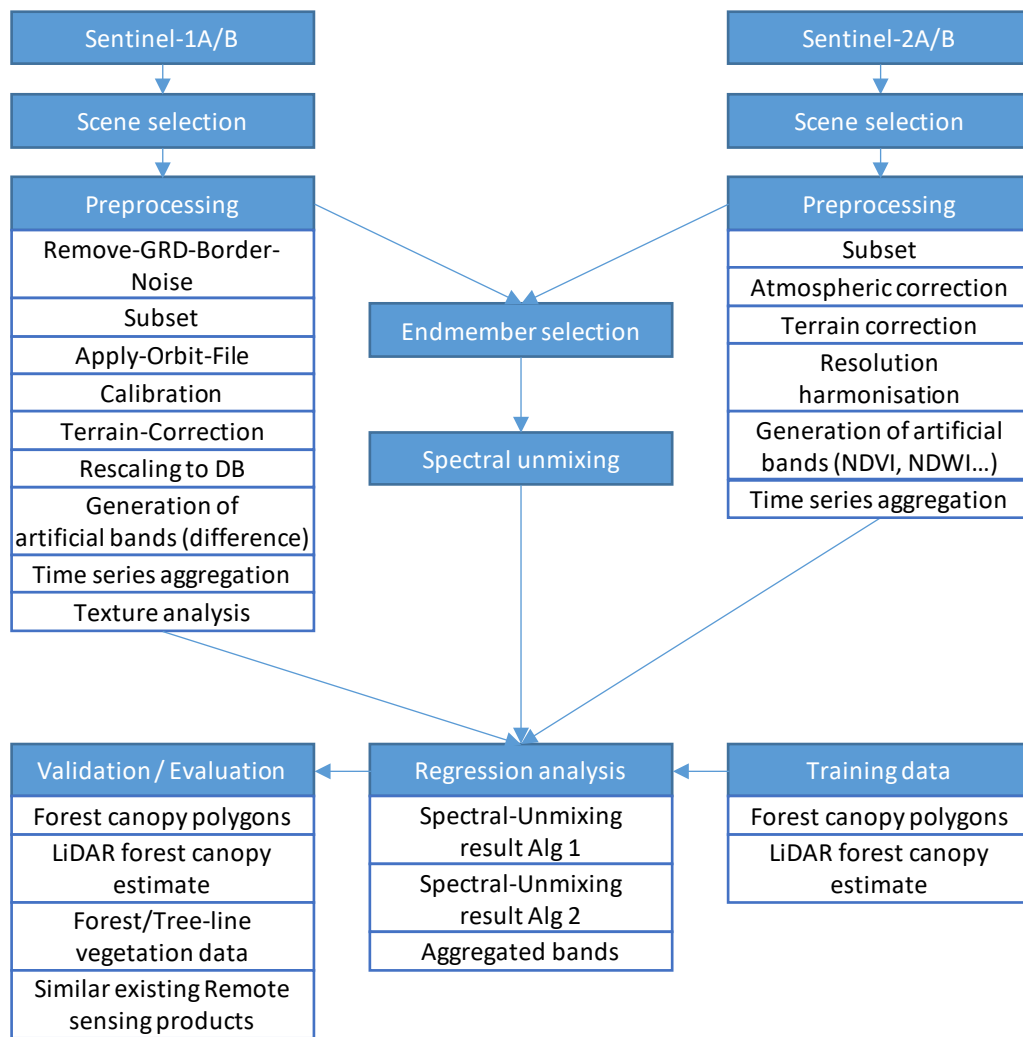
**Figure 23** *Workflow for development, evaluation and refinement of a model for Tree canopy cover (TT, NiN 1.0).*

Only uptakes under leaf-on conditions (July-September) were selected from both satellites in order to minimize differences across forest types. Additionally, for Sentinel-2, scenes with cloud coverage > 10% were filtered out.

#### 6.2.1.1 Data fusion

Besides combining Sentinel-1 and Sentinel-2 data, fusing auxiliary data e.g. from terrain models and indices derived from them has been considered in order to extend the layer stack of possibly relevant predictors for tree canopy cover. Relevant candidates were mainly

* slope, which is known to impact occurrence of forest and tree density
* altitude of the terrain with regards to forest line or tree line, which would delineate the climatic boundaries for forest and thus tree canopy cover

However, both variables were disregarded as artificial bands in further analysis. The effect of slope is mainly limited to very steep locations (> 64 degrees, Bryn et al. 2013), that cover only a very low percentage (~ 0.04%) of the total land area in Norway. Spatial data on forest line that covers entire Norway is only available at relative coarse scale (50m resolution) (Blumentrath & Hanssen 2010). It is derived from topographic maps and thus bound to update cycles in the topographic data. A similar dataset on tree line has not been available. Thus, it was expected

that the datasets mentioned above introduce more noise in the analysis of the high-resolution satellite imagery than they contribute to improve the predictive power of the tree canopy cover model. However, a future improved estimate on forest line could help to exclude false possible signals in the mountains.

For fusion of Sentinel-1 and Sentinel-2 images, data from both satellites were first co-registered to the terrain model during pre-processing (see **Figure 23**), in particular terrain correction (Sentinel-1) and atmospheric correction (Sentinel-2). During that pre-processing step, satellite images were resampled to the pixel alignment of the terrain model. That way all input data to the regression analysis had unified extent and resolution.

### 6.2.1.2   Scene selection
For each case study site, a rectangular study extent was defined prior to the analysis. The size and position of the rectangle was chosen so that it captured the training data sites, as well as a variety of topographical features (valleys, mountain tops of different heights) and a variation of forest types with varying tree canopy density. In the study sites Oslofjord and Lurøykalven, the extent is a 10 x 10 km rectangle and in case of Hjerkinn a 20 x 20 km rectangle. In Sunndalen, the extent was divided into two smaller rectangles (12 x 15 km and 7 x 15 km) because no Sentinel-2 scene covered the entire area.

### 6.2.1.3   Sentinel-1 data preprocessing
Sentinel-1 data was pre-processed based on the methodology of Dostálová et al. (2016) (see **Figure 23**). From Sentinel-1A/B IW Ground Range Detected (GRD) Level-1 products were selected, because the "combination of two polarization bands (VV and VH in this case) offers the possibility to use the backscatter intensities from the C-Band SAR sensor for a classification of various land cover types" (Dostálová et al. 2016). In addition, using multi-temporal data from Sentinel-1 helps to overcome limitations in precision compared to analysing single SAR images caused by speckle noise or topographic effects (Dostálová et al. 2016).

Removal of grid border noise (extremely low backscatter values (below -30 dB) occur at the image borders due to thermal noise), sub-setting to the area of interest, application of orbit file, radiometric calibration to sigma-0 values and Range-Doppler terrain correction were conducted using the graph processing command line tool (gpt) from ESAs SNAP tool box (version 5). For terrain correction, the 10m digital elevation model provided by the Norwegian Mapping authority was used. Because the Interferometric Wide swath (IW) data from Sentinel-1 have a spatial resolution of ~20m with the pixel spacing of 10m, band values were resampled to the resolution and pixel alignment of the terrain model used. As in Dostálová et al. (2016) no multi-looking or speckle filtering was applied because the aggregation of multi-temporal image stacks can compensate for the issues tackled by these techniques.

For each case study site, between 50 and 83 Sentinel-1 scenes were downloaded for the three-summer months (July to September) for 2015 to 2017. The downloaded scenes were visually checked for invalid data and the precision of the georeferencing.

Conversion from linear to decibel scale, computation of the difference between VV and VH polarisation per scene, as well as the aggregation of time series and texture analysis was conducted in GRASS GIS 7.4 (GRASS GIS Development Team 2017). From the single scenes in the time series of Sentinel-1 images, mean, median, quartiles, standard deviation, variance and the so-called dry-parameter were computed by year as well as across all three years. The dry-parameter is computed as the average pixel value of all pixels with values below the first quartile. The aggregated pre-products were then used in further analysis.

### 6.2.1.4  Sentinel-2 data pre-processing

For each case study site, Level-1C Sentinel-2 scenes covering the entire study extent were downloaded using the Sentinelsat utility (Wille & Clauss 2016). The Level-1C product[2] is composed of 100 x 100 km$^2$ tiles and contains the Top Of Atmosphere (TOA) reflectances along with the parameters to transform them into radiances.

In order to minimize the effect of seasonal variations in vegetation cover and at the same time minimize differences across forest types, leaf-on scenes (beginning of June – end of September) from years 2015 (launch of the first Sentinel-2 satellite), 2016 and 2017 were included in the analysis. Additionally, a constraint of maximum 10 % cloud cover was used.

To obtain the Bottom Of Atmosphere (BOA) reflectances from TOA reflectances, atmospheric corrections were applied to each individual band using *i.atcorr* module of GRASS GIS. The software uses the 6s algorithm (Second Simulation of Satellite Signal in the Solar Spectrum), in which following parameters need to be specified:
- geometrical conditions
- month, day, time, longitude and latitude of measurement
- atmospheric model
- aerosol model
- aerosol optical depth or visibility
- mean target elevation above sea level
- sensor height
- sensor band

**Table 3** provides an overview of 6s parameters used as static parameters for atmospheric correction at the different case study sites.

*Table 4 Parameters used for atmospheric correction at the different case study sites*

|  | Hjerkinn | Lurøykalven | Oslofjord | Sunndalen |
|---|---|---|---|---|
| Geometrical conditions | Sentinel-2A / Sentinel-2B | Sentinel-2A / Sentinel-2B | Sentinel-2A / Sentinel-2B | Sentinel-2A / Sentinel-2B |
| Atmospheric model | Subarctic summer | Subarctic summer | Subarctic summer | Subarctic summer |
| Aerosol model | Continental | Maritime | Urban | Continental |
| Aerosol optical depth | 0.1 | 0.1 | 0.1 | 0.1 |
| Sensor height | 1 000 km | 1 000 km | 1 000 km | 1 000 km |

Month, day, time, longitude and latitude of measurements, as well as mean target elevation above sea level, were computed individually for each scene. Aerosol optical depth was estimated to be 0.1 in average, but further research needs to be carried out to precisely estimate this parameter. Finally, sensor band number was set individually for each band.

Because two of the case study sites are located in a mountainous area, and a lot of shading occurs in the imagery, it was especially important to perform topographic corrections. In topographic corrections, the terrain, as well as position (zenith and azimuth) of the sun at the time of sensing is used to create an illumination model. Reflectance values in areas exposed to the sun are decreased, while reflectance values in areas in the shadow are increased. The atmospheric

---

[2] https://earth.esa.int/web/sentinel/user-guides/sentinel-2-msi/product-types/level-1c

corrections were performed for each band separately using the *i.topo.corr* module in GRASS GIS and minnaert method.

The Sentinel-2 Level-1C products were resampled with a constant Ground Sampling Distance (GSD) of 10, 20 and 60 m depending on the native resolution of the different spectral bands. To unify the resolution of spectral bands to 10 m, a Gaussian filter with a 3 x 3 neighbourhood was applied to the 20m and 60m bands.

Additional artificial bands were computed for each scene - The Normalized Difference Vegetation Index (NDVI) and the Modified Normalized Difference Water Index (MNDWI). NDVI is used for detection and quantification of green vegetation. It normalizes the green leaf scattering in the near infra-red wavelength and chlorophyll absorption in the red wavelength, and for Sentinel-2 products is computed as follows:

$$NDVI = \frac{B08 - B04}{B08 + B04}$$

The values span from -1 to 1. Negative values correspond to water, values close to 0 represent bare rock, sand or snow and vegetation has positive values. The higher the value, the higher the density of green leaves.

MNDWI is an index used for distinguishing water bodies, which strongly absorb in the range from visible to infrared wavelengths. For Sentinel-2 products MNDWI is computed as follows:

$$MNDWI = \frac{B03 - B11}{B03 + B11}$$

Small, negative values represent vegetation, while high (positive) values correspond to water.

Before the next steps were carried out, the atmospherically and topographically corrected scenes were manually checked for large patches of snow (especially in early or late summer in case study sites in Hjerkinn and Sunndalen). Since the 10 % cloud cover limit applies to the entire 100 x 100 km$^2$ scene, and not the study extent, several scenes had to be excluded due to large portions of their area being covered by clouds. Additionally, any otherwise corrupted scenes (e.g. shifted or containing no data) were excluded as well.

From all the remaining scenes, a median value of each band (including NDVI and MNDWI) was computed for each case study site in order to minimize the effect of seasonal variations in vegetation cover. Finally, shadow and water were masked out. Applying topographic corrections resulted in areas in complete shadow being masked out. Additionally, in order to avoid the negative effect of water bodies on spectral unmixing, water pixels were masked out using NDVI, MNDWI and slope thresholding. An overview of thresholds used in individual case study sides is provided in **Table 4** (pixels need to satisfy all conditions in order to be used in further analysis).

*Table 5 Threshold values used for masking water*

|  | NDVI | MNDWI | Slope |
|---|---|---|---|
| Hjerkinn | > 0.00 | < 0.02 | - |
| Lurøykalven | > 0.00 | - | - |
| Oslofjord | > -0.04 | < 0.40 | - |
| Sunndalen | > 0.00 | < 0.02 | > 0.5 |

### 6.2.1.5   Endmember selection and spectral unmixing
Linear spectral unmixing assumes that the spectrum of an image consists of a mixture of several spectrally distinct surface components. If the spectral response of these distinct components

(also called the endmembers) is known, and a linear mixture is assumed, it is possible to derive the abundance of each endmember in the pixel (Bai et al. 2012).

Many studies proved the usefulness of linear spectral unmixing in estimating the proportions of various land cover classes, including forest cover (Bai et al. 2012) and forest types (Gudex-Cross et al. 2017). Gudex-Cross et al. (2017) applied spectral unmixing to multi-temporal Landsat imagery to produce a thematic forest classification of a mixed composition of ten common tree species in northern New York and Vermont, USA. Additionally, the basal area maps were refined using a hierarchical ruleset classification. Similarly, Bai et al. (2012) examined the capability of linear spectral unmixing of Landsat-7 Thematic mapper imagery to improve forest cover estimation. In the case study carried out in a subtropical forest in southeast China, they achieved only a slight (0.8 %) underestimation of the forest area compared to the forest inventory statistics.

Inspired by the work of Schulte to Bühne & Pettorelli (2018), who argued that fusing multispectral and radar images can significantly improve the ability to assess the distribution of ecosystems, Sentinel 1 dry parameter images as well as the artificial NDVI band were included in the endmember selection and spectral unmixing alongside the atmospherically and topographically corrected Sentinel 2 bands.

The endmembers have to be selected prior to the analysis – either by selecting the spectral response of individual endmembers from a spectral library or by detecting the most distinct pixels in an image. In this study, several endmember extraction methods from the Python module PySptools (Therien 2016) were compared - the Fast Iterative Pixel Purity Index, N-FINDR and the Pixel Purity Index, out of which the N-FINDR algorithm outperformed the other two in terms of result interpretation. The Fast Iterative Pixel Purity Index and the Pixel Purity Index algorithms often detected edges of masked features (snow cover, clouds, water bodies).

The PySptools module offers three methods of linear spectral unmixing – Unconstrained Least Squares (UCLS), Non-negative Constrained Least Squares (NNLS) and Fully Constrained Least Squares (FCLS). All of them perform linear spectral unmixing by means of least square estimation of abundances from spectral signatures of input endmembers. They differ in terms of the constraint put on the values of output class abundances – while in UCLS, any value of abundance is allowed, in NNLS the resulting abundances must be non-negative, and in FCLS the abundances must be between 0 and 1, and together the abundances must fulfil the sum-to-one constraint. (Kumar et al. 2016, Therien 2016). When compared in terms of the interpretability of the results, the NNLS and FCLS algorithms proved to perform significantly better than the UCLS algorithm. Thus, UCLS was excluded at an early stage from model development.

## 6.2.2 Training and validation data

The model for forest canopy cover gradient requires both training and validation data because the final maps with forest canopy cover estimates are generated by means of regression analysis. From both detailed, manually digitized forest canopy and air-born laser scanning data (Light Detection and Ranging, LiDAR) forest canopy cover was estimated per pixel in the satellite imagery. 75% of each of these datasets were used to train the models for each case study site, while the other randomly chosen 25% were used for cross-validation.

In addition to such training and validation data, the model results were evaluated through visual inspection against orthophotos in comparison with existing, similar remote sensing products. Furthermore, a correlation analysis was conducted using tree canopy cover estimates collected at a transect along an altitudinal gradient that crosses forest and treeline and thus covers the transition from dense forest to alpine habitats.

### 6.2.2.1  Manually digitized tree canopy cover

For tackling the tree canopy cover gradient, recent, very high-resolution orthophotos were used to manually digitize tree canopy cover below the resolution of satellite pixels (see **Figure 24**). From these vector data, the percentage of canopy cover has been calculated per pixel of the

satellite imagery used (resolution and alignment of the pixels are equal to the satellite images). This results in a continuous value of percent of canopy cover per pixel, which is supposed to represent the tree canopy cover gradient from NiN.
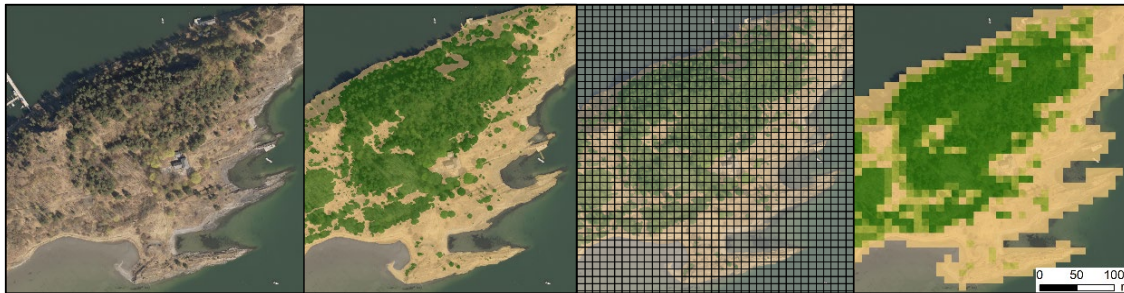


**Figure 24** *Manually digitized tree canopy cover of Gressholmen in Oslofjord study area. Left: Orthofoto, middle-left: manually digitized tree canopy polygons, middle-right: tree canopy polygons split by vector grid corresponding to pixels in the satellite imagery, right: raster representation of the percentage of tree canopy cover per pixel*

### 6.2.2.2 Tree canopy cover estimates from LiDAR

Because the manual digitization from orthophotos is very labour intensive, forest canopy was also estimated from air-born laser scanning data (Light Detection and Ranging, LiDAR), downloaded from hoydedata.no. This way a larger spatial extent could be covered with training and validation data, and thus a wider range of situations (tree canopy densities and spectral profiles within pixels) could be included in training and validation data. This is particularly important as the chosen modelling technique using Gradient Boosted Regression Trees is not able to extrapolate.

In order to generate suitable training and validation data from LiDAR data, tree canopy cover was estimated from ground and non-ground returns (see **Figure 25**). Using the resolution and alignment from the satellite imagery, the percentage of 0.5 m pixels with non-ground LiDAR returns with more than 2 m height above ground was calculated in relation to total density of 0.5 m pixels with LiDAR returns. This procedure accounts for differences in point density in the LiDAR data (e.g. because of overlap in flight strips) and gives a rough estimate of tree canopy cover. Since the LiDAR data does not distinguish between vegetation and non-vegetation returns in the non-ground LiDAR points, and because LiDAR data in the Lurøykalven case study site was partly outdated due to recent logging activities, areas with valid forest returns were manually (yet coarsely) delineated. Training and validation data was only generated within the areas where no logging activity could be identified and it could be assumed that the LiDAR data represent the current state.
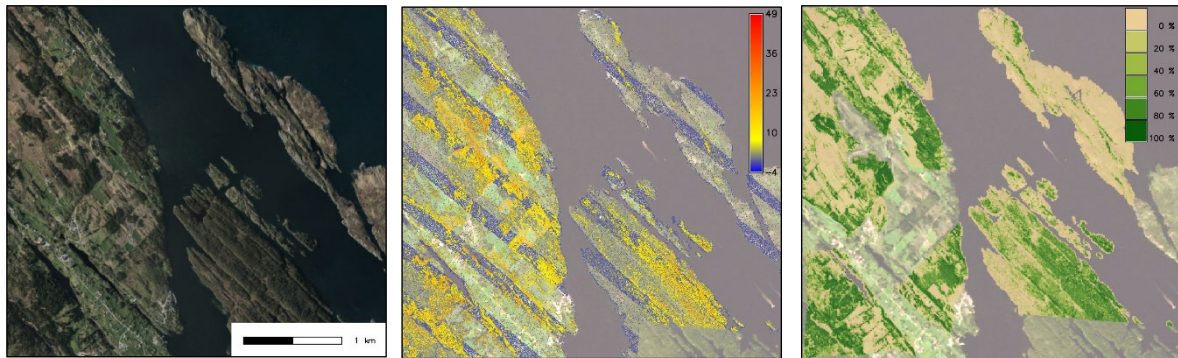
**Figure 25** *Tree canopy cover estimates from LiDAR of Lurøykalven. Left: Orthofoto, middle: height above ground of LiDAR returns, right: LiDAR derived tree canopy cover used as training data.*

### 6.2.2.3 Visual inspection against orthophotos and existing similar products

The maps resulting from modelling tree canopy cover were spot checked using recent orthophotos from "Norge i Bilder"[3] and compared to the following three remote sensing products with a more or less comparable scope:

- the Global forest cover change maps developed by Hansen et al. (2013)
- the Norwegian forest resource map SAT-SKOG developed by Gjertsen & Nilsen (2012)
- the Vegetation map for Norway developed by Johansen (2009)

### 6.2.2.4 Tree canopy and vegetation pattern across forest and tree line

Finally, detailed data on tree canopy and vegetation pattern along an altitudinal gradient were correlated with the estimates on tree canopy cover. These data (see **Figure 26**) were collected by Løkken & Hofgaard (unpublished) for the ECOFUNC project (from RCN grant MILJØ2015, project number: 244557) following a transect that crosses forest and tree line. These data were also used to compare the explanatory power of the newly developed models with the three existing remote sensing products listed above.

---

[3] https://kartkatalog.geonorge.no/metadata/norge-i-bilder/norge-i-bilder-wms-ortofoto/dcee8bf4-fdf3-4433-a91b-209c7d9b0b0f
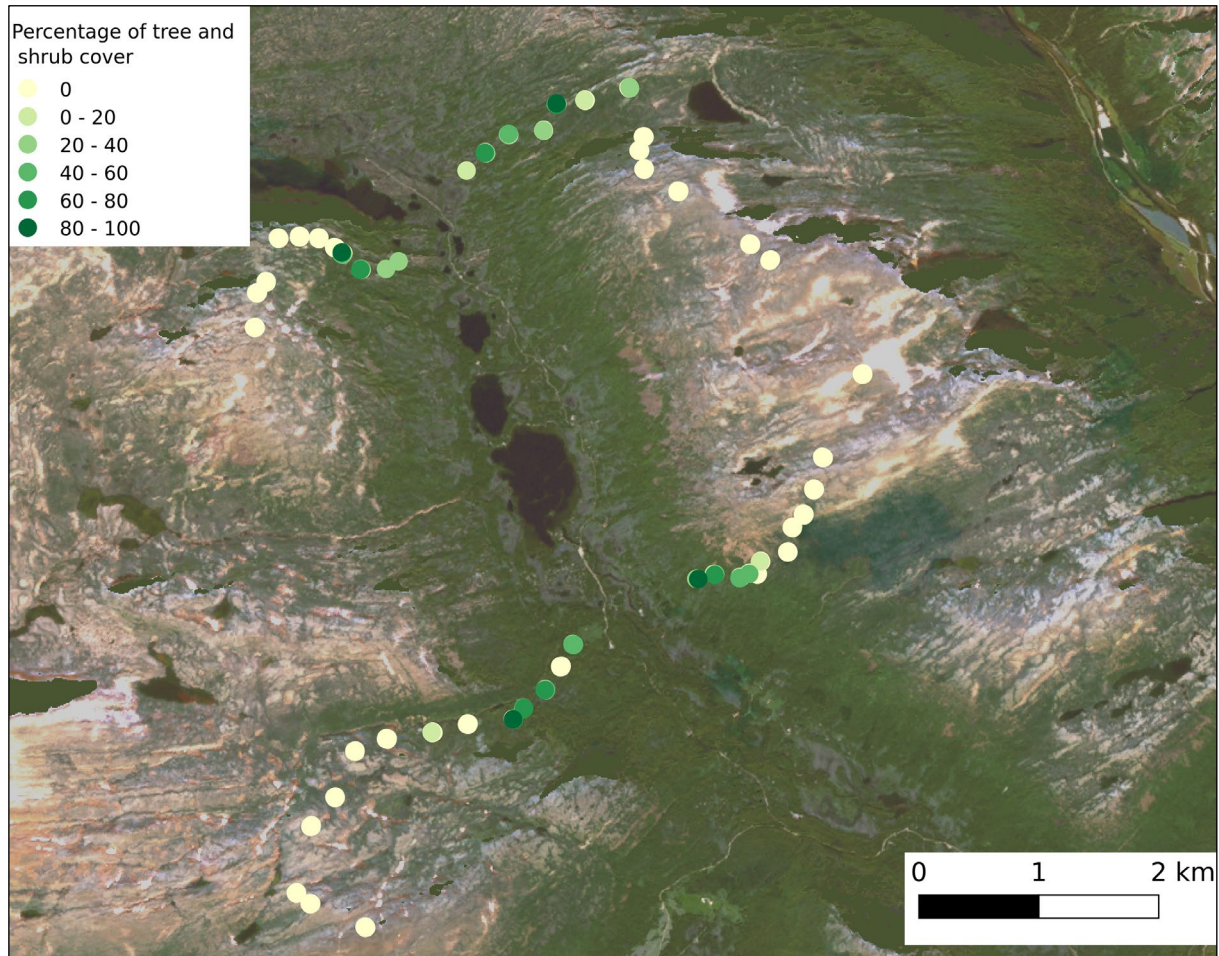
**Figure 26** *Data on tree canopy and vegetation pattern across forest and tree line in Sunndalen (Løkken & Hofgaard, unpublished)*

## 6.2.3 Model development

For the regression analysis Gradient Boosted Regression Trees (GBRT) were chosen as modelling technique due to their predictive power, robustness for outliers, and their ability to handle non-linear relations as well as feature interactions. The Python GBRT implementation from scikit-learn (scikit-learn 0.19.1) was used for model development.

For each case study site, a twofold modelling process was conducted, that consists of:
1. Automatic hyper-parameter optimization using a range of appropriate tuning parameters
2. Application of the hyper-parameters identified as optimal to a final model

That way a model on tree canopy cover was produced using either just the satellite bands and artificial bands generated from them or results from the two spectral un-mixing algorithms applied to the same bands. Here, the training and validation data from manually digitized forest canopy was used and root mean square error (RSME) and $R^2$ were tracked for every model. That way, performance of the different models could be compared using RSME and $R^2$.

However, because results from the models based on the manually digitized training data showed weaknesses due to the lack of variation covered in the training and validation data, another set of models was created the same way, but with training and validation data derived from LiDAR. In addition, the three most influential layers from the best-performing spectral un-mixing algorithm (judged by $R^2$) were added as input to the latter set of models. The reason for that was that the spectral un-mixing – although being less accurate compared to using satellite bands directly

- seemed to improve model performance regarding separation of moist vegetation and ground from forest / tree canopy.

For all models the following plots were generated to help interpret the modelling results:
- deviance plots that show test and training error with regards to number of boosting iterations
- plots of feature importance that show the influence of each input layer (e.g. satellite bands or spectral un-mixing results) on the final model
- partial dependence plots that show how a feature affects the estimate of tree canopy cover; such plots were also generated for the pair-wise interactions between the 5 most influential features

## 6.2.4 Results

For each of the four case study sites, three GBRT models based on manually digitized training data were created – one using satellite bands and artificial bands generated from them as predictors, and two using results of fully constrained least squares and non-negative least squares spectral unmixing as predictors. Furthermore, for Hjerkinn, Lurøykalven and Sunndalen case study sites, a GBRT model based on LiDAR-derived training data as response and satellite bands as predictors was created.

The result of each GBRT model is a prediction raster of tree canopy cover coverage, ranging from 0 % to 100 % in 10m resolution. Alongside the results, plots of predictor importance were created to estimate the most influential spectral bands. Furthermore, the Mean Square Error (MSE) and R squared ($R^2$) were computed to enable comparison amongst models. An overview of the created models is provided in **Table 5**. For each model, the six most important predictors (spectral bands) are stated, as well as Mean Square Error (MSE) and R squared ($R^2$).

*Table 6 Summary of tree canopy prediction results per case study site*

| Case study Site | Response | Manually digitized training data | | | LiDAR-derived training data |
|---|---|---|---|---|---|
| | Predictors | Satellite bands | FCLS unmixing | NNLS unmixing | Satellite bands |
| Hjerkinn | Predictors | B02, B04, B01, B05, NDVI, B09 | - | - | B02, B04, B01, B09, B05, B08 |
| | MSE | 0.02 | 0.06 | 0.06 | 81.01 |
| | R² | 0.77 | 0.31 | 0.40 | 0.78 |
| Lurøykalven | Predictors | NDVI, dry (VH), B01, B09, dry (VH-VV), dry (VV) | - | - | dry (VH), B04, dry (VV), B03, B05, B01 |
| | MSE | 0.019 | 0.03 | 0.02 | 415.68 |
| | R² | 0.34 | 0.20 | 0.18 | 0.64 |
| Oslo | Predictors | B04, dry (VH), B01, B09, B02, NDVI | - | - | - |
| | MSE | 0.03 | 0.05 | 0.05 | - |
| | R² | 0.79 | 0.71 | 0.71 | - |
| Sunndalen | Predictors | B05, B02, dry (VH-VV), NDVI, B01, B09 | - | - | B02, B05, dry (VH), B04, NDVI, B03 |
| | MSE | 0.02 | 0.04 | 0.03 | 107.46 |
| | R² | 0.74 | 0.45 | 0.51 | 0.82 |

The predictor importance plots of models using satellite bands were summarized into a frequency plot - the number of occurrences of each predictor (spectral band) amongst the six most important predictors was recorded (see **Figure 27**).
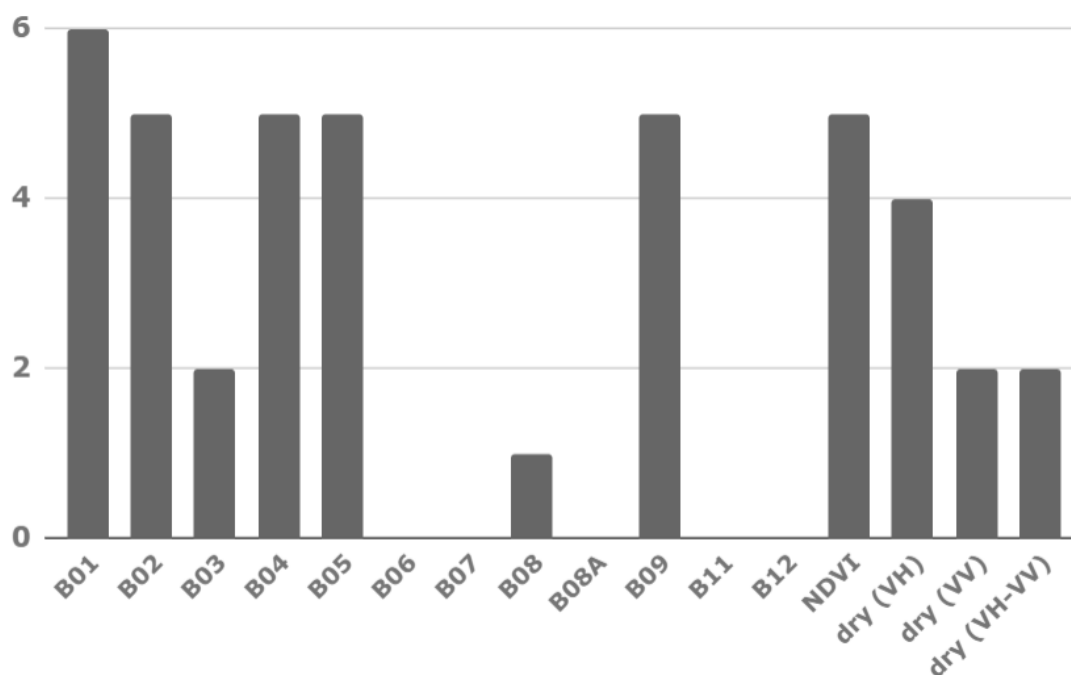


*Figure 27 Frequency at which spectral bands were represented among the 6 most important predictors across the different produced models*

## 6.2.5 Evaluation
The results were first evaluated visually by comparison to orthophotos, and then visually and statistically by comparison to existing forest products.

### 6.2.5.1   Visual inspection against orthophotos
*Hjerkinn*

In the Hjerkinn case study site, five regression models were applied to detect forest cover:
1. manually digitized training areas omitting water pixels as response, satellite bands and artificial bands generated from them as predictors
2. manually digitized training areas including water pixels as response, satellite bands and artificial bands generated from them as predictors
3. manually digitized training areas including water pixels as response, results of fully constrained least squares spectral unmixing as predictors
4. manually digitized training areas including water pixels as response, results of non-negative least squares spectral unmixing as predictors
5. LiDAR-derived training data as response, satellite bands and artificial bands generated from them as predictors

The model based on manually digitized training areas omitting water pixels (1) was excluded immediately, as it overestimated the tree canopy cover along the entire shore (see **Figure 30** and explanation below). In terms of explanatory values ($R^2$), the models using satellite bands and artificial bands as predictors (2 and 5) performed significantly better ($R^2$ = 0.77 and 0.78 for the model based on manually digitized (2) and LiDAR-derived (5) training datasets, respectively) than models using the results of spectral unmixing as predictors ($R^2$ = 0.32 and 0.40 for models using results of fully constrained least squares (3) and non-negative least squares (4) spectral unmixing, respectively).

Visual inspection revealed that the regression model based on LiDAR-derived training dataset overestimated the tree cover in the mountain area (see the upper left corner of the two images at the top of **Figure 28**) but performed better in terms of characterizing the non-uniform tree canopy cover along the forest line (see **Figure 29**).
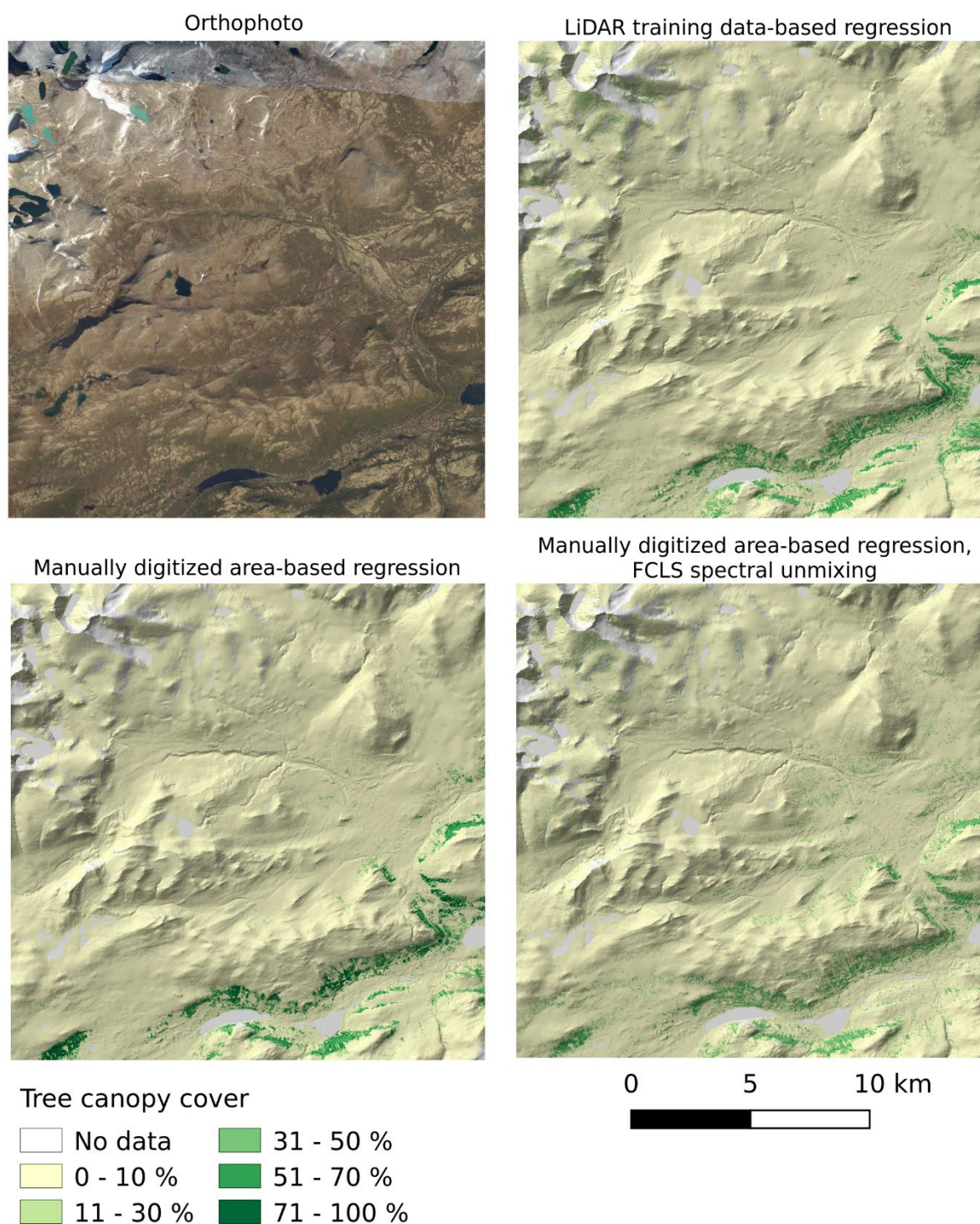
Orthophoto

LiDAR training data-based regression

Manually digitized area-based regression

Manually digitized area-based regression,
FCLS spectral unmixing

0          5          10 km

Tree canopy cover

☐ No data
☐ 0 - 10 %
☐ 11 - 30 %
☐ 31 - 50 %
☐ 51 - 70 %
☐ 71 - 100 %

**Figure 28** *Hjerkinn case study site – comparison of results with different training data and different predictors.*

Orthophoto

LiDAR training data-based regression

Manually digitized area-based regression

Manually digitized area-based regression, FCLS spectral unmixing

Tree canopy cover

No data
0 - 10 %
11 - 30 %
31 - 50 %
51 - 70 %
71 - 100 %

0    100 200 m
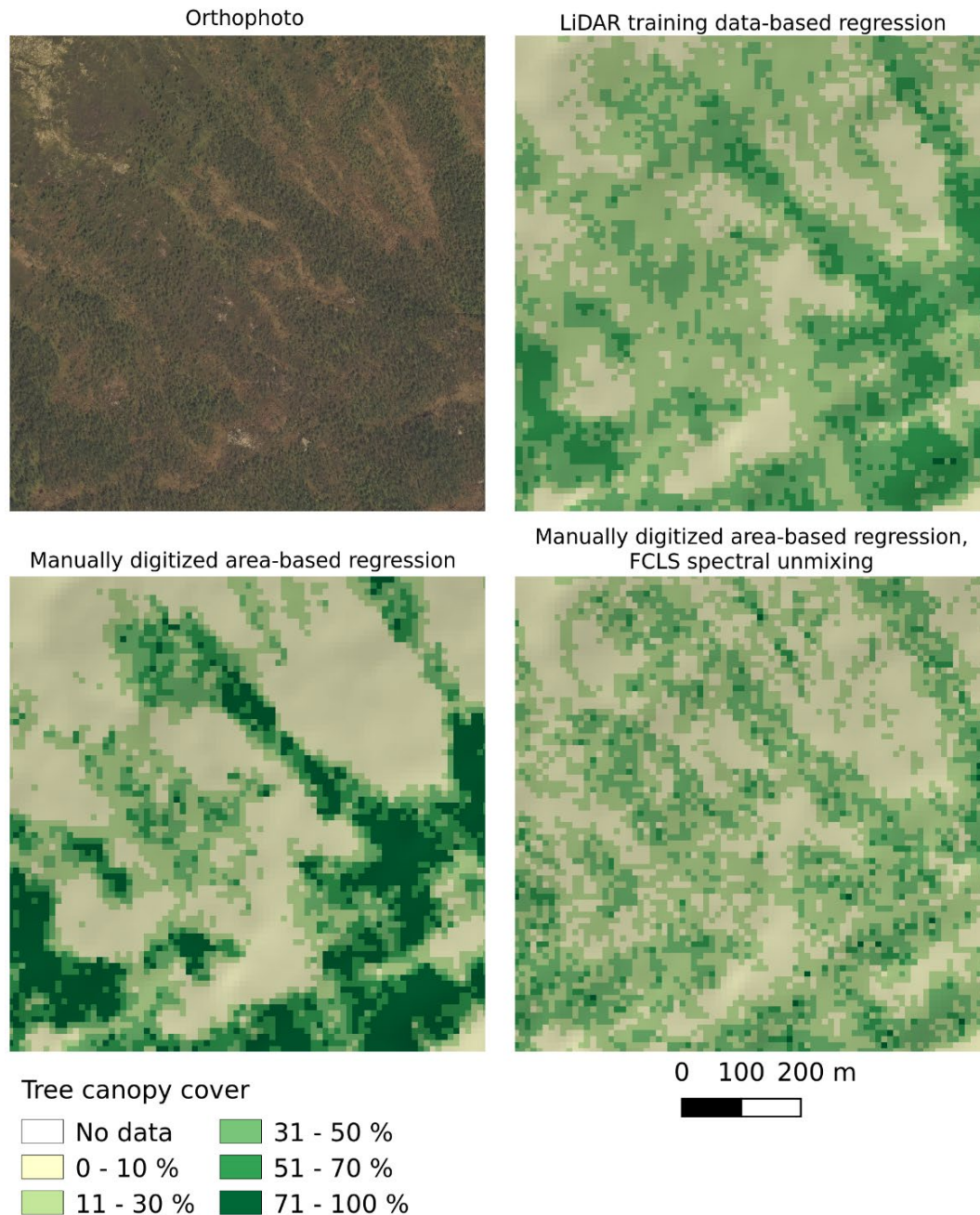
**Figure 29** *Zoom 1 into Hjerkinn case study site - comparison of results with different training data and different predictors.*

A detail from the Hjerkinn case study site illustrates the contribution of LiDAR training data-based regression (**Figure 29**). Whilst the output of the manually digitized area-based regression fails to detect sparse tree canopy and at the same time overestimates the canopy density in the continuous forest cover, the LiDAR training data-based regression succeeds in distinguishing between small nuances within the tree canopy and captures fine details. The result of the manually digitized area-based regression of FCLS spectral unmixing is overall underestimating the tree canopy cover density and fails to detect the continuous forest cover.
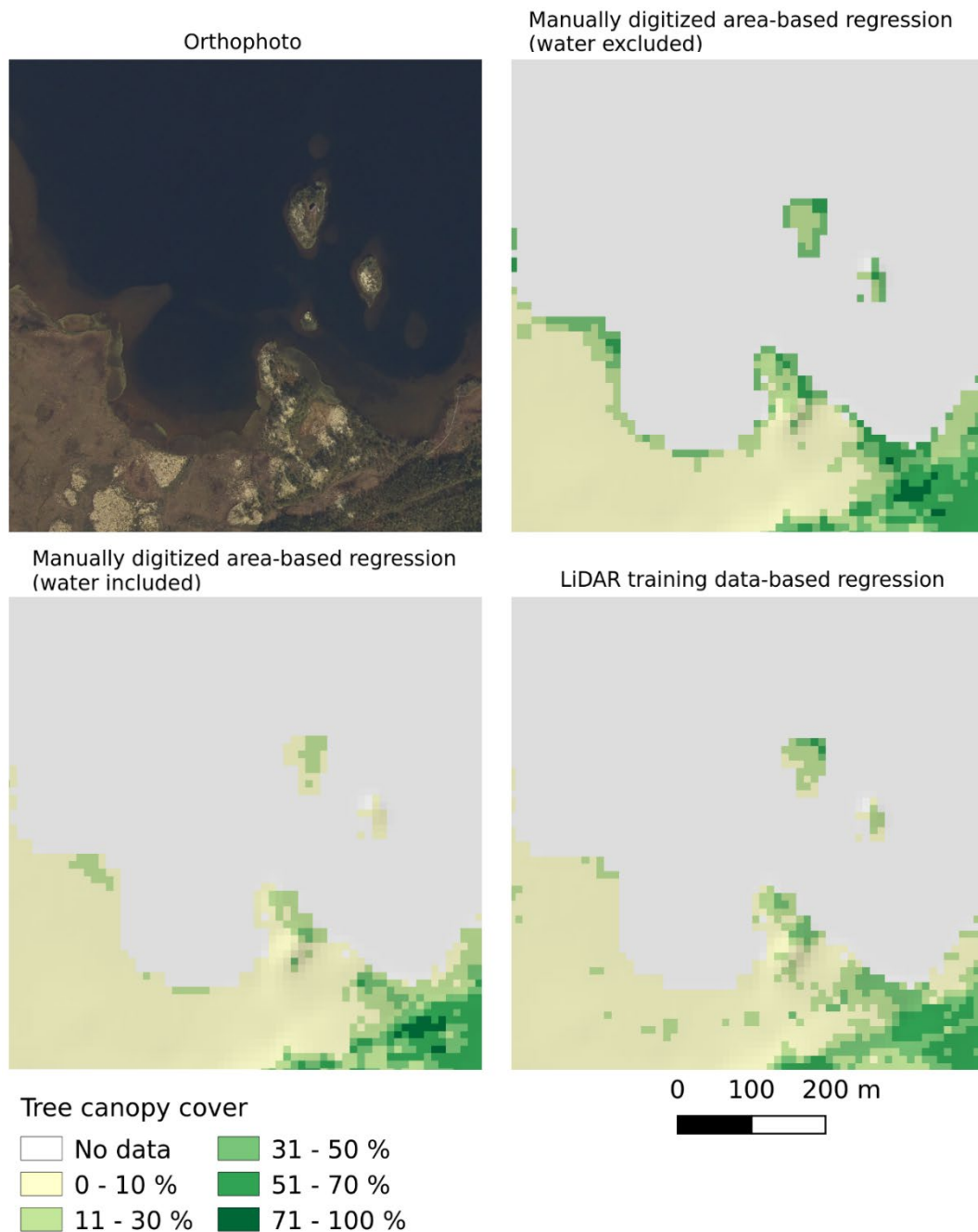
**Figure 30** *Zoom 2 into Hjerkinn case study site - comparison of results with different training data and different predictors.*

A second detail from the Hjerkinn case study stresses the importance of including areas of water bodies in the training data. In **Figure 30**, the upper right image illustrates the result of a regression based on a manually digitized area where pixels of water bodies were not included. The pixels along the entire shore line have tree canopy cover between 11 and 50 %. The problem diminishes when pixels of water bodies are added into the training dataset (bottom left image) or when LiDAR-derived tree canopy is used as training data (bottom right image). This effect of "mixed signal"-pixels at the land water interface is further explained in Section 3.3.2.

*Lurøykalven*

In the Lurøykalven case study area, four regression models were applied to detect forest cover:
1. manually digitized training areas including water pixels as response, satellite bands and artificial bands generated from them as predictors
2. manually digitized training areas including water pixels as response, results of fully constrained least squares spectral unmixing as predictors
3. manually digitized training areas including water pixels as response, results of non-negative least squares spectral unmixing as predictors
4. LiDAR-derived training data as response, satellite bands and artificial bands generated from them as predictors

Unlike the results in Hjerkinn case study area the regression model using LiDAR-derived training data as response and satellite and artificial bands as predictors (4) performed considerably better than the remaining regression models (1, 2, 3) – both in terms of $R^2$ (0.64 in case 4, 0.34, 0.20 and 0.18 in cases 1, 2 and 3, respectively) and visually (see **Figure 31**). The feeble performance of the regression models based on manually digitized training areas is caused primarily by the insufficient amount of tree canopy cover in the training data.
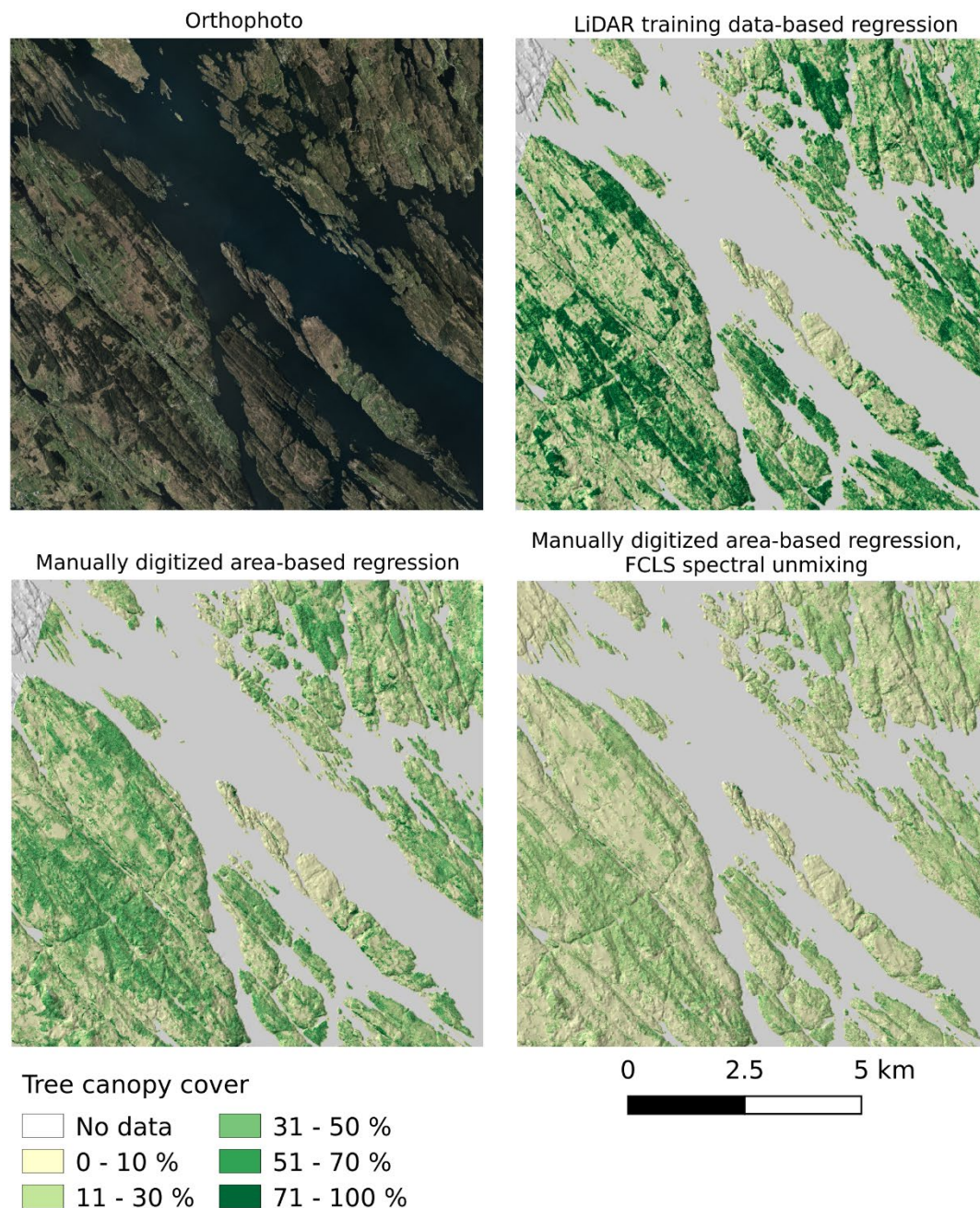
*Figure 31* Lurøykalven case study site - comparison of results with different training data and different predictors.

**Figure 32**, a detail from the Lurøykalven case study area, illustrates the importance of using a sufficiently large training dataset in the regression. The regression based on manually digitized training data performed poorly in both cases. Marshes and forest clearings were often confused with tree canopy. On the other hand, the regression based on LiDAR-derived training data managed to detect sharp forest edges as well as sparse vegetation.

Figure 32 *Zoom into Lurøykalven case study site - comparison of results with different training data and different predictors.*

*Sunndalen*

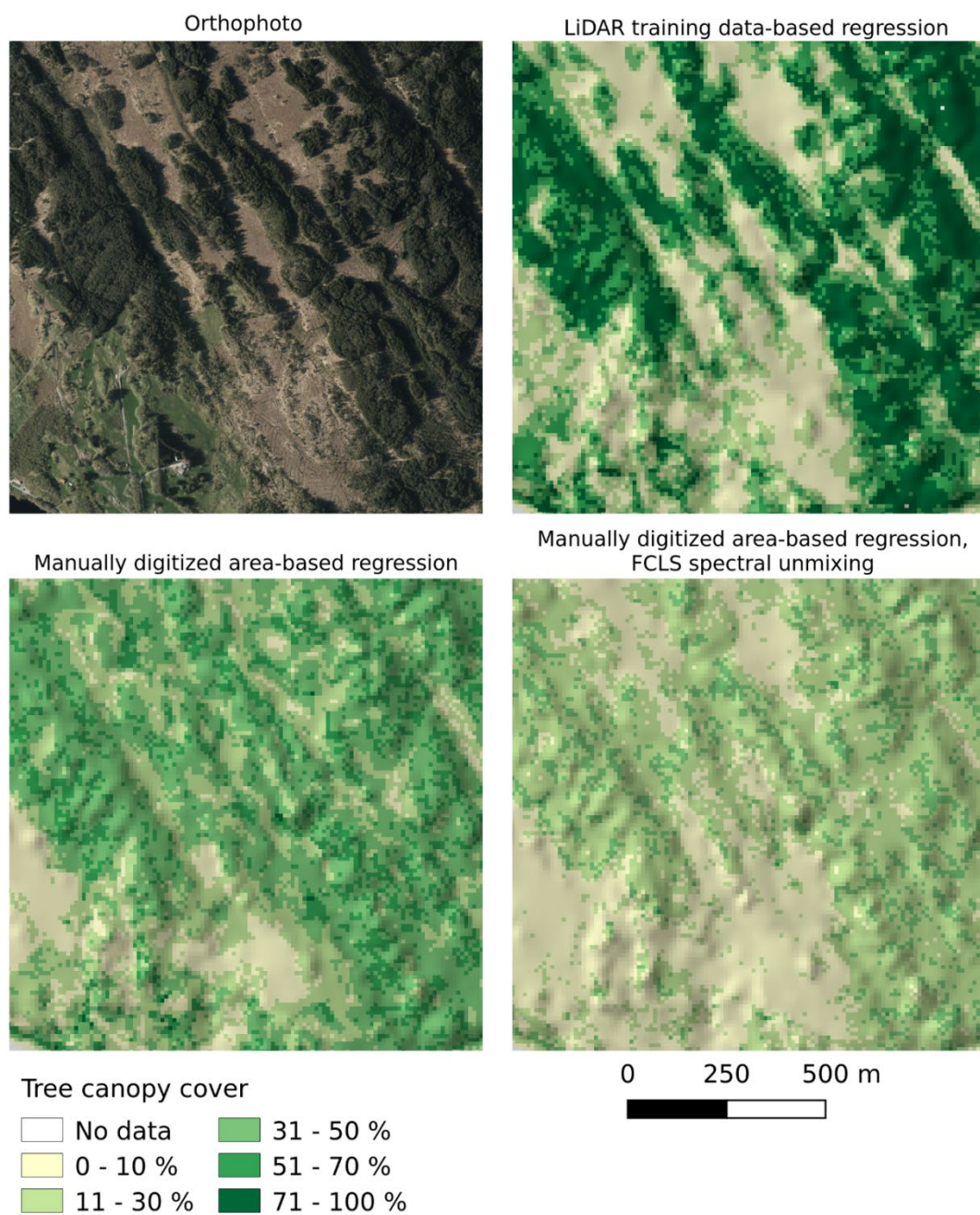In the Sunndalen case study area, four regression models were applied to detect forest cover:
1. manually digitized training areas including water pixels as response, satellite bands and artificial bands generated from them as predictors
2. manually digitized training areas including water pixels as response, results of fully constrained least squares spectral unmixing as predictors
3. manually digitized training areas including water pixels as response, results of non-negative least squares spectral unmixing as predictors
4. LiDAR-derived training data as response, satellite bands and artificial bands generated from them as predictors

Similarly to the previous case study areas, the regression model based on LiDAR-derived training data as response and satellite and artificial bands as predictors (4) outperformed the other models both in terms of $R^2$ (0.82 in case 4, 0.74, 0.45 and 0.51 in cases 1, 2 and 3, respectively) and visually. However, compared to the regression models based on manually digitized training areas carried out in the other case study sites, the regression model 1 in Sunndalen achieved results comparable to the best regression model (4). This fact emphasizes the influence of the quality of training data on the results. In the Sunndalen case study site, training data were obtained from several training sites in various parts of the tree canopy gradient. Consequently, the tree canopy cover was represented in the training data in various densities and compositions. The visual comparison of results for the Sunndalen case study area is provided in **Figure 33** and **Figure 34**.

Orthophoto

LiDAR training data-based regression

Manually digitized area-based regression

NORUT

SAT-SKOG

HANSEN

Tree canopy cover

- No data
- 0 - 10 %
- 11 - 30 %
- 31 - 50 %
- 51 - 70 %
- 71 - 100 %

0     2500     5000 m
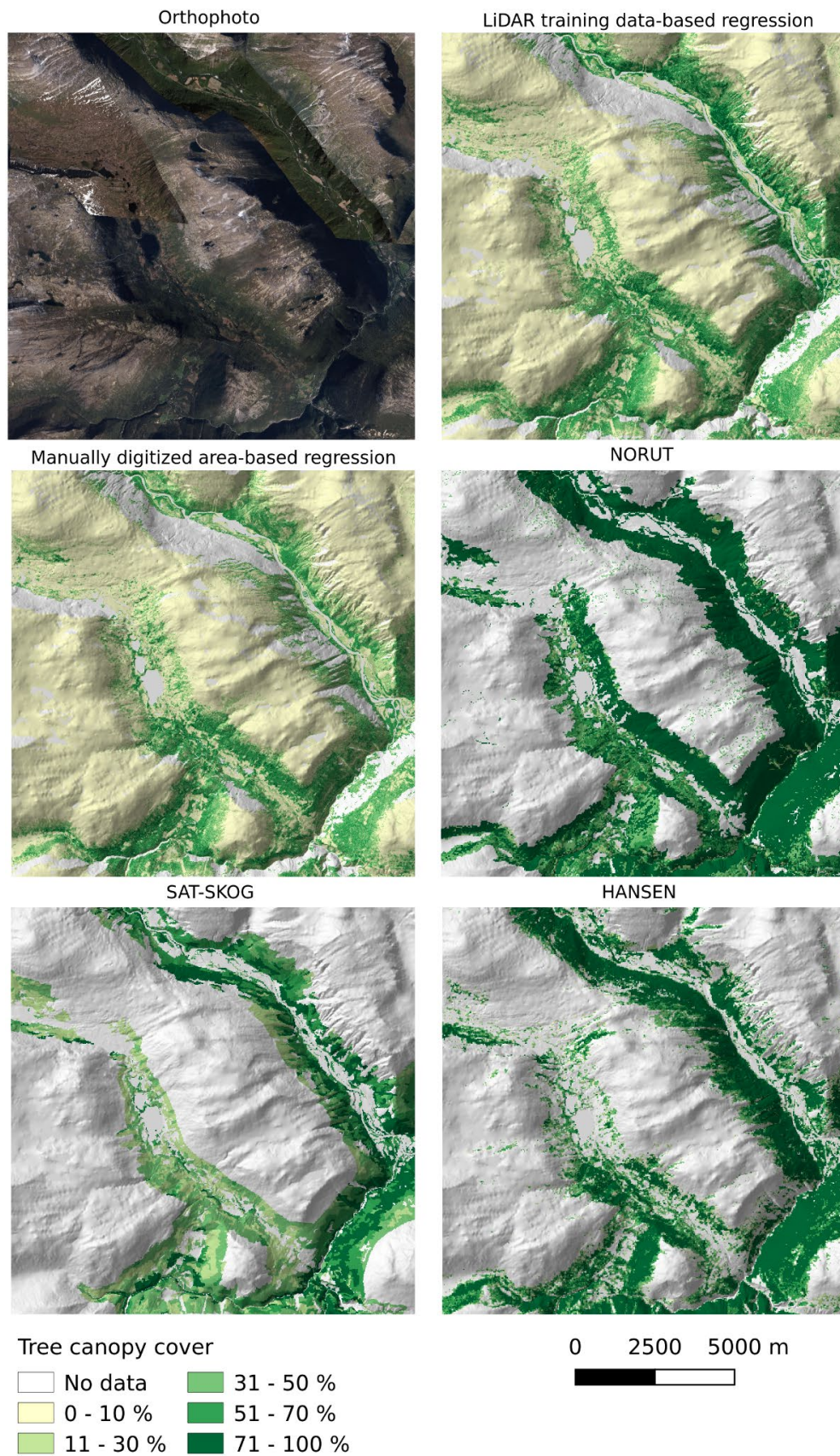
**Figure 33** *Sunndalen case study site - comparison of various forest products with different training data and different predictors.*
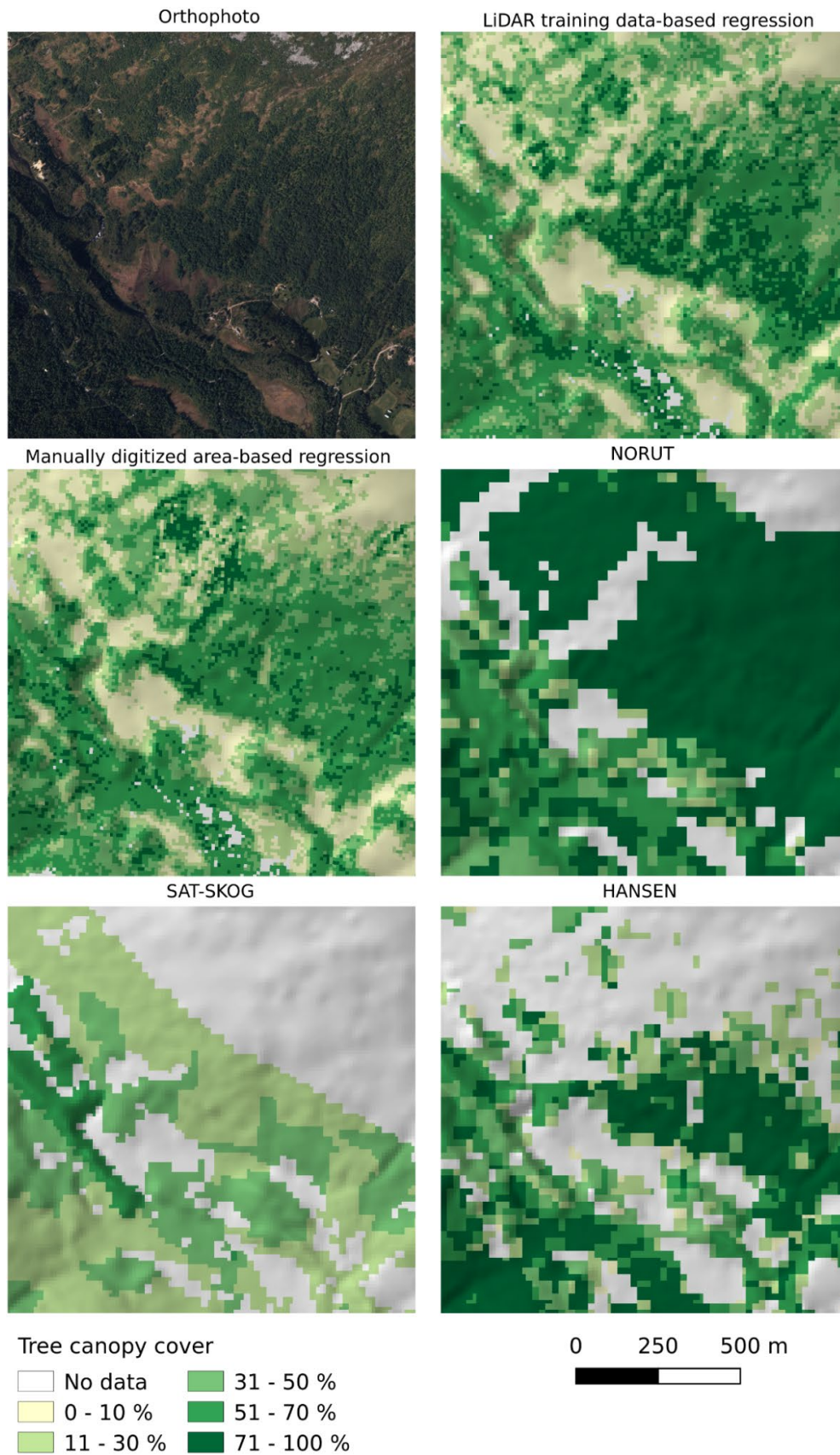
**Figure 34** *Zoom into Sunndalen case study site - comparison of various forest products*

### Oslofjord

In the Oslofjord case study site, three regression models were applied to detect forest cover:
1. manually digitized training areas including water pixels as response, satellite bands and artificial bands generated from them as predictors
2. manually digitized training areas including water pixels as response, results of fully constrained least squares spectral unmixing as predictors
3. manually digitized training areas including water pixels as response, results of non-negative least squares spectral unmixing as predictors

All three models are built on manually digitized training areas including water pixels as response. The Oslofjord case study site is comparably different than the other three case study sites. However, the regression model using satellite and artificial bands as predictors (1) again proved to be the best one. The $R^2$ values of the models are not dramatically different (0.75, 0.71 and 0.71 for models 1, 2 and 3, respectively), but visually the first model outperforms the other two (see **Figure 35** and **Figure 36**).



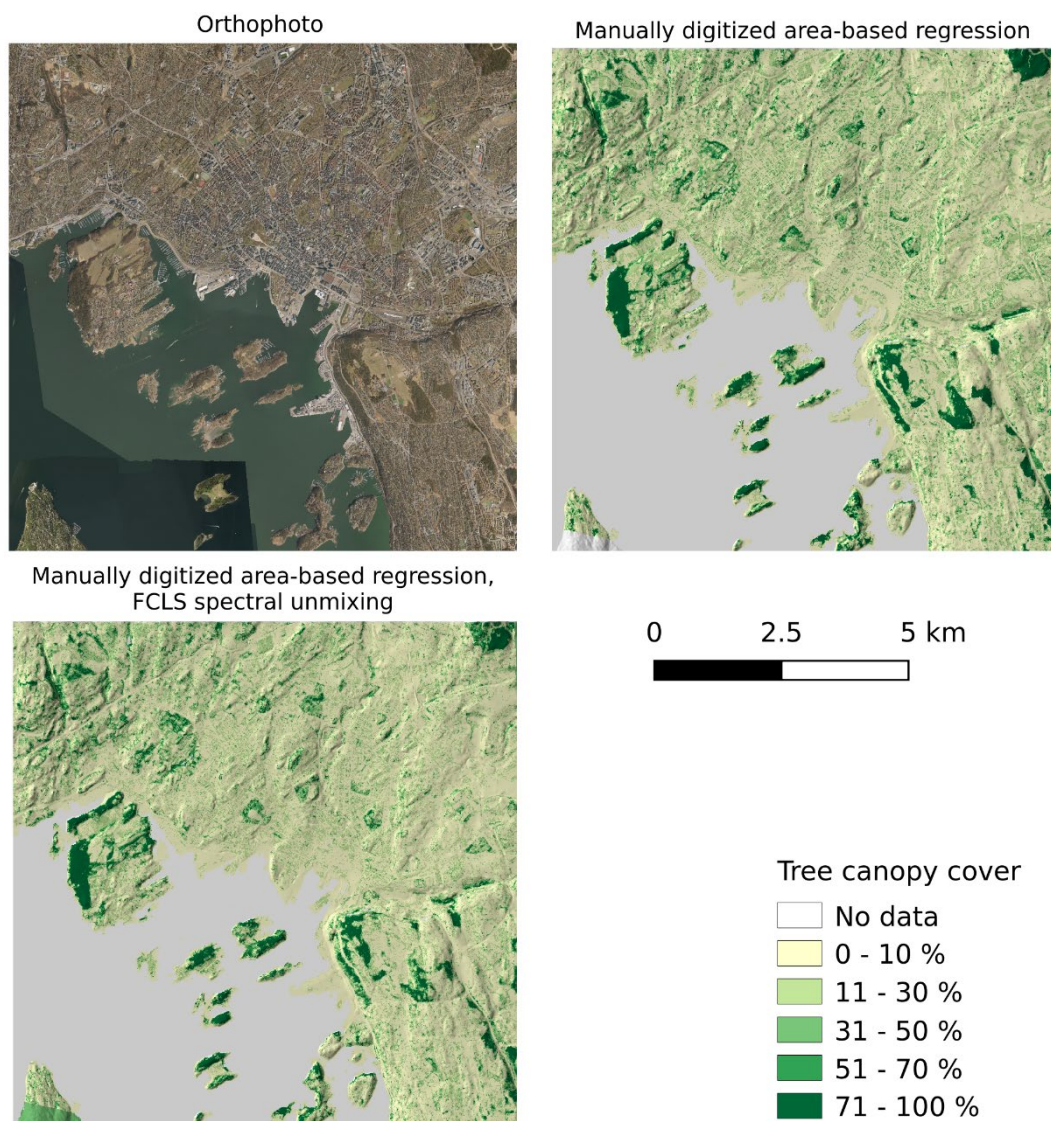**Figure 35** *Oslofjord case study site - comparison of results with different training data and different predictors.*

Orthophoto

Manually digitized area-based regression

Manually digitized area-based regression,
FCLS spectral unmixing



0            250            500 m

Tree canopy cover

No data
0 - 10 %
11 - 30 %
31 - 50 %
51 - 70 %
71 - 100 %
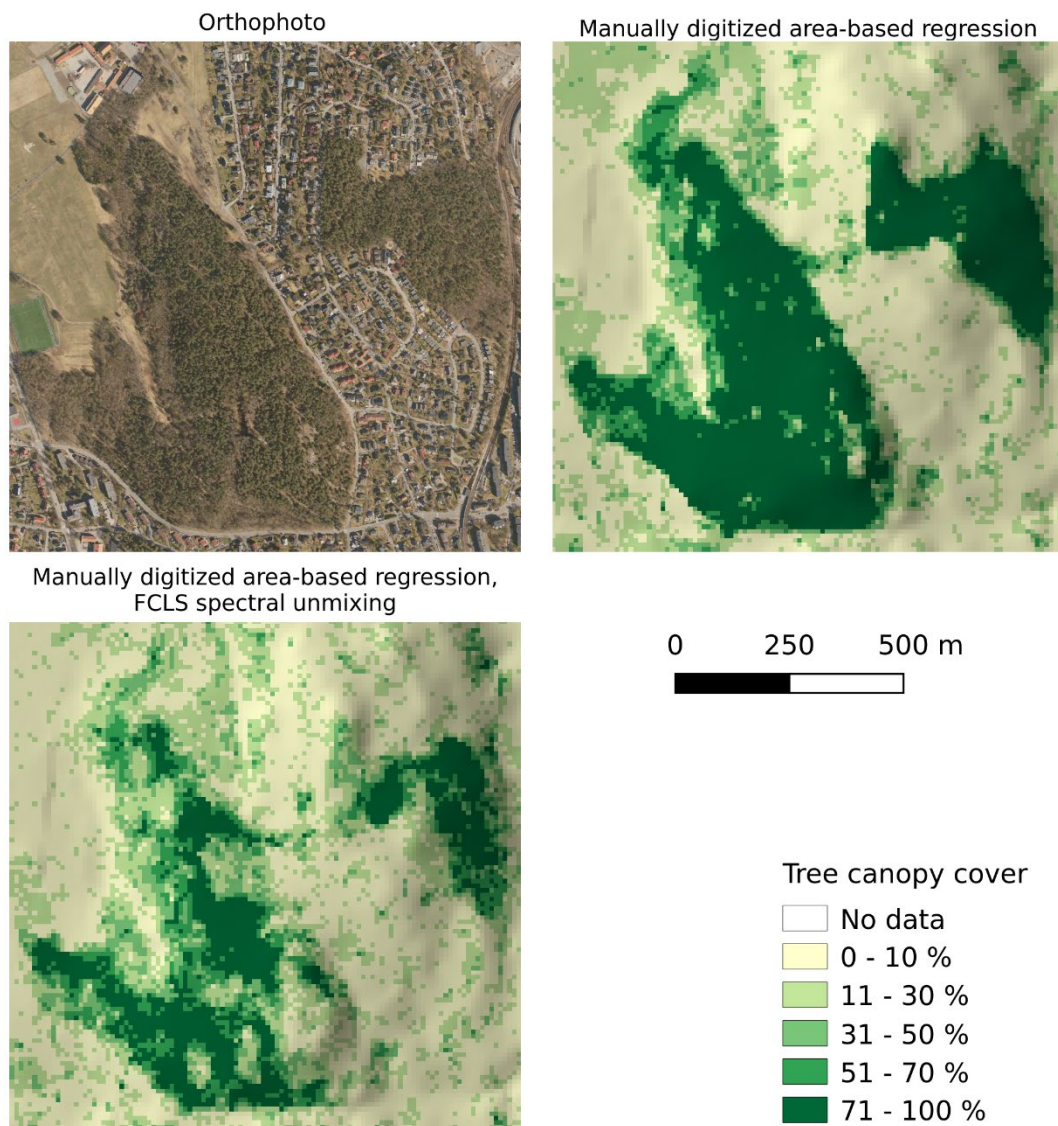
**Figure 36** *Zoom 1 into Oslofjord case study site - comparison of results with different training data and different predictors.*

In forested areas, the regression model using satellite and artificial bands as predictors (1) captures well both broad-leaf and coniferous trees. On the other hand, the regression model using results of FCLS spectral unmixing (2) fails at detecting compact broad-leaf tree canopy cover. **Figure 36** also illustrates the confusion caused by maintained grass cover (football pitch in the left part of the image). It is detected as sparse vegetation by both models.

Orthophoto

Manually digitized area-based regression

Manually digitized area-based regression, FCLS spectral unmixing

0    250    500 m

Tree canopy cover

- No data
- 0 - 10 %
- 11 - 30 %
- 31 - 50 %
- 51 - 70 %
- 71 - 100 %
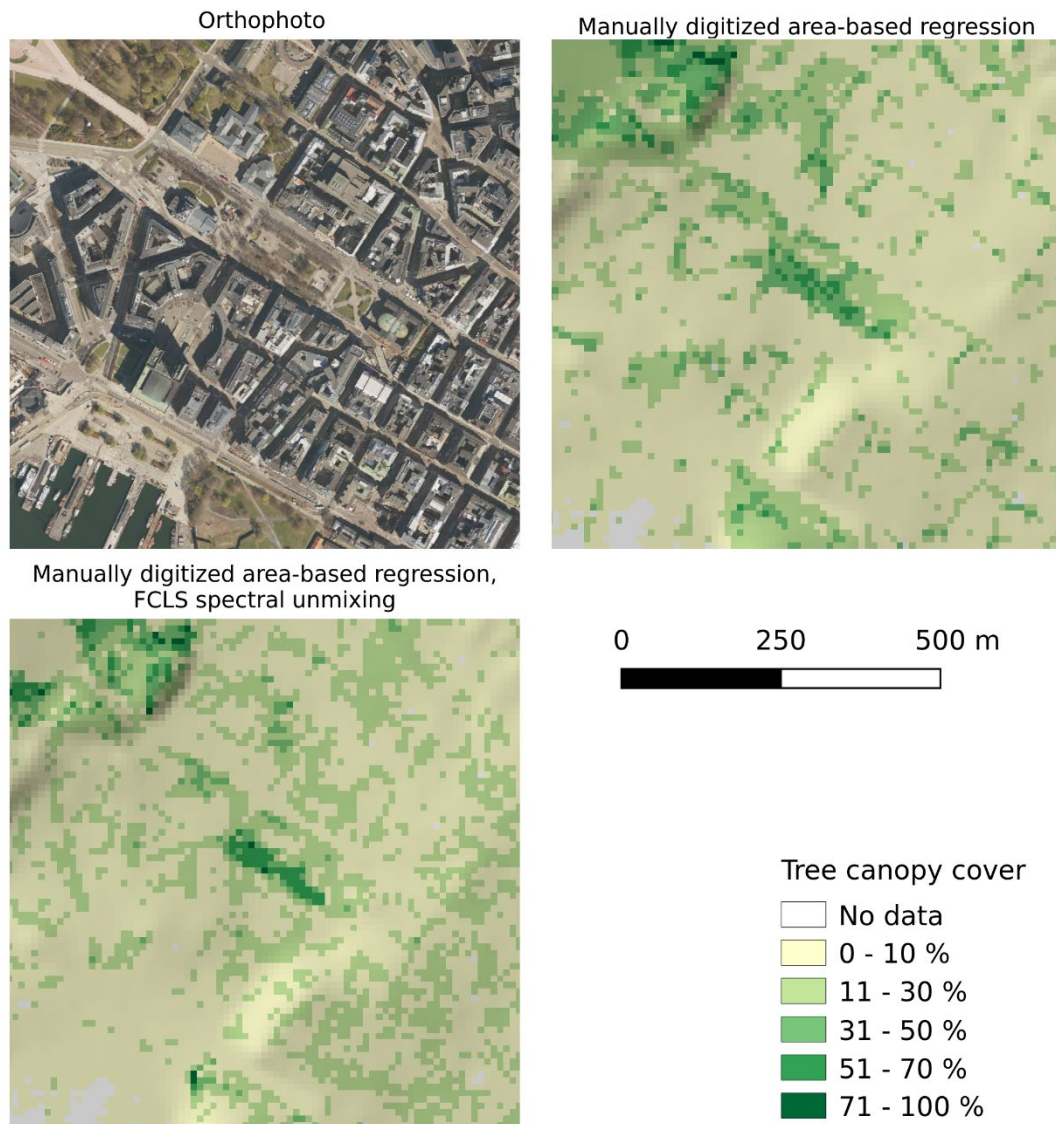
*Figure 37* Zoom 2 into Oslofjord case study site - comparison of results with different training data and different predictors.

In built-up areas, misclassifications occur due to shadows especially from lager buildings. Shadows are often detected as sparse vegetation. This issue is more relevant in case of the regression model using results of FCLS spectral unmixing (2). Closed canopy cover (parks) is again better detected by the regression model using satellite and artificial bands as predictors (1). On the other hand, this regression model misclassifies the gravel paths in the park in the upper left corner as sparse vegetation (**Figure 37**).

### 6.2.5.2   Tree canopy and vegetation pattern across forest and tree line in comparison to existing remote sensing products

Along with visual inspection, the contribution of remote sensing in modelling of tree canopy cover was assessed by comparison with similar products. These are the vegetation map of NORUT (Johansen 2009), High-Resolution Global Maps of 21st-Century Forest Cover Change by Hansen et al. (2013) and SAT-SKOG forest map from NIBIO (Gjertsen & Nilsen 2012).

The comparison was carried out in the Sunndalen case study site. Forest data from the three abovementioned sources, as well as the results of two best-performing regression models, were compared with ground vegetation measurements (Løkken & Hofgaard unpublished) by means of correlation coefficients. To ensure robustness of the comparison, three types of correlations – Pearson's, Spearman's and Kendall's coefficients were observed.

**Table 6** stresses the improved detectability of tree canopy using Sentinel-imagery. The developed Gradient boosted regression tree models based on Sentinel-1 and Sentinel-2 data (GBRT1 and GBRT2) perform constantly better than any other available data. However, comparing correlations of resulting data and trees (Layer A) and of resulting data and trees and high shrubs (Layers A+B) supports the conclusion that remote sensing fails to distinguish between different layers of vegetation with similar spectral response (i.e. trees and shrubs).

*Table 7 Comparison of existing remote sensing products on forest / tree canopy cover with the developed models*

| Layer A[4] | HANSEN | NORUT[5] | SAT-SKOG | GBRT 1 | GBRT 2 |
|---|---|---|---|---|---|
| **Pearson's** | 0.42 | 0.46 | 0.31 | 0.62 | 0.64 |
| **Spearman's** | 0.43 | 0.58 | 0.36 | 0.68 | 0.67 |
| **Kendall's** | 0.39 | 0.54 | 0.34 | 0.55 | 0.54 |
| **Layers A+B[4]** | HANSEN | NORUT | SAT-SKOG | GBRT 1 | GBRT 2 |
| **Pearson's** | 0.27 | 0.40 | 0.21 | 0.66 | 0.66 |
| **Spearman's** | 0.32 | 0.56 | 0.31 | 0.73 | 0.73 |
| **Kendall's** | 0.28 | 0.51 | 0.28 | 0.58 | 0.59 |

**Figure 33** and **Figure 34** illustrate the added value of the results of regression models. These provide significantly higher spatial precision and accuracy (the resolution is 10 m), as well as higher information resolution (continuous scale from 0 to 100 %). Moreover, they are capable of capturing small details in forest cover, such as variable densities, forest clearings, marshes etc.

## 6.2.6 Discussion and conclusions

Section 6.2 aimed at development, evaluation and refinement of a model for Tree canopy cover. Series of Sentinel-1 and Sentinel-2 data were combined and used in a regression model to derived the tree canopy cover, both directly, and also indirectly through spectral unmixing results. LiDAR data as well as manually-digitized training data were used to train and validate the model.

We used a Gradient boosted regression trees (GBRT) method to develop the regression model. GBRT is robust towards outliers and has the ability to handle non-linear relations as well as feature interactions. The result of the regression is a prediction of tree canopy cover density. For each case study site, three regression models were applied to detect tree canopy cover: 1) based on manually digitized training areas and satellite bands, 2) based on manually digitized training areas and results of spectral unmixing, and 3) based on LiDAR-derived training areas and satellite bands. The results were assessed both visually and in terms of statistical values (MSE, $R^2$).

---

[4] In Layer A, trees higher than 2 m were recorded, in Layer B, shrubs higher than 70 cm were recorded.

[5] NORUT data were assigned tree canopy density as follows: classes 1, 4, 5 – 100 %, class 6 – 75 %, classes 2, 3, 8 – 50 %, class 7 – 25 %, other classes – 0 %.

Using the LiDAR-derived training data led to consistently better results than using manually digitized training data. Furthermore, the models based on spectral unmixing results perform consistently poorer than those based on original spectral bands. Thus, spectral unmixing could not improve forest canopy cover estimates significantly. A further investigation for the causes of spectral unmixing failure needs to be carried out. In an ideal case, the spectral unmixing would directly lead to estimates of tree canopy cover, and no regression (and consequently no training data) would be required.

Alongside the various sources of inaccuracies caused by the input data, the largest influence on the quality of the result is caused by the training data. The number, distribution and land cover of the training sites turned out to have a fundamental effect on the results. It is preferable to include several training sites from various locations in the study area, and include both forested areas, as well as all kinds of non-forest land cover types (e.g. shrubs, open land and water). Excluding a land cover type, especially water, from the training data might lead to misclassifications. By including water pixels in the training data, the misclassification of mixed pixels (containing land and water) along the shoreline of water bodies as forest was dramatically reduced. The importance of good training data is particularly obvious in the Lurøykalven case study site, where only a small portion of the manually-digitized training area is covered by forest. Marshes and forest clearings were often confused with tree canopy. On the other hand, in the Sunndalen case study site the manually-digitized training data led to much better results, because the training sites were distributed in all parts of the tree canopy gradient. LiDAR measurements are generally a better source of training data, because they capture larger areas of various land cover types. However, problems occur as well – for example, buildings and boulders are sometimes confused with trees. Furthermore, despite the better performance of the regression based on LiDAR-derived training data, a question remains how to distinguish between tree canopy and shrub vegetation, which often have the same spectral response both in Sentinel-1 and Sentinel-2 bands.

Even with thorough model tuning applied, overfitting turned out to be a challenge during model fitting due to the large number of predictors. Therefore, further model simplification and reduction of the number of predictors would be recommended. However, the set of the six most important spectral bands used as predictors is not entirely consistent across the case study sites (see **Table 6**).This is on the one hand a possible result of overfitting and suggests on the other hand that model simplification should be applied with a broad set of training data across case study sites. Across sites, it is the bands of the visible spectrum (B01-B05) and some bands of the near infrared spectrum (B09) which are the most frequent ones. Moreover, the artificial bands (Sentinel-1 derived dry parameters, NDVI) turned out to be very frequent. This outcome stresses the importance of combining Sentinel-1 and Sentinel-2 data in the modelling. Furthermore, when only Sentinel-2 bands were used, grass was often mis-detected as forest, due to its similar response in the Sentinel-2 bands.

Still, the results produced by the best-performing regression model outperformed the current forest products used in Norway – both in terms of level of spatial detail (higher resolution) and information detail (tree canopy cover density). Also, small nuances especially at the forest line are captured in higher detail – compared to for example the SATSKOG product, which performed the poorest at forest line, most likely due to the fact that this data is limited to a manually mapped forest map (AR5) and that its focus is on productive forest and forestry. Furthermore, national products turned out to perform better than global products (Hansen et al. 2013).

In its current form, the developed approach for estimating tree canopy cover aggregates a time series of satellite scenes from several years, in order to minimize the seasonal variations in vegetation cover and at the same time minimize differences across forest types. However, when comparing scenes visually, we could identify large areas where significant changes in the landscape appeared relatively fast, caused e.g. by human intervention (logging) or natural causes (avalanches). Such phenomena need to be considered when training data is collected. Here, only areas with relatively constant land cover in time should be used in the training and a close temporal match between training data and satellite imagery is required.

At the same time this illustrates the potential of the approach for change detection in tree canopy cover. LiDAR can be used for relatively accurate estimates of tree canopy extent, but frequent LiDAR data acquisition over wide areas (e.g. entire Norway) cannot be expected to happen in the near future. Here, the developed methodology can bridge the gap. Locally collected LiDAR data could be used to train models based on satellite data for the same year that cover wider areas. If this would allow change detection on a year-to-year basis or if a two to three year period is required, depends on the availability of recent LiDAR acquisitions in space and time as well as on the availability of cloud free satellite images for the areas in question.

When it comes to the applicability of the model, urban areas turned out to be a special case where the developed approach is less suitable and in need of adjustments. Both algorithms (using satellite bands or spectral unmixing) based on the manually digitized training data tend to falsely classify urban areas as forest. For the specific context of mapping in urban areas, different parameters need to be selected. For SAR images Dekker (2003) showed that mean SAR intensity gives the best performance for delineating tree canopy in urban areas, but that it leads to over classification in hilly areas. Because the terrain is quite complex in most of the area of Norway, the so called dry-parameter was used in this study as it is more appropriate for these situations. However, another possibility to improve model precision in urban areas would be to use auxillary data, like topographic data on build-up areas and buildings, that is usually more frequently updated or to simply mask out urban areas using such auxiliary data (see Bossard et al. 2000).

Finally, there is some potential for improvements during the pre-processing of the satellite imagery. The partial results obtained in the pre-processing stressed the importance of terrain corrections, in particular the precision of the underlying terrain model. Especially in the areas with high terrain variations (e.g. in the built-up zone of Oslo), a detailed digital surface model is crucial so as not to misclassify building shadows as water. Furthermore, during pre-processing, the different resolution of the Sentinel-2 bands were unified to 10 m using a simple Gaussian filter. However, this approach may lead to inaccuracies especially at places where sharp edges occur in the nature (e.g. lake shores). More sophisticated algorithms exist (Brodu 2017) and could be utilized as a future improvement.

# 7 Overall conclusions

The Sentinel4Nature project identified reasonable potential for the applicability of satellite remote sensing to modelling and estimating NiN gradients. The literature review suggests that satellite remote sensing can be a useful source of information for more than 50 % of the 61 environmental gradients in NiN. The evaluation of the developed models for "Reduced growing season due to prolonged snow lie" (chapter 6.1) and "Tree canopy cover" (chapter 6.2) indicates the potential the new Sentinel satellites provide in terms of improved data compared to existing satellite imagery that has been available so far.

During the development and validation of the models for both case study gradients, supplemental auxiliary data turned out to be less important than expected for the performance of the developed models. Even for the strongly terrain related gradient on "Reduced growing-season due to prolonged snow-lie", the currently available terrain data for Norway, and terrain indices derived from them, improved the predictive power of the model only marginally. Also, comparing the developed remote sensing product with - even quite complex - models without satellite data, demonstrates the unique information satellite imagery adds. Because the models based on satellite imagery consistently explained the occurrence of snow sensitive plant species more accurate than models where only terrain information was used. However, supplemental data, and here terrain data in particular, has been important during pre-processing of the satellite imagery, both in terms of terrain correction, atmospheric correction and topographic correction. Fusing radar (Sentinel-1) and optical (Sentinel-2) data on the other hand significantly improved models for both case study gradients, underpinning findings by Schulte to Bühne & Pettorelli (2018) that radar and optical data are "better together". As the focus in terrestrial applied ecology is often on optical data, the potential of radar data in ecology is probably underestimated. Thus, the freely availability of Sentinel-1 radar data can help to unlock an important source of information for environmental monitoring in applied apology, especially for boreal and high latitude areas where light conditions can be limiting and cloud coverage is often a challenge.

The development of the model on tree canopy cover highlights the requirement for high quality training data that cover relevant variation in the imagery in order to achieve fairly accurate remote sensing products. Generating this kind of data manually is not only labour intensive, but also relatively error-prone due to continuous changes in nature and frequent revisits of the Sentinel satellites. Hence, utilizing efficient and frequently updated data sources, e.g. from in-situ sensors, crowd sourcing, "semi-remote sensing" (like LiDAR in the case of the tree canopy cover gradient, or drones) can be a means to address this issue for modelling approaches that require training data. Another possibility to handle this is to start focusing on gradients where the availability of training data is not a hard requirement. This has been the case for the gradient "Reduced growing season due to prolonged snow lie", and it is likely similar for gradients related to e.g. moisture or temperature related gradients. Here, in-situ data mainly plays a role as validation data and for such spot checks a lower amount of in-situ data would be required.

Comparison of the tree canopy cover model to existing similar forest related products indicates that the spectral, spatial and temporal resolution of the Sentinel satellites contributes to increasing the accuracy of remote sensing for environmental monitoring. It also suggests that the development of national and targeted products can be meaningful as the developed models correspond significantly better to data collected in the field than data for global applications (Hansen et al. 2013) or data for other purposes like forestry (Gjertsen & Nilsen 2012).

Although the presented methods already perform quite well, they are not yet production-ready on national scale. They are extendible to larger areas, but adjustments in the processing chains and also parameter tuning have to be expected when they are applied at larger extents and especially towards arctic environments of the Scandinavian peninsula. These areas have not been covered with study sites in this project and differ amongst others to available daylight over the year.

# 8 References

Bai, L., Lin, H., Sun, H., Mo, D. & Yan, E. 2012. Spectral Unmixing Approach in Remotely Sensed Forest Cover Estimation: A Study of Subtropical Forest in Southeast China. Physics Procedia 25: 1055-1062.

Blaschke, T. 2010. Object based image analysis for remote sensing. ISPRS journal of photogrammetry and remote sensing 65: 2-16.

Blumentrath, S. & Hanssen, F. 2010. Beregning av areal. *Datagrunnlag for Naturindeks*, pp.8-19.

Blumentrath, S. & Kudrnovsky H. 2016. v.in.pygbif - Search and import GBIF species distribution data. GRASS GIS addon. https://grass.osgeo.org/grass74/manuals/addons/v.in.pygbif.html

Blumentrath, S., Cimburova, Z. & Rød-Eriksen L. 2018: Using wildlife camera traps to collect in-situ data for remote sensing applications with high temporal resolution. NINA Report 1584. Norwegian Institute for Nature Research.

Bojinski, S., Verstraete, M., Peterson, T. C., Richter, C., Simmons, A. & Zemp, M. 2014. The Concept of Essential Climate Variables in Support of Climate Research, Applications, and Policy. Bulletin of the American Meteorological Society 95 (9): 1431-1443

Bossard, M., Feranec, J. & Otahel, J. 2000. CORINE land cover technical guide: Addendum 2000.

Brodu, N. 2017. Super-Resolving Multiresolution Images With Band-Independent Geometry of Multispectral Pixels. IEEE Transactions on Geoscience and Repote Sensing 55(8) : 4610-4617.

Bryn, A., Dourojeanni, P., Hemsing, L.Ø. & O'Donnell, S. 2013. A high-resolution GIS null model of potential forest expansion following land use changes in Norway. Scandinavian Journal of Forest Research 28(1): 81-98.

Bryn, A. and Potthoff, K. 2018. Elevational treeline and forest line dynamics in Norwegian mountain areas–a review. Landscape Ecology, pp.1–21.

Crawford, C.J., Manson, S.M., Bauer, M.E. & Hall, D.K. 2013. Multitemporal snow cover mapping in mountainous terrain for Landsat climate data record development. Remote Sensing of Environment 135: 224-233.

Dekker, R.J. 2003. Texture analysis and classification of ERS SAR images for map updating of urban areas in the Netherlands. Geoscience and Remote Sensing, IEEE Transactions on 41: 1950-1958.

Dostálová, A., Hollaus, M., Milenković, M. & Wagner, W. 2016. Forest area serivation from Sentinel-1 data. ISPRS Annals of the Photogrammetry, Remote Sensing & Spatial Information Sciences 3: 227.

Eide, N. E. 2017. Temperature logger data from Hjerkinn 2014 - 2017, Norway. Unpublished. Norwegian Institute for Nature Research.

Eriksen, E. L., Ullerud, H. A., Halvorsen, R., Aune, S., Bratli, H., Horvath, P., Volden, I. K., Wollan, A. K. & Bryn, A. 2018. Point of view: error estimation in field assignment of land-cover types. Phytocoenologia (2018): 1-14.

European Space Agency. 2010. Copernicus Programme. http://www.copernicus.eu/

Evju, M., Hagen D., & Hofgaard A. 2012. Effects of disturbance on plant regrowth along snow pack gradients in alpine habitats. Plant ecology 213: 1345-1355.

Gao, B.C. 1996. NDWI—A normalized difference water index for remote sensing of vegetation liquid water from space. Remote sensing of environment. 58(3): 257-266.

Gelman, A., Jakulin, A., Pittau, M.G. & Su, Y.S. 2008. A weakly informative default prior distribution for logistic and other regression models. The Annals of Applied Statistics 2 : 1360-1383.

Gjertsen, A.K. & Nilsen, J.E. 2012. SAT-SKOG. Et skogkart basert på tolking av satellittbilder. Rapport fra Skog og landskap 23.

Gudex-Cross, D., Pontius, J. & Adams, A. 2017. Enhanced forest cover mapping using spectral unmixing and object-based classification of multi-temporal Landsat imagery. Remote Sensing of Environment. 196: 193-204.

Group on Earth Observations Biodiversity Observation Network. 2016. Essential Biodiversity Variables - Getting most for your money. Learn more about our Essential Biodiversity Variables (EBVs). https://geobon.org/ebvs/what-are-ebvs/ visited 20.11.2018

Havorsen, R., Bryn A., Erikstad L. & Lindgaard A. 2015. Natur i Norge - NiN. Versjon 2.0.0. http://www.artsdatabanken.no/nin

Halvorsen, R., Bryn, A. & Erikstad, L. 2016. NiNs systemkjerne – teori, prinsipper og inndelingskriterier. Natur i Norge, Artikkel 1 (versjon 2.1.0): 1–358 (Artsdatabanken, Trondheim; http://www.artsdatabanken.no.)

Hansen, M.C., Potapov, P.V., Moore, R., Hancher, M., Turubanova, S.A.A., Tyukavina, A., Thau, D., Stehman, S.V., Goetz, S.J., Loveland, T.R. & Kommareddy, A. 2013. High-resolution global maps of 21st-century forest cover change. Science. 342 (6160): 850-853.

He, K.S., Rocchini, D., Neteler, M. & Nagendra, H. 2011. Benefits of hyperspectral remote sensing for tracking plant invasions. Diversity and Distributions, 17(3): 381-392.

Ichter, J., Evans D. & Richard D. 2014. Terrestrial habitat mapping in Europe: an overview. ISSN 1725-2237, European Environmental Agency, Copenhagen, Denmark.

Johansen, B. 2009. Vegetasjonskart for Norge basert Landsat TM/ETM+ data. Norut-Tromsø Rapport, 4:86.

Kumar, U., Milesi, C., Nemani, R. R., Raja, S. K., Wang, W. & Ganguly, S. 2016. Partially and fully constrained least squares linear spectral mixture models for subpixel land cover classification using Landsat data. International Journal of Processing Systems 4(3): 245-251.

Løkken, J. O. & Hofgaard A. 2017. Data on vegetation cover changes along an altitudinal gradient. unpublished. collected for the ECOFUNC project, funded by the Norwegian research council (RCN grant MILJØ2015, project number: 244557). Norwegian Institute for Nature Research.

Maher, A. I., Treitz P. M., & Ferguson M. A. 2012. Can Landsat data detect variations in snow cover within habitats of arctic ungulates? Wildlife Biology 18 (1): 75-87.

McCullagh, P. & Nelder J. A. 1989. Generalized linear models. Vol. 37. CRC press.

McFeeters, S.K., 1996. The use of the Normalized Difference Water Index (NDWI) in the delineation of open water features. International journal of remote sensing 17 (7): 1425-1432.

Metsämäki, S., Hiltunen, M., Luojus, K. & Pulliainen, J. 2014. Spring-time fractional snow cover mapping in Northern Hemisphere with NPP Suomi/VIIRS within ESA DUE GlobSnow-2 project. Pages 4002-4005 in Geoscience and Remote Sensing Symposium (IGARSS), 2014 IEEE International.

Metsämäki, S., Pulliainen, J., Salminen, M., Luojus, K., Wiesmann, A., Solberg, R., Böttcher, K., Hiltunen, M. & Ripper, E. 2015. Introduction to GlobSnow Snow Extent products with considerations for accuracy assessment. Remote Sensing of Environment, 156: 96-108.

Metz, M.; Rocchini, D.; Neteler, M. 2014. Surface Temperatures at the Continental Scale: Tracking Changes with Remote Sensing at Unprecedented Detail. Remote Sens. 2014 (6): 3822-3840.

Mulder, V.L., De Bruin, S., Schaepman, M.E. and Mayr, T.R. 2011. The use of remote sensing in soil and terrain mapping—A review. Geoderma 162 (1-2): 1-19.

Norwegian Ministry of Climate and Environment 2016. Arbeidet med det økologiske grunnkartet er i gang. https://www.regjeringen.no/no/aktuelt/arbeidet-med-det-okologiske-grunnkartet-er-i-gang/id2525650/. 23.12.2016

Nybø, S. & Evju, M. (red) 2017. Fagsystem for fastsetting av god økologisk tilstand. Forslag fra et ekspertråd. Ekspertrådet for økologisk tilstand, 247 s.

Odland, A. & Munkejord H.K. 2008a. The importance of date of snowmelt for the separation of different oligotrophic and mesotrophic mountain vegetation types in Southern Norway. Phytocoenologia 38 (1-2): 3-21.

Odland, A. & Munkejord H.K. 2008b. Plants as indicators of snow layer duration in southern Norwegian mountains. Ecological Indicators 8 (1): 57-68.

Olsen, S. 2017. Indcator species for snow cover duration in the Norwegian Mountains. Personal communication. August 2017.

Pachauri, R. K., Allen M.R., Barros V.R., Broome J., Cramer W., Christ R., et al. 2014. Climate change 2014: synthesis report. Contribution of Working Groups I, II and III to the fifth assessment report of the Intergovernmental Panel on Climate Change. IPCC.

Pirrone, N., Trombino, G., Cinnirella, S., Algieri, A., Bendoricchio, G. & Palmeri, L. 2005. The Driver-Pressure-State-Impact-Response (DPSIR) approach for integrated catchment-coastal zone management: preliminary application to the Po catchment-Adriatic Sea coastal zone system. Regional Environmental Change, 5 (2-3): 111-137.

Nagler, T., & Rott H. 2000. Retrieval of wet snow by means of multitemporal SAR data. Geoscience and Remote Sensing, IEEE Transactions on Geoscience and Remote Sensing 38 (2): 754-765.

Neteler, M., Grasso, D., Michelazzi, I., Miori, L., Merler, S. & Furlanello, C. 2005. An Integrated Toolbox for Image Registration, Fusion and Classification. International Journal of Geoinformatics 1 (1).

Rott, H. & Mätzler C. 1987. Possibilities and limits of synthetic aperture radar for snow and glacier surveying. Annals of Glaciology 9: 195-199.

Salberg, A. B. 2011. Retraining maximum likelihood classifiers using a low-rank model. Pages 166-169 *in* Geoscience and Remote Sensing Symposium (IGARSS), 2011 IEEE International. IEEE.

Salberg, A. B., Erikstad L. & Zortea M. 2013. Fusion of satellite and aerial images for identification and modeling of nature types. Vol. 8892, Page 889214 *in* Image and Signal Processing for Remote Sensing XIX. International Society for Optics and Photonics.

Scherer, D., Hall, D.K., Hochschild, V., Konig, M., Winther, J.G., Duguay, C.R., Pivot, F., Matzler, C., Rau, F., Seidel, K., Solberg R. & Walker A. E. 2005. Remote sensing of snow cover. GEOPHYSICAL MONOGRAPH-AMERICAN GEOPHYSICAL UNION 163: 7.

Schulte to Bühne, H. & Pettorelli, N. 2018. Better together: Integrating and fusing multispectral and radar satellite imagery to inform biodiversity monitoring, ecological research and conversation science. Methods in Ecology and Evolution 9 (4): 849-865..

Small, D. 2011. Flattening gamma: Radiometric terrain correction for SAR imagery. IEEE Transactions on Geoscience and Remote Sensing 49 (8): 3081-3093.

Stanners, D., Bosch, P., Dom, A., Gabrielsen, P., Gee, D., Martin, J., Rickard, L. & Weber, J.L. 2007. Frameworks for environmental assessment and indicators at the EEA. Sustainability Indicators–A Scientific Assessment.

Thakur, P. K., Garg, P.K., Aggarwal, S.P., Garg, R.D. & Mani, S. 2013. Snow cover area mapping using synthetic aperture radar in Manali watershed of Beas River in the Northwest Himalayas. Journal of the Indian Society of Remote Sensing 41 (4): 933-945.

Therien, Ch. 2016. pysptools Documentation, Release 0.13.4.

Vermaat, J.E., Hellmann, F.A., van Teeffelen, A.J., van Minnen, J., Alkemade, R., Billeter, R., Beierkuhnlein, C., Boitani, L., Cabeza, M., Feld, C.K. & Huntley, B. 2017. Differentiating the effects of climate and land use change on European biodiversity: A scenario analysis. Ambio 46 (3): 277-290.

Wille, M. & Clauss, K. 2016. Search and download Copernicus Sentinel satellite images https://sentinelsat.readthedocs.io

Zhu, Z., & Woodcock C. E.. 2012. Object-based cloud and cloud shadow detection in Landsat imagery. Remote Sensing of Environment 118: 83-94.

# Appendix

The electronic appendix, covering "The suitability of remote sensing (Sentinel) for estimating environmental gradients and properties in NiN" as referred to in chapter 3 can be accessed here:
https://brage.bibsys.no/xmlui/bitstream/handle/11250/2575962/1545%20vedlegg.xlsx?sequence=6&isAllowed=y


Code from the Sentinel4Nature project is documented here:
https://github.com/NINAnor/sentinel4nature


Data produced in the Sentinel4Nature project can be accessed here:
http://geodata.nina.no/search/?title__icontains=Sentinel4Nature

*The Norwegian Institute for Nature Research, NINA, is as an independent foundation focusing on environmental research, emphasizing the interaction between human society, natural resources and biodiversity.*

*NINA was established in 1988. The headquarters are located in Trondheim, with branches in Tromsø, Lillehammer, Bergen and Oslo. In addition, NINA owns and runs the aquatic research station for wild fish at Ims in Rogaland and the arctic fox breeding center at Oppdal.*

*NINA's activities include research, environmental impact assessments, environmental monitoring, counselling and evaluation. NINA's scientists come from a wide range of disciplinary backgrounds that include biologists, geographers, geneticists, social scientists, sociologists and more. We have a broad-based expertise on the genetic, population, species, ecosystem and landscape level, in terrestrial, freshwater and coastal marine ecosystems.*

**1545**

**NINA** Report

NINA

Cooperation and expertise for a sustainable future